

THE LARGE SCALE STRUCTURE OF THE SOLAR WIND

By

John H. Wolfe

→ KSS-10

Presented at

Solar Wind Conference

Asilomar Conference Grounds

Pacific Grove, California

March 21-26, 1971

(NASA-TM-X-69342) THE LARGE SCALE
STRUCTURE OF THE SOLAR WIND (NASA)
100 p HC \$7.00

CSSL 03B

N73-28826

G3/29

Unclas
15128

NASA-Ames Research Center
Moffett Field, California 94035

AA
6/15

A B S T R A C T

A review of the large scale structure of the solar wind is presented based on experimental space measurements acquired over approximately the last decade. The observations cover the fading portion of the last solar cycle up through the maximum of the present cycle. The character of the interplanetary medium is considered from the viewpoint of the temporal behavior of the solar wind over increasingly longer time intervals, the average properties of the various solar wind parameters and their interrelationships. A brief discussion of interplanetary-terrestrial relationships and the expected effects of heliographic latitude and radial distance is also included.

The Large Scale Structure of the Solar Wind

John H. Wolfe

Introduction

The purpose of this paper is to review our knowledge of the large scale structure of the solar wind. This review will be considered from measurements made from 1962 to the present. Results discussed represent data obtained during the fading portion of the last solar cycle (cycle 19) up to approximately the peak of the present cycle. Only proton results will be considered here since they represent the major energy carrying constituent of the solar wind and discussions of solar wind composition and solar wind electrons will be covered separately later in the conference. The first consideration will be given to the average behavior of the solar wind as observed over many days and up to several solar rotations. This will be followed by a comparison of the variations in the solar wind with the large scale interplanetary magnetic field observations and the behavior of the solar wind over much longer intervals up through the major portion of a solar cycle. The above is followed by an overall view of the average properties of the solar wind, the interrelationship between solar wind parameters and finally, a discussion of interplanetary-terrestrial relationships and present speculation of the behavior of the solar wind closer to the sun, far beyond the Earth's orbit and at high heliographic latitudes.

Short term variations

For the purposes of this review, short term variations are defined here to pertain to the solar wind behavior over periods of

days and months as contrasted to years for long term variations. Figure 1 is taken from the Mariner 2 results reported by Neugebauer and Snyder (1966) and shows the variation in the solar wind velocity and temperature averaged over 3 hour intervals. The data were taken over approximately $4\frac{1}{2}$ solar rotations in late 1962. One of the most interesting features of these results is the great variability in the solar wind over a time period on the order of days. The velocity is observed to frequently rise from a quiescent value between 300 and 350 km/sec up to as high as approximately 700 km/sec and indicates a high degree of temperature inhomogeneity in the solar corona. Note that these high velocity streams are often times asymmetric showing a sharper rise in velocity on the leading edge with a slower decay in the descending portion. The temperature is observed to be approximately in phase with the velocity although frequently tending to high values on the leading edge of the stream somewhat prior to the velocity peak. Although some high velocity streams tend to persist from one solar rotation to the next, they change in width and amplitude and some streams do not repeat at all. The data thus indicate, at least at the time of the Mariner 2 flight, dramatic coronal changes take place on a time scale less than one solar rotation. Neugebauer and Snyder (1966) also reported the proton number density for this same period of time as shown in Figure 2. For comparison purposes the velocity is again plotted here as the darker curve and the density on the lighter curve. The approximate in phase relationship between velocity and temperature is in contrast to the striking anticorrelation between velocity and density observed here. In addition to the velocity-density anticorrelation, note also a

frequent tendency for large increases in density associated with the leading edge of a high velocity stream. This density pile up is dramatically observed, for example, in the streams beginning September 1, September 30 and October 7.

Three hour averages of various solar wind parameters obtained during the last two weeks of December, 1965 are shown in Figure 3. The data are taken from the Ames Research Center plasma probe on Pioneer 6 (Wolfe, 1970) and show the solar wind bulk velocity, proton density and temperature, the two angular components of the flow direction and the geomagnetic disturbance index K_p . The angular components of the flow direction are defined in terms of a spacecraft centered, solar ecliptic coordinate system. The azimuthal flow direction represents the angle of flow in the ecliptic plane with positive angles defined as flow from the west with respect to the spacecraft-sun line and negative angles from the east. This angle has been corrected for the aberration due to the motion of the spacecraft around the sun and has also been corrected for an apparent systematic error of a negative 2.6° . The polar flow direction represents the angle of flow in the plane normal to the ecliptic containing the spacecraft-sun line with positive angles defined as flow from the north and negative from the south. As was the case for the Mariner 2 data, the stream structure in the velocity is quite evident in the Pioneer 6 results. The density is observed to pile up in front of the leading portion of the streams with a sharp temperature rise associated with the positive gradient in the velocity. Also note that associated with the leading edge of each stream, the azimuthal

flow angle shows that the flow shifts to a direction first from the east and then from the west across the positive gradient in velocity. This is a very persistent stream feature and is even more dramatically observed in Figure 4. These data were also obtained from the Pioneer 6 Ames Research Center plasma probe (Wolfe, 1970) and shows the solar wind bulk velocity and flow directions for the first two weeks of January 1966. Note the one for one correlation of the east-west shift in the azimuthal flow direction with the positive gradients in velocity. Although large shifts in the polar flow direction are observed, frequently associated with velocity gradients, there is no particular flow pattern discernible in this angular component.

Similar results obtained during the rising portion of the present solar cycle have been reported by Lyon et al. (1968) using data taken from the Explorer 33 earth satellite. Figure 5 shows 3-hour average values of the solar wind bulk velocity, density (logarithmic scale), most probable thermal speed (related to temperature by $w = (2kT/m)^{1/2}$) and the azimuthal and latitude (polar) angles. Note that the azimuthal angle, ϕ_{SE} , has been defined here in a sense opposite to that described for Figures 3 and 4. The data were taken over the interval July 3-12, 1966. Again, the influence of the solar wind high velocity stream structure is apparent. Note the striking examples of the density pile-up at the leading edges of the high velocity streams and the east-west shift in azimuthal flow direction across the positive gradient in velocity.

With respect to short term variations in the solar wind behaviour as observed over averages of several hours and considered on a time scale of weeks to months, the dominant feature seems to be the solar wind stream structure. Coronal temperature inhomogeneities which presumably

lead to this stream structure, leads one to a picture (as observed) near 1 AU) of numerous coronal high temperature regions which give rise to high velocity solar wind streams which interact, due to the rotation of the sun, with the quiescent plasma associated with the ambient coronal solar wind. The stream interactions manifest themselves as a positive gradient in the solar wind convective velocity associated with the leading edge of the stream which is typically much steeper than the negative gradient in velocity associated with the trailing portion of the stream. Although the velocity and temperature are observed to be approximately in phase, the steep positive gradient in velocity frequently indicates an interaction mechanism for heating the solar wind gas. Although the velocity and density are approximately anti-correlated, anomalous density pile-up ~~is~~ frequently observed associated with the leading edge of the stream presumably due to a "snowplow" effect associated with the high velocity plasma overtaking the slower ambient gas. Of particular significance is the east-west shift in the azimuthal component of the solar wind flow direction across the positive gradient in bulk velocity associated with the leading edge of the stream. This azimuthal shift in flow direction is consistent with that expected for the azimuthal stresses set up along the average Archimedian spiral of the interplanetary field which presumably defines the interaction geometry between the high velocity plasma stream and the ambient gas. It should be noted here that the westward flow shifts at the positive velocity gradients are usually of higher amplitude (in angle) than the eastward flow shifts.

In addition, there seems to be a frequent tendency for slight eastward flow associated with the more gradual negative gradient in the velocity on the trailing edge of a stream.

Solar Wind Streams and Magnetic Field Sector Structure

Results from the IMP-1 satellite (Wilcox and Ness, 1965) indicated the presence of a definite pattern in the dominant polarity of the interplanetary magnetic field. This polarity pattern or sector structure was fairly repetitive over approximately 3 solar rotations observed by the IMP-1 flight. These results are shown in Figure 6 where three-hour averages of the interplanetary magnetic field are plotted starting on November 27, 1963 with the plus symbols representing field lines predominantly outward from the sun and the negative symbols representing field lines predominantly inward toward the sun. The Archimedian spiral lines represent the best fit sector boundaries which separated the differing field polarities. The only gross exception to the repeating pattern appears to be the early polarity reversal associated with a geomagnetic storm commencing on December 2, 1963. At the time, Wilcox and Ness (1965) presumed this early polarity reversal to be due to a higher than expected solar wind velocity associated with the storm.

The obvious next question concerns the relationship between the interplanetary magnetic field sector structure and the high velocity solar wind stream pattern. Twenty-four hour average values of the solar wind velocity obtained from the Ames Research Center plasma probe on IMP-1 are shown in Fig. 7. The dominant orientation of the interplanetary magnetic field is also shown together with the geomagnetic disturbance index A_p . The recurring solar wind streams are identified by letter.

The most striking feature is the almost one-for-one correspondence between the solar wind stream pattern and the magnetic field sector structure. Note that the field changes its dominant polarity near the beginning of each stream and that the width of any given stream and corresponding sector are almost identical. If the solar wind streams define the magnetic sector structure then the earlier than expected polarity reversal on December 2, 1963 can be explained as due to a change in the solar wind stream width on the successive solar rotation rather than a change in velocity as discussed previously. This can be seen in Fig. 7 by noting that the stream identified as "A" from its first observed occurrence to its recurrence on the next solar rotation has decreased in width by approximately 2 to 3 days whereas the peak velocity has remained about the same near 700 km/sec. It is interesting to note that although the A_p index in general follows the solar wind stream structure, the peak velocity frequently tends to lag the peak in A_p by as much as a day.

Using the method of superposed epoch analysis, Wilcox and Ness (1965), compare the interplanetary magnetic field sectors observed by IMP-1 with preliminary MIT plasma data. The results for solar wind velocity are shown in Fig. 8 where the ordinate is a 3-hour average value of the solar wind velocity and the abscissa is the position within the four large sectors previously shown in Fig. 6. Note that both "toward" and "away" sectors are used. It can be seen that the velocity tends to reach a maximum on the order of 1/4 to 1/3 of the way through the sector. The second peak near 4 days for the "away" sectors is considered to be

an artificial feature related to the perigee passage of the spacecraft near the middle of these "away" sectors. The same analysis was performed for the solar wind density and is shown in Fig. 9. Here the density is observed to rise to a maximum value at about one day after the sector beginning, decrease to a minimum near the center and then rise again at the end of the sector. Note by comparison with Fig. 8 that the large peak in density at the beginning of the sector coincides with the positive gradient in the velocity which in turn is associated with the beginning of a new solar wind stream.

Fig. 10 shows the sector pattern of the interplanetary magnetic field as given by Wilcox and Colburn (1969) covering the period from the flight of Mariner 2 in 1962 through Explorer 35 in mid-1968. The sector structure is shown overlaying the daily geomagnetic character index C9 with light shading indicating sectors with fields predominantly away from the sun and dark shading for sectors with fields predominantly toward the sun. The diagonal bar indicates an interpolated quasi-stationary structure during 1964. Although it might be argued that the 1964 interpolations could be misleading, it is certainly clear that the sector structure was much more repetitive from one solar rotation to the next up through the IMP-2 flight as compared to after that time. The period from 1965 through mid-1967 is particularly chaotic with no discernible repeating pattern. This period occurred during the steeply rising portion of the present solar cycle (cycle 20) as compared to near solar minimum for the time of the IMP-1 flight. Note that the sector pattern becomes somewhat more regular in 1968 near solar maximum.

The relationship between the solar wind stream structure and the more chaotic interplanetary magnetic field sector pattern associated with the steeply rising portion of the solar cycle is illustrated in Fig. 11. The solar wind data are taken from Pioneer 6 (Wolfe, 1970) and 24-hour average values of the proton temperature (fitted to an isotropic Maxwellian distribution), number density and velocity have been plotted together with the geomagnetic disturbance index A_p . The data are shown for slightly more than one solar rotation beginning December 18, 1965. The bar graph at the top gives the interplanetary magnetic field sector structure with the extent of the away ("A") and toward ("T") sectors as shown. The vertical-lines designate the sector boundaries. As was the case for the IMP-1 results discussed earlier, the sector boundaries appear to be associated with the beginning of new solar wind streams. Here, however, more than one stream is observed to appear within a given magnetic sector. The sector commencing on December 25, 1965, for example, is "classic" in that it is quite similar to that observed by IMP-1 in late 1963. The velocity is observed to peak approximately 1/3 of the way through the sector with the density high at the extremes of the sector and at a minimum near the center. In addition, the temperature is seen to peak early in the sector and then descend throughout the remainder of the sector. By contrast, the wide sector beginning January 2, 1966 is seen to contain two distinct solar wind streams. Note, however, that when the sector boundaries do occur, they appear near the beginning of a new solar wind stream.

Another interesting feature of the data is the nature of the solar wind streams themselves and their relationship to geomagnetic activity.

Within the general appearance of correlation of temperature and anti-correlation of density with respect to velocity, anomalously high densities and temperatures are observed associated with the positive gradients in velocity which define the leading edge of a solar wind stream. With respect to geomagnetic activity the maxima in velocity tends to lag and the density tends to lead the peaks in the A_p index whereas the temperature appears to be roughly in phase. For the set of data shown here, the correlation coefficient between temperature and A_p was 0.88 indicating a surprisingly high degree of correlation. Although not necessarily cause and effect, it seems apparent that the temperature might be a fairly reliable index of the state of disturbance in the solar wind which in turn determines the level of geomagnetic activity.

A perhaps even more complex example of the relationship between the solar wind streams and the magnetic field sector structure is shown in Fig. 12. The plots are similar to the previous figure with the solar wind data taken from Pioneer 7 (Wolfe, 1970) and are shown for slightly more than one solar rotation beginning August 19, 1966. As was the case with Pioneer 6, more than one solar wind stream is observed within a given magnetic field sector. The sector with field predominantly toward the sun which ends on September 4, 1966 contains three distinct solar wind streams. Note again, however, that when the sector boundaries do occur they appear near the beginning of a new solar wind stream. An exception to this appears to be the September 4, 1966 sector boundary. Investigation of the detailed data (Wolfe, 1970) shows, however, that the solar wind stream beginning at this time

was somewhat anomalous with a 6-hour "spike" in velocity to values over 530 km/sec associated with this sector boundary. This short period velocity increase has been washed out in the averaging process in Fig. 12. The peak in geomagnetic activity on August 30, 1966 illustrates a striking example of the lag, lead and in phase relationship between respectively velocity, density and temperature and the A_p index.

The interplanetary investigations reported thus far clearly indicate an apparent dominance of the magnetic field sector structure by solar wind streaming. The solar wind high velocity streams are apparently the interplanetary manifestations (observed near 1 AU) of coronal temperature inhomogeneities. According to the classical Parker (1969) model, higher temperature regions in the corona would lead to higher interplanetary solar wind velocities. Due to the rotation of the sun, these higher velocity streams would be expected to interact with the lower velocity gas associated with the quiescent corona. Based on the observed interplanetary magnetic field and solar wind characteristics, it is postulated that an interaction region forms along the Archimedian spiral of the interplanetary magnetic field between the high velocity plasma and the lower velocity gas associated with the quiescent corona. For some hypothetical boundary, perhaps associated with the initial velocity increase at the leading edge of a new stream, the leading ambient gas would be accelerated with the loss of kinetic energy and therefore velocity decrease for the higher velocity driving gas giving rise to the observed asymmetry in the stream velocity profile. Due to the essentially

infinite conductivity of the medium, the streams cannot penetrate one another so that the plasma density increases forward of this hypothetical boundary in a "snowplow" like effect. The observed east-west shift in the solar wind azimuthal flow direction is then simply the reaction of the gas to the tangential stresses set up at the interaction boundary. It is quite likely that waves are generated at this boundary which, in the moving frame of reference of the gas, propagate both upstream and downstream giving rise to plasma heating throughout the entire interaction region. Since the interaction region is likely to be the most disturbed, it follows that geomagnetic disturbance indices and interplanetary solar wind ion temperatures should be correlated. Since the interaction boundary separates different plasma regimes, the change in the dominant interplanetary magnetic field polarity might be expected to most likely occur at this boundary. Finally, the occurrence of more than one solar wind stream in a given magnetic field sector may be simply due to the greater frequency of coronal temperature inhomogeneities and wider magnetic field sectors associated with increased solar activity as compared to the state of the corona closer to solar minimum.

Long Term Variations

It is appropriate now to consider the long term variations of the solar wind characteristics taken over period of many solar rotations up to a time interval covering the entire period of solar wind observations from 1962 to the present. Fig. 13 shows the solar wind velocities and temperatures averaged over each solar rotation as observed by the Vela 2 satellites (Strong et al., 1967) from July 1964 to July 1965. The

last value in the velocity averages was taken from the Vela 3 satellite as indicated. This time interval included solar minimum which occurred in October 1964 during solar rotation number 1795. Perhaps the most interesting feature of the data is the great variability of the solar wind parameters over the one year period. The 27-day averages of the solar wind velocity shows a range from slightly over 500 km/sec for rotation number 1792 to approximately 360 km/sec for rotation number 1799 for an overall variation of roughly 140%. Similarly the temperature shows a range from approximately 2.6×10^5 °K for rotation number 1792 to about 9×10^4 °K for rotation number 1802 for an overall variation of almost a factor of 3. It is enticing to speculate that the decline in temperature and velocity from rotation 1792 to 1799 is associated with the decline in solar activity. It should be pointed out, however, that the actual minimum in the sun spot number occurred during rotation number 1795 (October 1964) and in addition the geomagnetic activity in July 1964 and October 1964 was about the same. As will be seen later, the total range in solar wind parameters observed here is not significantly different from that observed throughout the entire portion of the solar cycle observed to date.

The variations in the azimuthal flow direction of the solar wind observed by Vela 2 (Strong et al., 1967) over the same time interval is shown in Fig. 14. The angles have been averaged over each successive solar rotation with the area of each circle representing the statistical weight for each value. The last value was taken from the Vela 3 satellite as indicated. As was the case for velocity and temperature, great

variability in the azimuthal flow direction is observed throughout the one year period. The values of the average azimuthal flow direction are seen to range from a minimum of approximately -0.5° for rotation number 1793 to a maximum of approximately -3.5° for rotation number 1805. The overall mean value, indicated by the dashed line, was approximately -1.4° indicating a mean azimuthal velocity component of about 10 km/sec. Note that negative angles refer to flow directions from east of the sun.

Using the interplanetary magnetic sector structure results from a variety of satellites and deep space probes, Wilcox and Colburn (1970), have reported the variation in the synodic rotation period of the interplanetary field from 1963 to 1968. The synodic period is plotted in Fig. 15 together with the smoothed sun spot numbers for the present solar cycle and the mean of cycles 1 through 19. The synodic period is seen to vary from near 27.0 days close to solar minimum up to 28.0 days at the beginning of the solar cycle and then gradually decline back to 27.0 days at solar maximum. Wilcox and Colburn (1970) postulate that the increase from 27.0 to 28.0 days represents the dominance of the interplanetary field by the high solar latitude spot groups associated with the beginning of the solar cycle. The decline in synodic rotation period thereafter is the result of the decrease in latitude of the spot groups as the solar cycle progresses. One might expect then that the synodic period would remain near 27.0 days throughout the remainder of the present solar cycle and not increase until the beginning of the next cycle.

Fig. 16 gives a table of selected solar wind parameters reported from the time of Mariner 2 to the present. The left hand columns give

spacecraft and institutional group reporting the results and the right hand column shows the dates over which the observations were made. With respect to the sun spot cycle recalled in Fig. 15, it is seen that the Mariner 2 observations were obtained during the waning portion of the previous cycle, and IMP-2 and Vela 2 observations near solar minimum, Vela 3, Pioneer 6 and Pioneer 7 during the steeply rising portion of the present cycle, Explorer 34 near solar maximum and finally HEOS-1 slightly past solar maximum. Since the time distributions of velocity, density and temperature are non-gaussian and highly skewed (to be discussed in the next section) both the most probable and the average values of these parameters are given in the table. In addition, the average values (where available) of the components of the flow direction are also given. Here φ is the azimuthal component with positive values for flow from west of the sun and θ is the polar component of the flow with positive values for flow from north of the sun. The most surprising feature of the data is the absence of any definite trend in any of the parameters with respect to the solar cycle. One is tempted to visualize an increase in the average velocity from the time of IMP-1 near solar minimum up through Pioneer 7 during the rising portion of the cycle and then a decline up through solar maximum. Unless there is a significant increase in velocity with declining solar activity (which seems unlikely) then the Mariner 2 velocity average is anomalously high. In addition, the Vela 3 velocity average which includes the entire rising portion of the solar cycle is anomalously low compared to the Pioneer 6 and Pioneer 7 averages which were obtained

within the time period of the Vela 3 observations. In addition, the Vela 3 averages are anomalously low with respect to the Vela 2 results which were obtained at solar minimum.

With the possible exception of the angle ϕ which is highly susceptible to systematic error, it is hypothesized that the lack of any discernible trend in the various solar wind parameters is primarily due to a sample aliasing problem. It is intended here to consider sample aliasing in a very long term sense. For example, in recalling Fig. 13, the range in the solar wind velocity averages per solar rotation obtained by Vela 2 for the year period including solar minimum is approximately the same as the range in averages reported by all spacecraft observations for the better part of an entire solar cycle. This surprising result clearly indicates that any effects on the solar wind parameters due to the solar cycle must indeed be subtle compared to the variations which are observed from one solar rotation to the next regardless of the time of observations within the entire solar cycle. The above leads to the inevitable conclusion that the effects of the solar cycle can only be unfolded by continuous monitoring of the interplanetary medium throughout a complete solar cycle.

Average properties

The average properties of the various solar wind parameters are best considered from the point of view of their frequency distributions. Figs. 17 through 22 show histograms of solar wind velocity obtained from 7 separate spacecraft observations. Fig. 17 was obtained from IMP-1 (Olbert, 1968) and covers the time period from December 1963 to February 1964. The velocities shown are 3-hour averages with each bar

representing a 20 km/sec velocity interval. Here the most probable velocity was approximately 330 km/sec and the average velocity was 360 km/sec. The velocity histogram shown in Fig. 18 was obtained from the Vela 2 satellites (Strong et al., 1967) and covers the one-year interval from July 1964 to July 1965. Individual cases have been included here in the velocity intervals shown. The location and widths of the velocity intervals were chosen to coincide with the energy acceptance windows of the Vela 2 plasma analyzers. For these observations the most probable velocity was approximately 325 km/sec and the average velocity was 420 km/sec. Fig. 19 shows the velocity histogram obtained from the Vela 3 measurements (Hundhausen et al., 1970) obtained from July 1965 to November 1967. Here the individual cases are included in 25 km/sec intervals. The Vela 3 results indicate a most probable velocity of approximately 350 km/sec and an average velocity of 400 km/sec. Fig. 20 gives the velocity distribution results from both Pioneer 6 (lighter curve) from December 1965 to March 1966 and Pioneer 7 (darker curve) from August 1966 to October 1966 (Mihalov and Wolfe, 1971). The velocities given are individual cases included in 10 km/sec intervals. For Pioneer 6 the most probable velocity was approximately 340 km/sec and the average velocity was 422 km/sec. For Pioneer 7 the most probable velocity was not determined and the average velocity was 455 km/sec. The velocity histogram for Explorer 34 (Burlaga and Ogilvie, 1970a) is shown in Fig. 21. The results were obtained over the period from June to December 1967. The velocities given are 3-hour averages included in 20 km/sec velocity intervals. Here the most probable velocity was approximately 390 km/sec

and the average velocity was 438 km/sec. The last velocity histogram, shown in Fig. 22, was obtained from HEOS-1 (Egidi et al., 1970) from 2100 hours of observations in the period from December 1968 to April 1969 and from August 1969 to January 1970. Individual cases are shown in 20 km/sec velocity intervals. For the HEOS-1 results, the most probable velocity was 390 km/sec and the average velocity was 409 km/sec.

In comparing the various velocity histograms, the most common feature is the skew in the distributions out to a high velocity tail. This high velocity skewing evidently indicates that in general the solar wind exists in the more quiescent state between streams than at the high velocities associated with the peak of the streams themselves. Another contributing factor is the frequent observation of a much more gradual slope for the negative gradient of velocity associated with the trailing edge of the high velocity stream as compared to the steep slope at the leading edge. Comparing the results of Pioneer 6 and Pioneer 7 in Fig. 20, for example, the skew is much more pronounced for Pioneer 6. Although the statistics are not as good for the Pioneer 7 data, the detailed parameters (recall Fig. 12) reveal a much higher frequency of streams during the observations of Pioneer 7 than that observed during the time of Pioneer 6 (see Fig. 11).

Similar plots of the frequency distributions of the solar wind proton number density from 5 separate spacecraft observations are given in Figs. 23 through 26. The density histogram shown in Fig. 23 was obtained from IMP-1 observations (Olbert, 1968) from December 1963 to February 1964. The results shown are 3-hour average values of the density in one proton/cm³ density intervals. For these

data the most probable density was approximately 4 cm^{-3} and the average density was 7 cm^{-3} . Fig. 24 gives the density histogram from the Vela 3 measurements (Hundhausen et al., 1970). Individual cases were used with a density interval of one proton/ cm^3 . Here the most probable density was approximately 4 cm^{-3} and the average density was 7.7 cm^{-3} . The density histograms shown in Fig. 25 (Mihalov and Wolfe, 1971) were obtained from Pioneer 6 from December 1965 to February 1966 and from Pioneer 7 from August to October 1966. Individual cases were used here with a density interval of 0.4 protons/ cm^3 . The most probable densities for the Pioneer 6 and Pioneer 7 observations were respectively 3.2 and 2.4 cm^{-3} . The corresponding average densities were 5.7 and 4.4 cm^{-3} . The last density histogram, shown in Fig. 26, was obtained from the HEOS-1 observations (Egidi et al., 1970) over two time intervals from December 1968 to April 1969 and from August 1969 to January 1970. Individual cases are used and the density interval was one proton/ cm^3 . From the HEOS-1 results the most probable density was approximately 2 cm^{-3} and the average density was 4.3 cm^{-3} .

As was the case for velocity, all of the density histograms show a high degree of skewing. Note that the distributions of density all show a tail out to 20 cm^{-3} and beyond. The skewing to high values for both the velocity and density might at first be surprising since the velocity and density are expected to be roughly anti-correlated. Careful examination of the data, however, shows that a velocity-density anti-correlation is a gross oversimplification. For example, recalling the Pioneer 6 results shown in Fig. 11, it is noted that of the 30 days

of data presented, only on 4 of those days did the 24-hour average values of the density exceed approximately 8 cm^{-3} . Assuming December 17-18, 1965 was a positive gradient in velocity, these high density averages were all associated with the density pile-up region at the leading edge of the solar wind streams discussed previously. By inspection one sees in Fig. 11 that the majority of the time outside of the pile-up regions the density varies between approximately 3 and 6 cm^{-3} regardless of velocity. Comparing now with the Pioneer 6 density histogram of Fig. 25 one sees that the above is precisely what the histogram indicates.

Of the three convective properties of the solar wind; bulk speed, number density and flow direction, the latter is the least well understood. This is probably due to the relatively small variations in the flow directions that one observes and the susceptibility of the measurements to systematic error. Historically, the solar wind flow direction has been considered in terms of its azimuthal and polar components in a solar-ecliptic coordinate system. The azimuthal angle is usually defined as that component of the flow which lies in the ecliptic and is measured with respect to the spacecraft-sunline. This definition of the azimuthal angle is convenient for most spacecraft since it readily allows the subtraction of the aberration of this angle due to the motion of the spacecraft around the sun. The polar angle is measured with respect to the spacecraft-sunline in the orthogonal plane containing the spacecraft, sun and ecliptic poles. Figs. 27 through 29 show the frequency distribution of the azimuthal component of flow from 5 separate spacecraft

observations. For all histograms shown, negative angles represent flow from east of the sun, positive angles for flow from the west and aberration effects have been removed from all the data. For the case of the Vela 2 data shown in Fig. 27 (Strong et al., 1967) and the Vela 3 data shown in Fig. 29 (Hundhausen et al., 1970), the azimuthal angle is measured in the spin plane of the spacecraft which were tilted with respect to the ecliptic on the order of 30° . The Pioneer data shown in Fig. 28 (Mihalov and Wolfe, 1971) is in the ecliptic which coincides with the spin plane of all Pioneer spacecraft. The mean azimuthal flow angles from the Vela 2, Pioneer 6, Pioneer 7, Vela 3a and Vela 3b measurements are respectively: -1.4° , $+3.0^\circ$, $+0.31^\circ$, -2.52° and -0.93° . The $+3.0^\circ$ value obtained from Pioneer 6 was considered a possible systematic error and for comparative purposes was subtracted in the histogram in Fig. 28. The significant variance in the reported mean values of the azimuthal flow direction leads one to suspect systematic error problems. This is particularly supported by the 1.6° difference in the mean values reported by the Vela 3a and 3b observations which were taken over the same time interval by presumably identical spacecraft. Long term sample aliasing due to non-continuous observations could also be a contributing factor. In any event, subtle effects on the solar wind azimuthal flow direction due to solar angular momentum (expected to be only a fraction of a degree) must await more accurate measurements from continuously monitored spacecraft. One of the most interesting features of the azimuthal flow direction distributions is the tendency toward skewing in the direction of flow from west of the sun.

Although the azimuthal flow histogram is much more symmetric than the velocity or density distributions, the slight skewing appears to be real. The skewing is particularly evident in the Pioneer and Vela 3 data. Although conceivably statistical, it is postulated that the skewness is due to the solar wind stream structure. Recalling the stream structure discussed previously, note that the flow from west of the sun, associated with the leading edge of the stream (positive gradient in velocity) was accompanied by high amplitude shifts in the flow direction from west of the sun whereas the negative gradients in velocity which were associated with azimuthal flow shifts from east of the sun, were of much lower amplitude and much more gradual. This alone seems adequate in accounting for the skewness observed in the azimuthal flow histograms.

Fig. 30 shows the distribution in flow direction from the polar component as observed by Pioneer 6 and Pioneer 7 (Mihalov and Wolfe, 1971). The polar flow histograms are the most symmetric of any of the solar wind parameter distributions. The mean values are within experimental error of zero thus indicating that the polar component of the solar wind flow is symmetric about the ecliptic. Note that the widths of the polar and azimuthal histograms (See Fig. 28) are comparable and lead one to conclude that the stresses on the flow do not have any particular preferred orientations.

The distributions of the solar wind temperature as observed by six different spacecraft are illustrated in Figs. 31 through 35. The temperature histogram given in Fig. 31 was obtained from the Vela 2 results (Coon, 1968) from observations made between July 1964 and

July 1965. The most probable and mean temperatures are as indicated. Note the skew in the temperature distribution out to approximately 6×10^5 °K. Fig. 32 shows the temperature distribution obtained from Vela 3 measurements (Hundhausen et al., 1970) from July 1965 to November 1967. The histogram is plotted out to 2×10^5 °K with 9% of the measured values greater than this temperature. The most probable temperature here is approximately 4×10^4 °K and the average temperature is 9.1×10^4 °K. Measurements obtained from Pioneer 6 from December 1965 to February 1966 and Pioneer 7 from August and September 1966 yielded the temperature histograms shown in Fig. 33 (Mihalov and Wolfe, 1971). The mean temperatures for the two spacecraft are as indicated. The most probable temperatures for Pioneer 6 and Pioneer 7 were respectively 0.4×10^5 °K and 0.3×10^5 °K. Note the tendency for greater skewing toward higher temperatures for the Pioneer 7 results as compared to Pioneer 6. This evidently reflects the more highly disturbed character of the interplanetary medium and more complex solar wind stream structure at the time of the Pioneer 7 measurements. Fig. 34 shows the temperature distribution obtained from Explorer 34 measurements (Burlaga and Ogilvie, 1970) taken from June to December 1967. The most probable temperature was approximately 4.6×10^4 °K. The average temperature was not reported but is estimated here to be near 10^5 °K. The temperature distribution obtained from HEOS-1 measurements (Egidi et al., 1970) is shown in Fig. 35. These results were obtained from 2100 hours of observations during two time intervals from December 1968 to April 1969 and from August 1969 to January 1970. The average temperature is about

$6.6 \times 10^4 \text{ }^\circ\text{K}$ where the temperature, T , is related to the thermal speed, W , by $W = (2kT/m)^{1/2}$. The most probable temperature is estimated here to be about $5.5 \times 10^4 \text{ }^\circ\text{K}$.

The most common feature of all of the temperature histograms is the large skewing in the distribution forming a long, high temperature tail. The temperature distributions are generally the most skewed of any solar wind parameter. It is interesting to note that although the average temperature varies by almost a factor of 3 among the various observations, the most probable temperatures are all comparable, near $4-6 \times 10^4 \text{ }^\circ\text{K}$. The above might be explained by differing degrees of complexity in the solar wind stream structure which were present during the various observations. A complex stream structure tends to elevate the high temperature tail leading to a higher average temperature. On the other hand, the solar wind resides a greater percentage of the time in the "between stream" state where the temperatures are lower and comparable regardless of the period of observation.

With the exception of the Vela 3 results, all of the temperature histograms shown are plotted in terms of an isotropic temperature. The Vela 3 histogram is plotted using an effective temperature and will be discussed later. An isotropic temperature assumes that the random motions of the protons obey an isotropic Maxwellian distribution law. Although valid to a first approximation, this is not strictly true. This is illustrated in Fig. 36 (Hundhausen et al., 1967) which shows contours of constant flux in a plane in velocity space from Vela 3b in August 1965. The contours are plotted in 10% increments decreasing

outward from the maximum central contour. The abscissa is the velocity radially outward from the sun and the ordinate is the perpendicular velocity in the spin plane of the Vela 3b satellite. At the time of these measurements, the spin plane was tilted approximately 35° with respect to the ecliptic. The arrow represents the orientation of the interplanetary magnetic field projected onto the coordinate plane. The magnetic field orientation was determined by the Goddard Space Flight Center magnetometer on IMP-3 for the period of the Vela 3b measurements. The triangle near the center of the distribution represents the bulk velocity which was, for this case, 347 km/sec in the radial direction and 20 km/sec in the orthogonal direction. The distribution around the bulk velocity is due to the random motions of the protons and deviations from a circular pattern centered above the bulk velocity are a result of anisotropy. The particular distribution shown in Fig. 36 is highly anisotropic with an elongated tail symmetric about the magnetic field projection and outward away from the sun.

Assuming the random motion in the distribution shown in Fig. 36 to be thermal, Hundhausen et al., (1967), derived the polar plot of temperature given in Fig. 37. The coordinates and magnetic field are as before. For this case, the maximum temperature seem to be near 120° and is approximately 9.2×10^4 K. The minimum temperatures lie near the 30° and 210° radials. Defining the anisotropy as the ratio of the maximum to minimum temperatures gives, for this case, a value of about 3.4. Comparison of Vela 3 and IMP-3 data at other times seems to confirm that the anisotropy is, in general, aligned with the magnetic field but that the elongated tail is always outward from the sun

regardless of the polarity of the field. This elongated tail in the temperature distribution outward from the sun was interpreted as an energy transport or heat conduction away from the sun and estimated to be on the order of 10^{-5} ergs cm^{-2} sec^{-1} . This proton heat conduction is small, however, compared to the electron heat conduction (Montgomery et al., 1968) which is about 3 orders of magnitude larger.

The anisotropy value of 3.4 for the case discussed above is unusually high as can be seen in the anisotropy histogram shown in Fig. 38 (Hundhausen et al., 1970). This histogram was obtained from the Vela 3 measurements over the time period from July 1965 to November 1967. The most probable value of the anisotropy is between 1.2 and 1.3 and the average value is about 1.9. Note that only 9.6% of the determined anisotropy values are greater than 3.0. The anisotropy arises from simple conservation of the magnetic moment of the proton as the collisionless solar wind flows outward from the sun. Theoretical calculations, however, typically predict anisotropy values generally 1 to 2 orders of magnitude greater than those observed. This clearly indicates that instabilities and wave-particle interactions must play an important role in inhibiting the growth of the anisotropy to such high values.

Solar wind parameter relationships

Up to the present, only the temporal behavior and variance or frequency distribution of the individual solar wind parameters have been dealt with. Consider now a more detailed investigation of the relationships between various solar wind parameters. Fig. 39 shows

the solar wind proton density as a function of flow speed from measurements made by the Vela 3 satellites (Hundhausen et al., 1970) during the period from July 1965 to November 1967. The density is plotted as the average within a 25 km/sec flow speed interval. For these observations the density is observed to decrease with increasing velocity almost as V^{-1} (constant flux) up to about 500 km/sec beyond which the density tends to level off. The relationship between density and velocity observed by the Ames Research Center plasma probe on Pioneer 6 from December 1965 to March 1966 is shown in Fig. 40. Here the results are presented somewhat differently than in the previous figure with each point representing a 24-hour average value of the proton density and velocity. These results suggest a much more exponential fall off of density with increasing velocity, particularly at the lower velocities. Note the large scatter in the density for low velocities. This can be accounted for by recalling that densities in the range of about 4 to 7 cm^{-3} are typical of the solar wind in the "between stream" state where the velocity is low. On the other hand, densities greater than 7 cm^{-3} are more typical of the "pile up" regions ahead of new streams where the velocity is also relatively low. The exponential character of the density-velocity relationship clearly indicates why the density and velocity frequency distributions both tend to peak at low values with skewing toward the higher values of both parameters. The density-velocity relationship obtained by Explorer 34 (Burlaga and Ogilvie, 1970b) and some average values obtained from several other spacecraft observations are given in Fig. 41. The Explorer 34 observations cover the period from June to

December 1967 and the horizontal lines represent the average density within 50 km/sec velocity intervals. The individual points represent the average values of density and velocity for the various spacecraft observations indicated. The open points are further observations which have been added to the original figure of Burlaga and Ogilvie (1970b). The lower density IMP-1 average is a corrected value (Olbert, 1968) and the higher density IMP-1 point should be ignored. The best fit curve to the Explorer 34 results indicate a density dependence on velocity of $V^{-1.5}$. Although the various observations show some scatter, it is clear that density decreases exponentially with velocity and that on the average the solar wind flux is not a constant. The above must be accounted for by any theory which attempts to determine the solar wind source function.

Consider next the relationship between the solar wind flow direction and velocity. Fig. 42 (Hundhausen et al., 1970) gives the average flow direction in the Vela 3a and 3b spin planes as a function of the flow speed in 25 km/sec intervals. The results were obtained from measurements made during the interval from July 1965 to November 1967. Since the Vela 3 spin planes are tilted approximately 35° with respect to the ecliptic, then in a solar-ecliptic coordinate system, the flow directions given here contain contributions from both the azimuthal and polar components. Wolfe (1970), however, has shown from Pioneer 6 results that there is no discernible correlation between the polar component and the flow speed, therefore the results shown here presumably reflect only contributions from the azimuthal component. Due to the likelihood of systematic error and for comparative purposes, the

obvious trend toward more positive flow with increasing velocity should be considered the important feature of the flow direction-velocity relationship rather than the absolute values. Note in the Vela 3a data the tendency for the return of the flow toward the negative direction at the highest velocities. Although conceivably statistical, this trend is also seen in the Pioneer 6 results (Wolfe, 1970) shown in Fig. 43. Plotted here are 3-hour average values of the azimuthal flow direction and corresponding velocity from measurements made over one complete solar rotation beginning December 18, 1965. The average azimuthal flow direction for this entire time interval was $+2.6^\circ$ (flow from west of the sun). This average is considered to be possibly a systematic error and has been arbitrarily subtracted from all the data in order to investigate trends in the azimuthal flow direction with respect to a zero mean. The trend toward more positive flow with increasing velocity is also readily seen in the Pioneer 6 results, however, the return to more nearly radial flow at the higher velocities is quite pronounced. Note also the large scatter in azimuthal angles most prominent between about 400 and 450 km/sec. Recalling the more detailed data discussed in connection with the solar wind stream structure, the largest amplitude variations in the azimuthal flow direction (particularly positive) were associated with the leading edge (sharp positive velocity gradient) of a new stream where the velocity was typically on the order of 400-450 km/sec. Recall also that near the peak of the stream (highest velocity) the flow tended to be more radial. Thus the correspondence between the azimuthal flow

direction and velocity seen here seems clearly to be highly dependent on the solar wind stream structure.

Fig. 44 (Wolfe, 1970) shows the relationship between the polar and azimuthal flow directions obtained from Pioneer 6 over the same time interval as the previous figure. As before, the azimuthal angles have been corrected by 2.6° for comparative purposes. By inspection it is seen that the polar and azimuthal flow components are completely independent. It is interesting to note, however, that the amplitude in the flow angle variations are comparable for the two components.

The relationship between temperature and velocity is very strong as can be seen in the Vela 3 results shown in Fig. 45 (Hundhausen et al., 1970). These results were compiled from observations made from July 1965 to November 1967. The temperatures are averages in 25 km/sec flow speed intervals. A similar strong temperature-velocity relationship is also seen in Fig. 46 obtained by Ames Research Center plasma observations from Pioneer 6 from December 1965 to March 1966. The values given are 24-hour averages with the temperature plotted on a logarithmic scale. For reference purposes the square root of T relationship with velocity determined by Burlaga and Ogilvie (1970a) derived from Explorer 34 observations is also plotted on the Pioneer 6 data. Although the Pioneer 6 results seem to fit this relationship fairly well there is a great deal of scatter and a linear relationship seems to fit about as well. This is also true for the Vela 3 results of the previous figure. Note, however, the particularly large amount of scatter (in the direction of higher temperature with respect to the curve) between about 350 and 500 km/sec. This is conceivably

due to the heating one observes associated with the positive gradient in velocity on the leading edge of a solar wind stream where the velocities are typically in this range. Fig. 47 shows the relationship between the anisotropy, defined by T_{\max}/T_{\min} (Hundhausen et al., 1970), and the flow speed. These results were obtained from Vela 3 measurements over the period from July 1965 to November 1967 with the anisotropy averaged in 50 km/sec flow speed intervals. The average anisotropy is seen to peak near 375 km/sec at a value of approximately 2.0 and to drop off slightly for lower velocities and much more steeply for higher velocities. Hundhausen et al. (1970) postulated the fall off of anisotropy for the low velocities as consistent with coulomb collision effects and the decrease in anisotropy with increasing velocity above 375 km/sec to be the result of the dominance of instabilities associated with a more disturbed medium.

Interplanetary-terrestrial relationships

The historical interplanetary-terrestrial relationship which has been sought has been that between the character of the solar wind and the state of the geomagnetic field. The first attempt at this was by Snyder et al. (1963) using Mariner 2 observations. Of all the solar wind parameters or combinations thereof, the best correlated parameter with the geomagnetic disturbance index, K_p , was the solar wind flow speed. These results are shown in Fig. 48 where the 24-hour average velocity is plotted against the daily sum of K_p for that particular day. The results were obtained during the period from late August through late December 1962. The line through the data represents the least squares linear fit to the points. Although the trend of increasing

K_p with increasing velocity is certainly evident, the large amount of scatter in the data leaves one somewhat unsatisfied with respect to a definite, strong velocity- K_p relationship. Similar results were reported by Olbert (1968) from the M.I.T. IMP-1 observations obtained from November 1963 to February 1964 shown in Fig. 49. Although the relationship (assumed linear) between velocity and K_p is somewhat different than the Mariner 2 results, there is still a large amount of scatter in the data. The correlation coefficient for these results was approximately 0.8. Fig. 50 indicates the relationship between the 24-hour average solar wind velocities obtained by Pioneer 6 (Wolfe, 1970) and the daily geomagnetic disturbance index, A_p . Although the correlation coefficient here is approximately 0.7, as was the case with the Mariner 2 and the IMP-1 results, there is a large scatter in the data. Perhaps the best explanation of the scatter is the frequently observed phase lag between the solar wind velocity and geomagnetic disturbance indices discussed earlier. During the rising portion or leading edge of a solar wind stream (positive gradient in velocity) the geomagnetic field tends to be much more disturbed than during the trailing portion (more gradual negative gradient) of the stream. Thus for a given value of solar wind velocity the K_p or A_p indices would be double valued leading to the scatter observed in the previous three figures. As discussed earlier, the density tends to lead, the velocity lag and the temperature is approximately in phase with the daily geomagnetic disturbance index, A_p (or ΣK_p). Fig. 51 gives the 24-hour average values of the Ames Research Center Pioneer 6 solar wind proton temperature observations as a function of the A_p index. These measurements were obtained over

the same period as the previous figure. Even though the correlation coefficient here is approximately 0.9, there is still a fair degree of scatter in the data. It is inconceivable that the amplitude of the random motion in the protons should really have any strong effect on the geomagnetic field. What seems more plausible is that the solar wind proton temperature represents a large scale indication of the degree of disturbance in the interplanetary medium and it is changes in the momentum flux or simply flux fluctuations which are conceivably responsible for geomagnetic disturbance. The above, however, can only be confirmed by higher time resolution plasma measurements than are presently available. The result that solar wind proton temperature seems to give the best correlation with geomagnetic disturbance indices is considered here to be an effect, not a cause.

Effects of solar latitude and radial distance.

Unfortunately, space observations to date have been restricted to near the plane of the ecliptic between the orbits of Venus and Mars. In a spherical coronal expansion model, the solar wind density is expected to decrease as the square of the distance. This has been tentatively verified by the Mariner 2 results (Neugebauer and Snyder, 1966) shown in Fig. 52. Twenty-seven day averages of the daily averages of proton density, flux and total momentum flux are plotted versus distance from the sun. The slopes for an inverse square relationship are also shown. Considering the variations which are observed from one solar rotation to the next, the density here seems to fit the expected inverse square relation remarkably well. The Mariner 2 results showed no radial dependence for either the velocity or temperature. This is not unexpected since the radial dependence for these

parameters are conceivably much more subtle. As the solar wind flows outward from the sun, it is expected to quickly approach a terminal velocity which would be essentially constant beyond the Earth's orbit. The radial variation of the proton temperature is less certain and would be dependent on the proton heating mechanisms. For example, adiabatic, constant speed expansion with isotropic pressure requires that the proton temperature decrease as $R^{-4/3}$, whereas conduction dominated flow gives an $R^{-2/7}$ dependence and flow dominated by proton-electron energy exchange has an $R^{-6/7}$ dependence. It seems likely that these dependencies would be difficult to separate from the temporal variations for observations which only extend over a radial distance of approximately 0.3 AU.

Gosling (1971) compared Pioneer 6 and Pioneer 7 velocity observations during the period from January 1969 to July 1970. Specifically, the velocity observed by one spacecraft was compared to the velocity observed by the other spacecraft after a period corresponding to the co-rotation delay due to their heliocentric azimuthal separation. Fig. 53 shows the results when the two spacecraft are separated in co-rotation by less than two days. With a few exceptions, most of the points tend to lie close to the equal velocity line, although there is some scatter. When the two spacecraft have a separation of 2 to 4 days, shown in Fig. 54, the fit is not as good. A separation of greater than 4 days, shown in Fig. 55, indicates a very poor correlation. This implies that there are significant coronal changes taking place on a time scale of a few days (at least at the time of these measurements) and predicts the difficulty of determining the solar wind radial

gradients from a single spacecraft. One cannot discount, however, that this is a heliographic latitude effect due to the tilt of approximately 7° of the sun's equatorial plane with respect to the ecliptic.

In considering what might be expected in the way of heliographic latitude effects on the solar wind, a coronagraph photo of the March 7, 1970 solar eclipse is shown in Fig. 56 (Smith, 1970). This is a composite of three separate pictures with the north pole of the sun at the top. Note in particular that the coronal streamers are just as prevalent near the solar pole as they are near the equator. If these streamers play an important role in solar wind dynamics, then one might not expect any significant solar wind latitude effects. One might expect, however, drastic effects on the character of the stream interactions since with increasing heliographic latitude the interplanetary magnetic field becomes less and less spiralled. The observation of these effects will probably require space measurements up to at least 30° to 40° heliographic latitude.

References

1. Burlaga, L. F. and K. W. Ogilvie, Heating of the Solar Wind, Ap. J., 159, 659-670, 1970a.
2. Burlaga, L. F. and K. W. Ogilvie, Magnetic and Kinetic Pressures in the Solar Wind, Solar Phys., 15, 61-71, 1970b.
3. Coon, J. H., Solar Wind Observations, in Earth's Particles and Fields, edited by B. M. McCormac, 359-372, Reinhold, New York, 1968.
4. Egidi, A., V. Formisano, G. Moreno, F. Palmiotto and P. Saraceno, Solar Wind and Location of Shock Front and Magnetopause at the 1969 Solar Maximum, J. Geophys. Res., 75, 6999-7006, 1970.
5. Gosling, J. T., Variations in the Solar Wind Speed along the Earth's Orbit, Solar Phys., 1971 (in press).
6. Hundhausen, A. J., S. J. Bame and N. F. Ness, Solar Wind Thermal Anisotropies: Vela 3 and IMP-3, J. Geophys. Res., 72, 5265-5274, 1967.
7. Hundhausen, A. J., S. J. Bame, J. R. Asbridge and S. J. Sydorik, Solar Wind Proton Properties: Vela 3 Observations from July 1965 to June 1967, J. Geophys. Res., 75, 4643-4657, 1970.
8. Lyon, E., A. Egidi, G. Pizzella, H. Bridge, J. Binsack, R. Baker and R. Butler, Plasma Measurements on Explorer 33, (1) Interplanetary Region, in Space Research VIII, edited by A. P. Mitra, L. G. Jacchia and W. S. Newman, 99-106, North-Holland Publishing Co., Amsterdam, 1968.

9. Mihalov, J. D. and J. H. Wolfe, Average Solar Wind Properties from Pioneers 6 and 7, Cosmic Electrodynamics, 1971 (in press).
10. Montgomery, M. D., S. J. Bame and A. J. Hundhausen, Solar Wind Electrons: Vela 4 Measurements, J. Geophys. Res., 73, 4999, 1968.
11. Neugebauer, M. and C. W. Snyder, Mariner 2 Observations of the Solar Wind, 1. Average Properties, J. Geophys. Res., 71, 4469-4484, 1966.
12. Olbert, S., Summary of Experimental Results from M.I.T. Detector on IMP-1, in Physics of the Magnetosphere, edited by R. L. Carovillano, 641-659, D. Reidel, Dordrecht-Holland, 1968.
13. Parker, E. N., Dynamics of the Interplanetary Gas and Magnetic Fields, Astrophys. J., 128, 664, 1958.
14. Smith, S., Solar Eclipse 1970 Bulletin F, National Science Foundation, 157, 1970.
15. Snyder, C. W., M. Neugebauer and U. R. Rao, The Solar Wind Velocity and its Correlation with Cosmic-Ray Variations and with Solar and Geomagnetic Activity, J. Geophys. Res., 68, 6361-6370, 1963.
16. Strong, I. B., J. R. Asbridge, S. J. Bame and A. J. Hundhausen, Satellite Observations of the General Characteristics and Filamentary Structure of the Solar Wind, in The Zodiacal Light and the Interplanetary Medium, edited by J. L. Weinberg, 365-372, National Aeronautics and Space Administration, Washington, D. C., 1967.

17. Wilcox, J. M. and N. F. Ness, A Quasi-stationary Co-rotating Structure in the Interplanetary Medium, J. Geophys. Res., 70, 5793-5805, 1965.
18. Wilcox, J. M. and D. S. Colburn, Interplanetary Sector Structure in the Rising Portion of the Sunspot Cycle, J. Geophys. Res., 74, 2388-2392, 1969.
19. Wilcox, J. M. and D. S. Colburn, Interplanetary Sector Structure Near the Maximum of the Sunspot Cycle, J. Geophys. Res., 75, 6366-6370, 1970.
20. Wolfe, J. H., Solar Wind Characteristics Associated with Interplanetary Magnetic Field Sector Structure, Trans. Am. Geophys. Union, 51, 412, 1970.

FIGURE CAPTIONS

- Figure 1: Three hour average values of velocity and temperature versus time observed by Mariner 2 in late 1962. The time base is chosen to show the 27-day recurrence features associated with solar rotation.
- Figure 2: Mariner 2 3-hour average values of plasma velocity and proton number density versus time.
- Figure 3: Pioneer 6 3-hour average values of velocity, density, temperature, azimuthal flow direction, polar flow direction and K_p versus time.
- Figure 4: Pioneer 6 3-hour average values of velocity, azimuthal flow direction and polar flow direction versus time.
- Figure 5: Explorer 33 3-hour averages of azimuthal flow direction, latitude flow direction, thermal speed, proton density and bulk velocity versus time.
- Figure 6: IMP-1 interplanetary magnetic field sector structure for approximately 3 solar rotations starting late November 1963. The pluses represent fields which are predominantly away from the sun and minuses predominantly toward the sun.
- Figure 7: Comparison of the IMP-1 solar wind velocity and magnetic field orientation with the A_p index.
- Figure 8: Superposed epic analysis of the magnitude of the solar wind velocity as a function of position within the 2/7ths sectors shown in Fig. 6.

Figure 9: Superposed epic analysis of the solar wind density of as a function of position within the 2/7ths sectors.

Figure 10: Observed sector structure of the interplanetary magnetic field overlaying the daily geomagnetic character index C9. Light shading indicates sectors with field predominantly away from the sun and dark shading indicates sectors with field predominantly toward the sun.

Figure 11: Pioneer 6 24-hour average values of the solar wind velocity, proton density and temperature plotted versus time. The interplanetary magnetic field sector structure is shown at the top.

Figure 12: Pioneer 7 24-hour average values of the solar wind velocity, proton density and temperature versus time. The interplanetary magnetic field sector structure is shown at the top.

Figure 13: Solar wind flow speed and proton temperature averaged over solar rotations as measured on the Vela 2 satellites from July 1964 to July 1965.

Figure 14: Solar wind flow directions averaged over solar rotations as measured by the Vela 2 satellites from July 1964 to July 1965.

Figure 15: Synodic rotation period of the interplanetary magnetic field superimposed on the observed smoothed sunspot number from October 1962 to October 1972.

- Figure 16: Average and most probable values of the various solar wind parameters from all reported spacecraft measurements.
- Figure 17: IMP-1 solar wind bulk velocity histogram.
- Figure 18: Vela 2 solar wind bulk velocity histogram.
- Figure 19: Vela 3 solar wind bulk velocity histogram.
- Figure 20: Pioneer 6 and Pioneer 7 solar wind bulk velocity histogram.
- Figure 21: Explorer 34 solar wind bulk velocity histogram.
- Figure 22: HEOS-1 solar wind bulk velocity histogram.
- Figure 23: IMP-1 proton density histogram.
- Figure 24: Vela 3 proton density histogram.
- Figure 25: Pioneer 6 and Pioneer 7 proton density histogram.
- Figure 26: HEOS-1 proton density histogram.
- Figure 27: Vela 2 solar wind flow direction histogram.
- Figure 28: Pioneer 6 and Pioneer 6 azimuthal flow angle histograms.
- Figure 29: Vela 3a and Vela 3b flow direction histograms.
- Figure 30: Pioneer 6 and Pioneer 7 polar flow angle histograms.
- Figure 31: Vela 2 solar wind proton temperature histogram.
- Figure 32: Vela 3 proton temperature histogram.
- Figure 33: Pioneer 6 and Pioneer 7 proton temperature histograms.
- Figure 34: Explorer 34 proton temperature histogram.
- Figure 35: HEOS-1 proton thermal speed histogram.
- Figure 36: A contour mapping in the Vela 3 spin plane of an example proton velocity distribution function. The small triangle indicates the mean velocity. The B_p indicates the magnetic field orientation of the time of the measurements.

- Figure 37: A polar graph of the temperature for the proton distribution function of Fig. 26.
- Figure 38: Vela 3 thermal anisotropy histogram.
- Figure 39: Vela 3 proton density versus solar wind flow speed.¹
- Figure 40: Pioneer 6 proton number density versus velocity.
- Figure 41: Explorer 34 proton number density versus velocity. Average values from other spacecraft are shown in the circles.
- Figure 42: Vela 3a and Vela 3b flow directions versus flow speed.
- Figure 43: Pioneer 6 3-hour average values of the azimuthal flow angle as a function of velocity.
- Figure 44: Pioneer 6 polar flow angle as a function of azimuthal flow angle.
- Figure 45: Vela 3 proton temperature versus flow speed.
- Figure 46: Pioneer 6 proton temperature versus velocity.
- Figure 47: Vela 3 anisotropy versus flow speed.
- Figure 48: Mariner 2 scatter diagram of daily mean plasma velocity versus ΣK_p . The line is the least squares linear fit to the points.
- Figure 49: IMP-1 daily averages of the solar wind velocity plotted versus the daily sum of the K_p index.
- Figure 50: Pioneer 6 24-hour average values of solar wind velocity versus the A_p index.
- Figure 51: Pioneer 6 24-hour average values of proton temperature versus the A_p index.

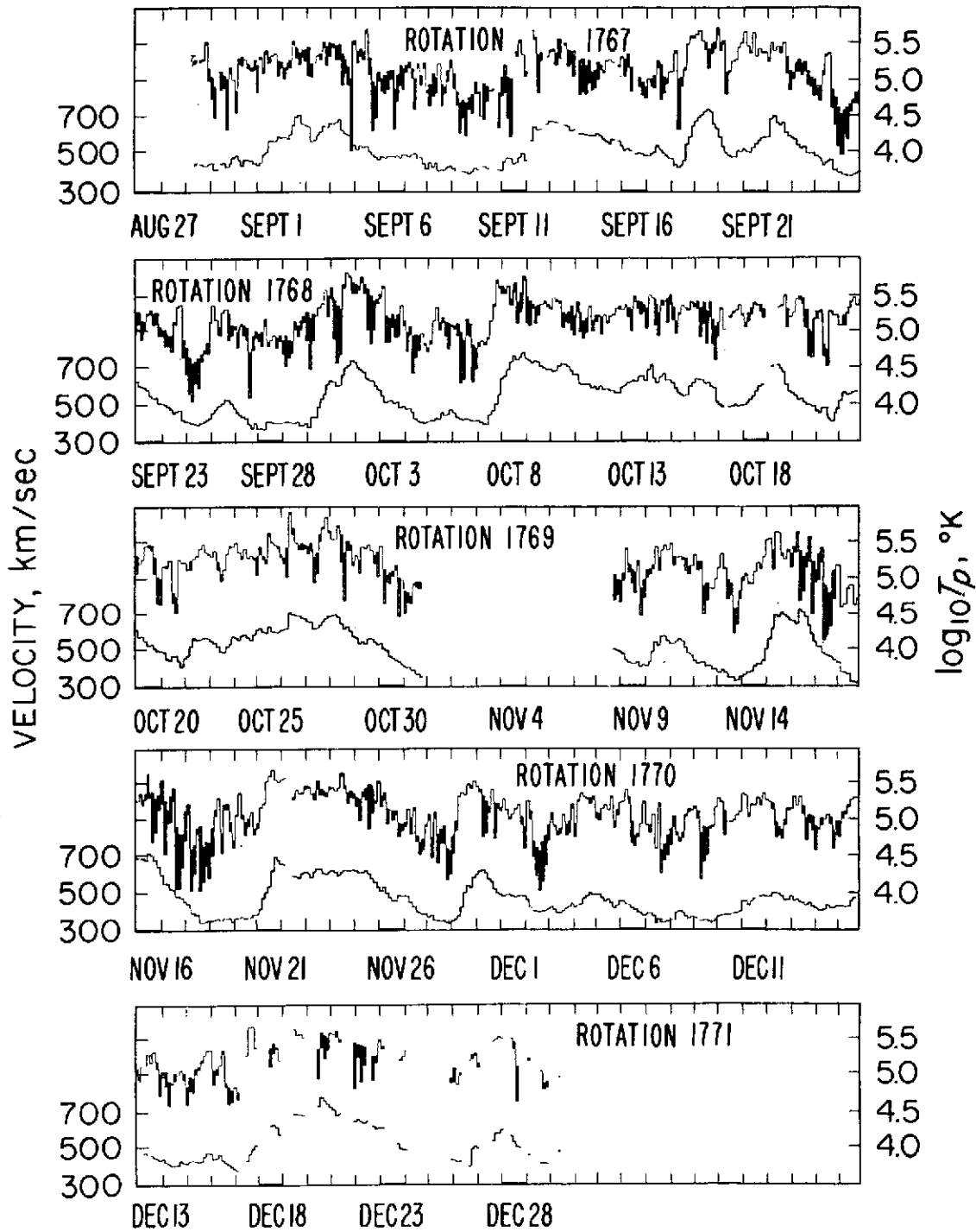
Figure 52: Mariner 2 27-day averages of the daily averages of proton number density, proton flux and total momentum flux versus distance from the sun. The slope for an inverse square relation are also given.

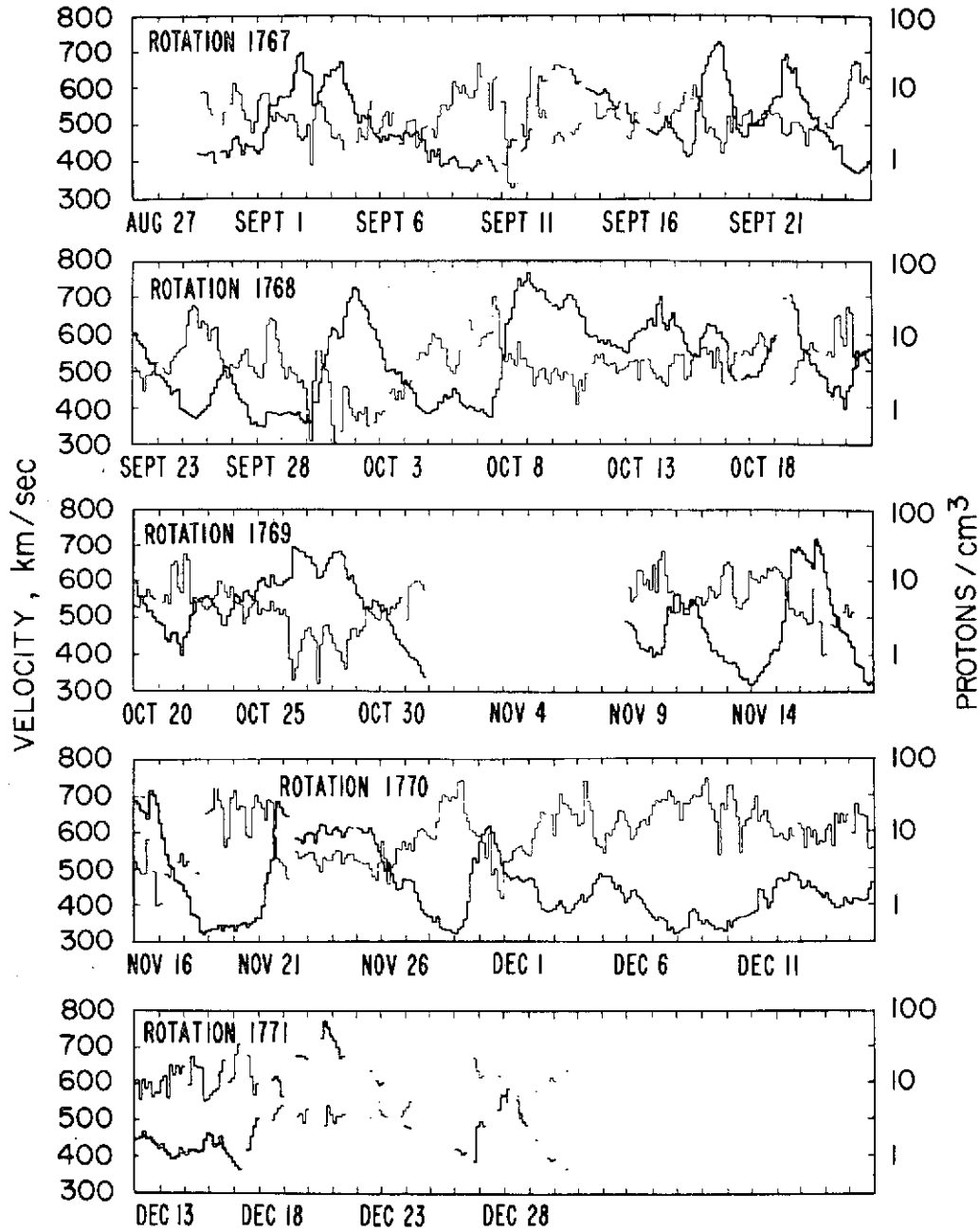
Figure 53: Comparison of Pioneer 7 and Pioneer 6 solar wind flow speeds when the two spacecraft are separated by less than 2 days co-rotation delay.

Figure 54: Comparison of Pioneer 7 and Pioneer 6 solar wind flow speeds when the two spacecraft are separated by 2 to 4 days co-rotation delay.

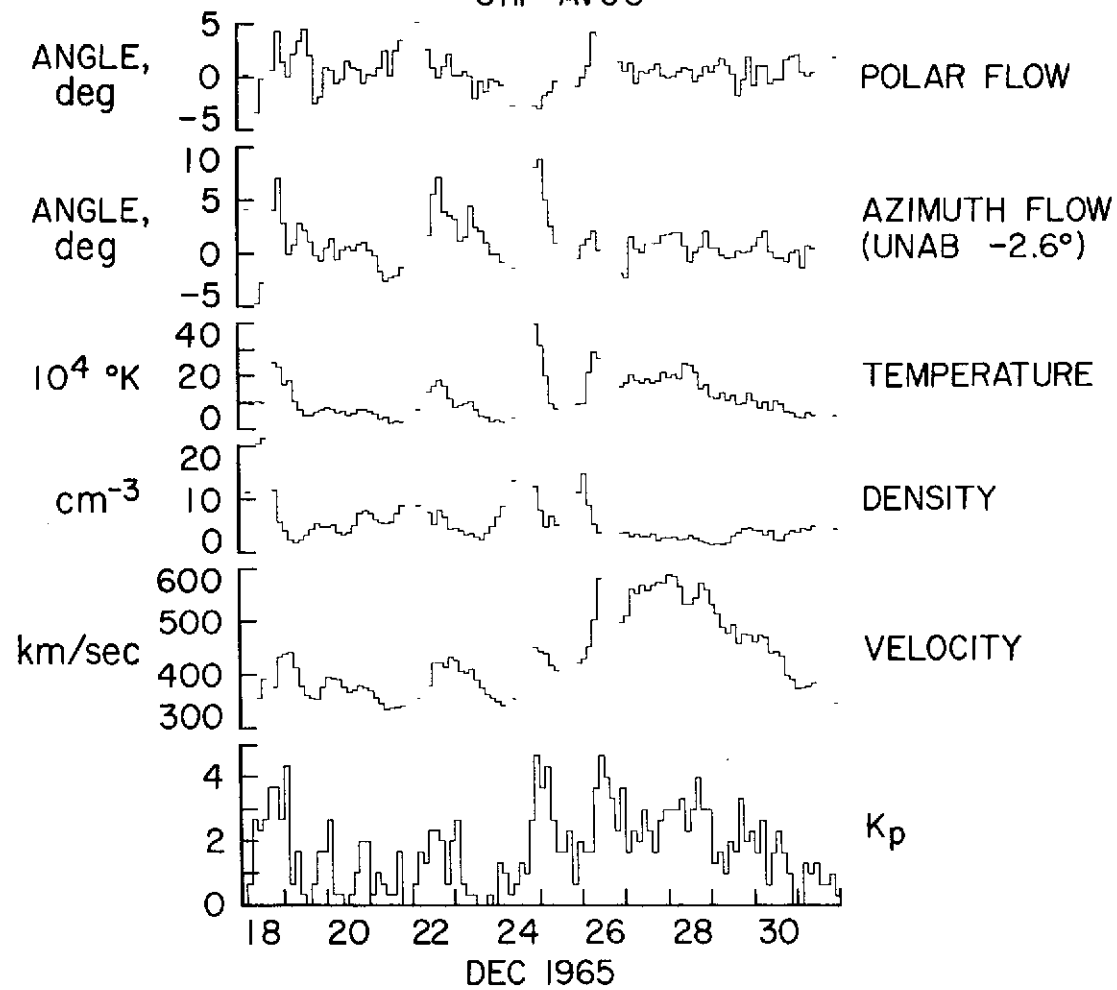
Figure 55: Comparison of Pioneer 7 and Pioneer 6 solar wind flow speed when the two spacecraft are separated by greater than 4 days co-rotation delay.

Figure 56: Composite of 3 coronagraph photos of the March 7, 1970 solar eclipse.

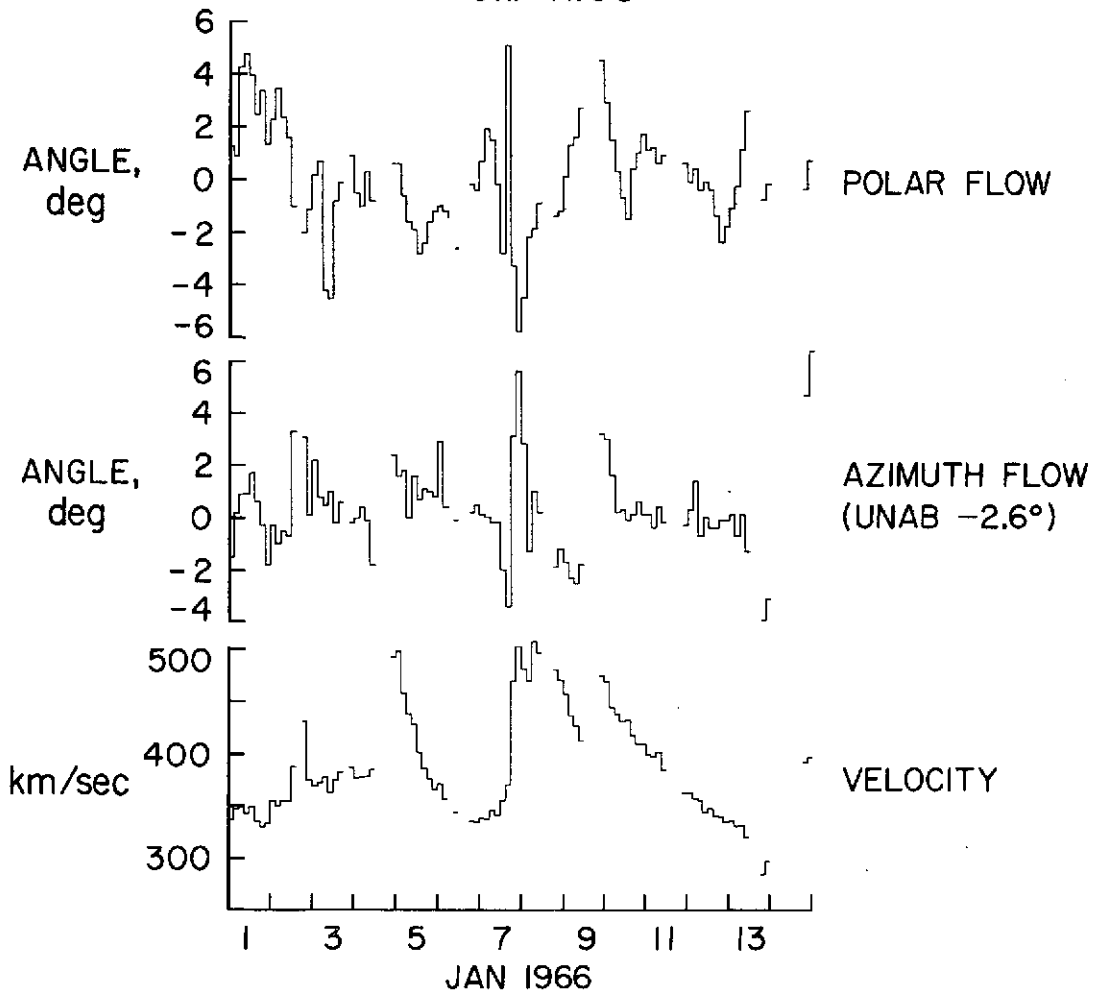




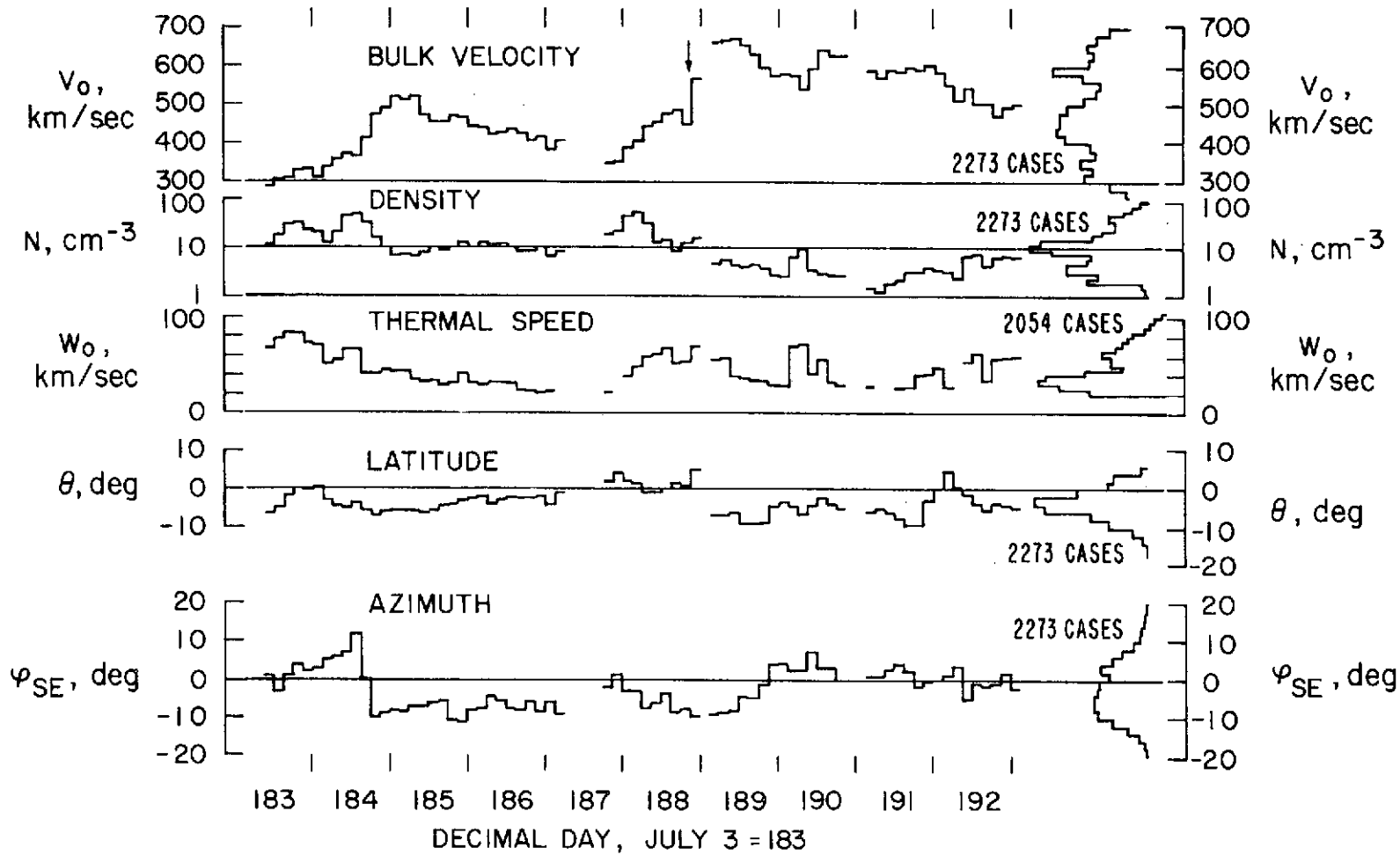
PIONEER 6
3hr AVG'S

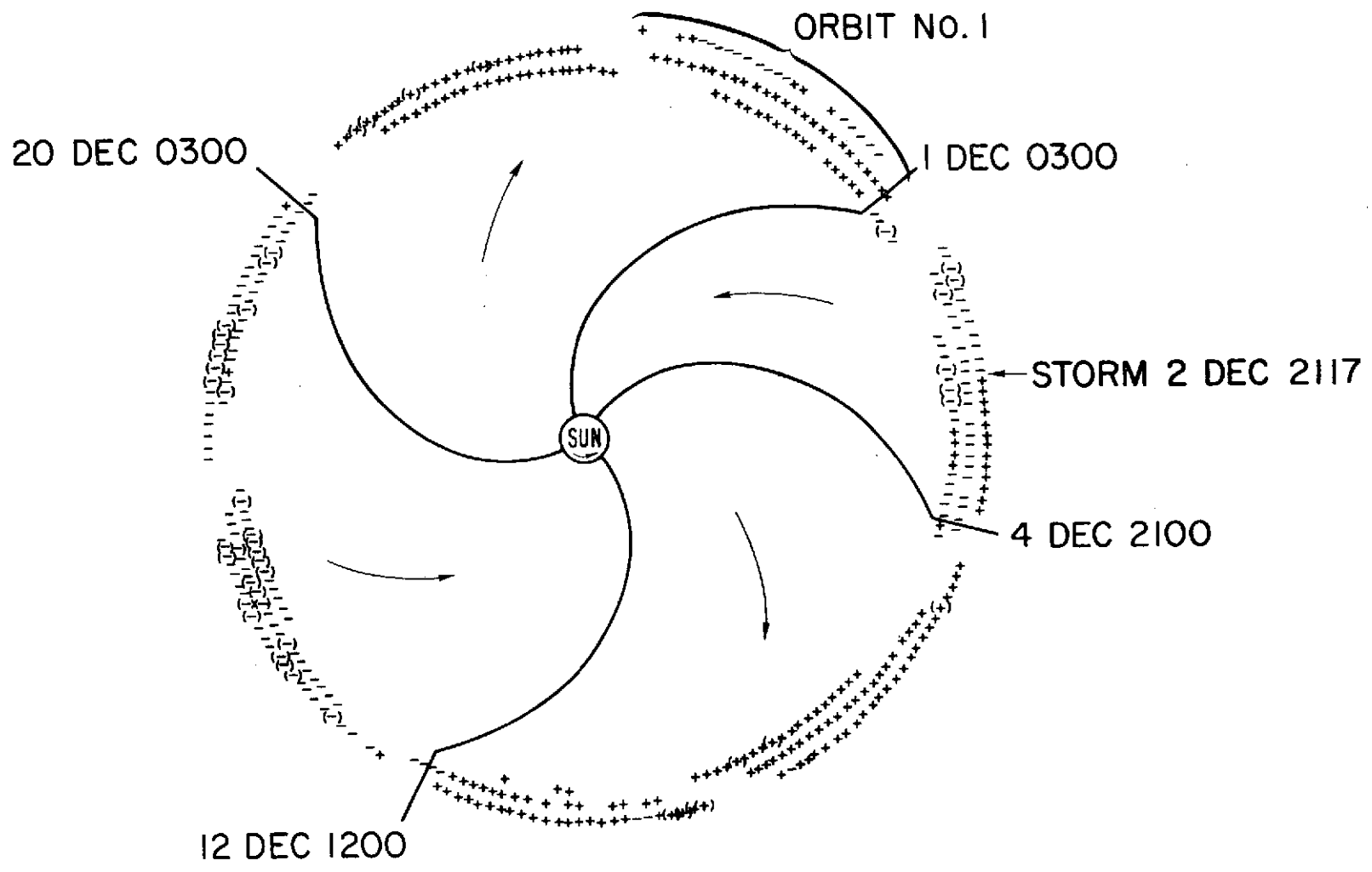


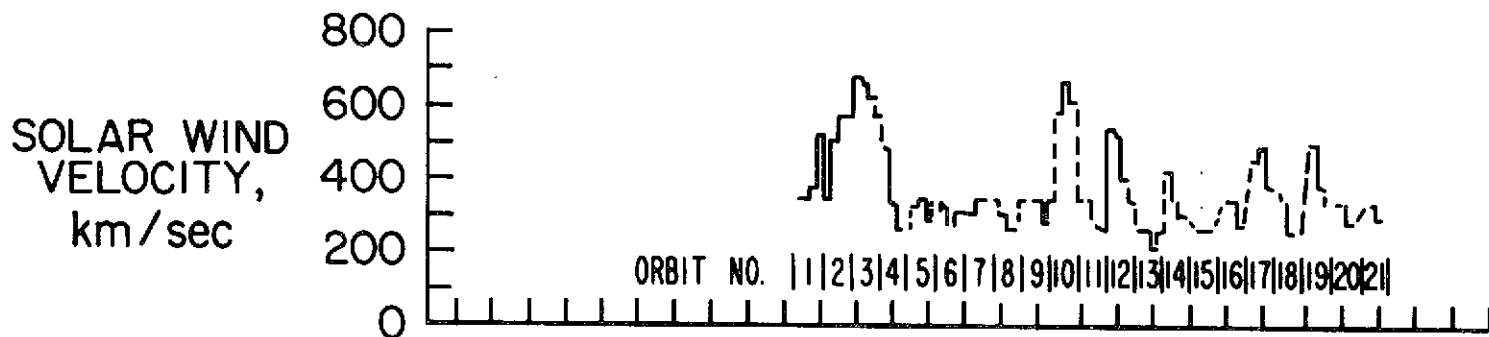
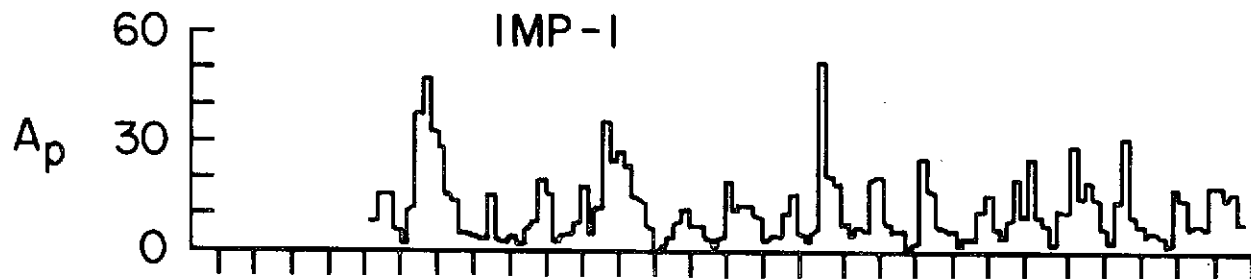
PIONEER 6
3hr AVG's



217







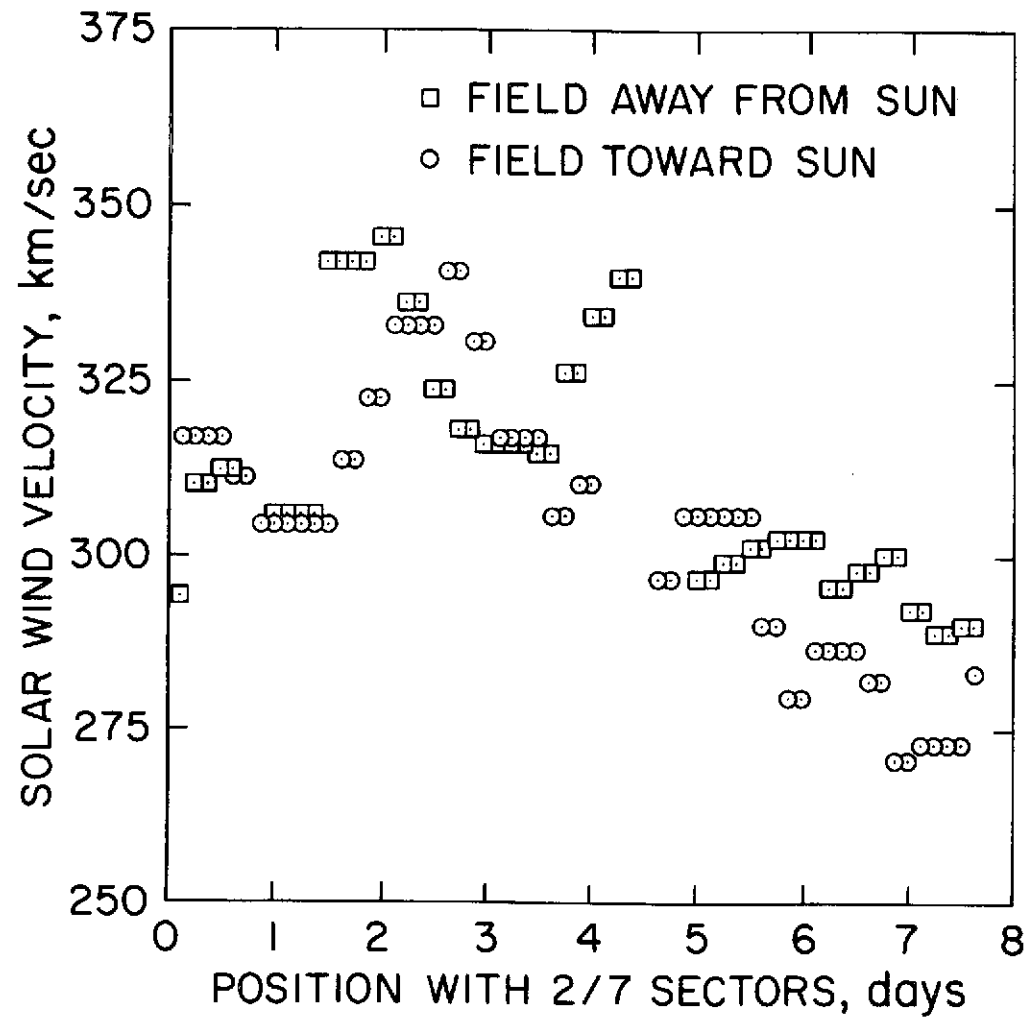
BEAM IDENTIFICATION → D | A | B | C | D | A | B | C | D | A | B | C

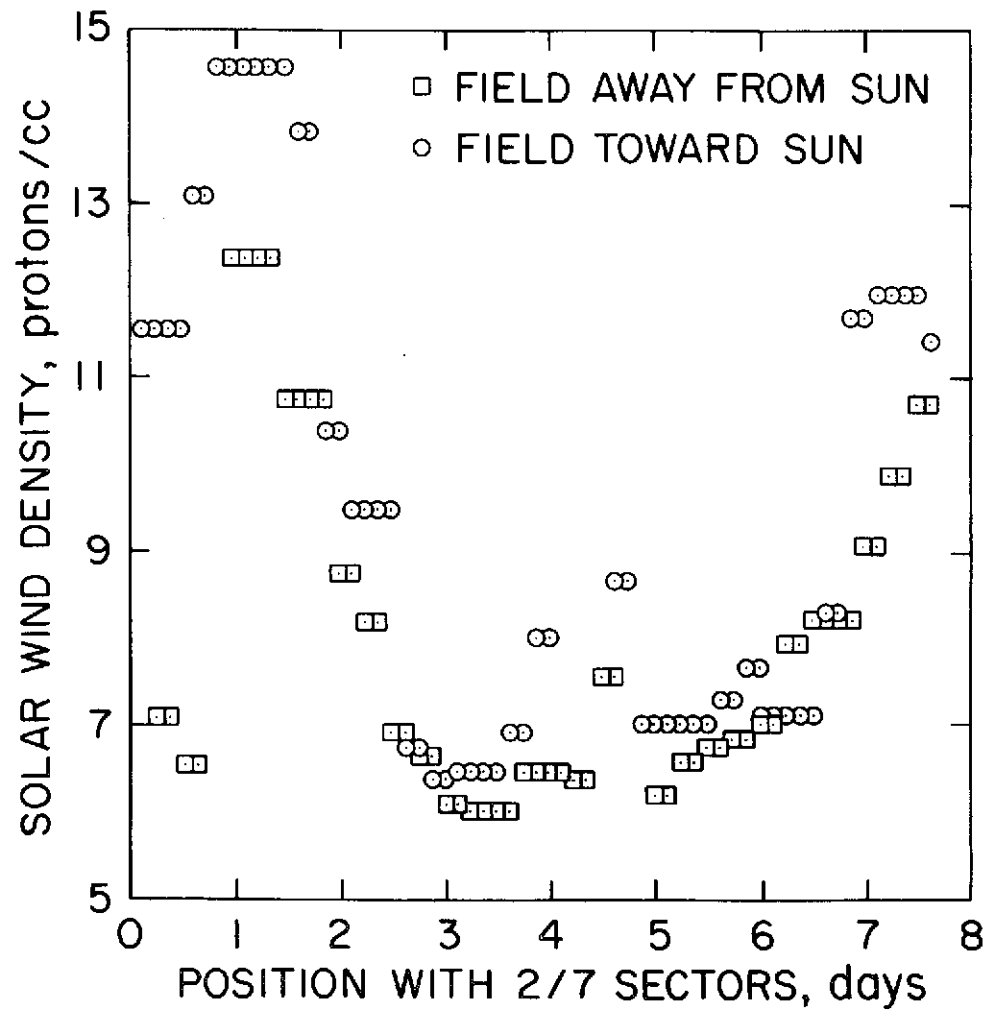
MAGNETIC FIELD ORIENTATION

AWAY FROM SUN → - - - - -

TOWARD SUN → - - - - -

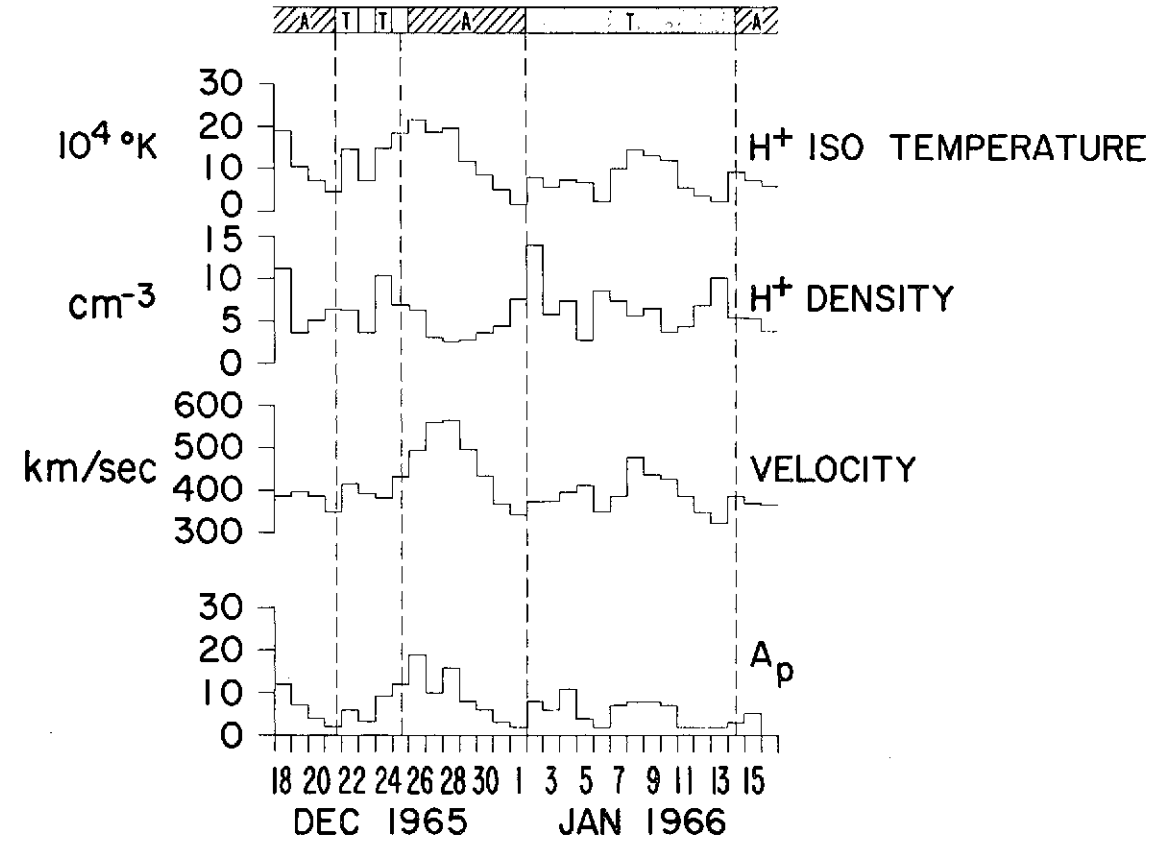
10 20 30 10 20 30 10 20 30 10 20 30 10 20 30
 OCT 63 NOV 63 DEC 63 JAN 64 FEB 64





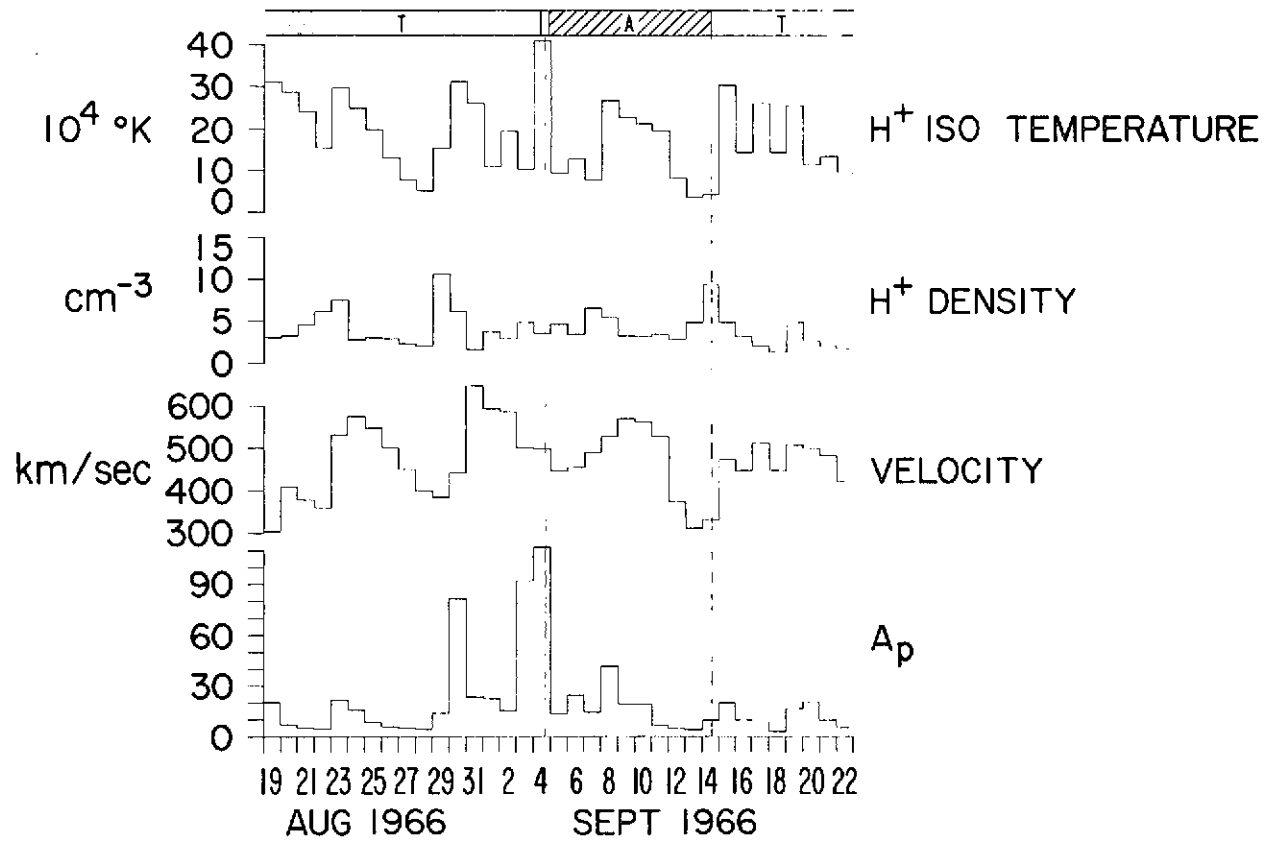
PIONEER 6
24 hr AVG'S
DEC 18, 1965 - JAN 16, 1966

MAGNETIC FIELD SECTOR STRUCTURE

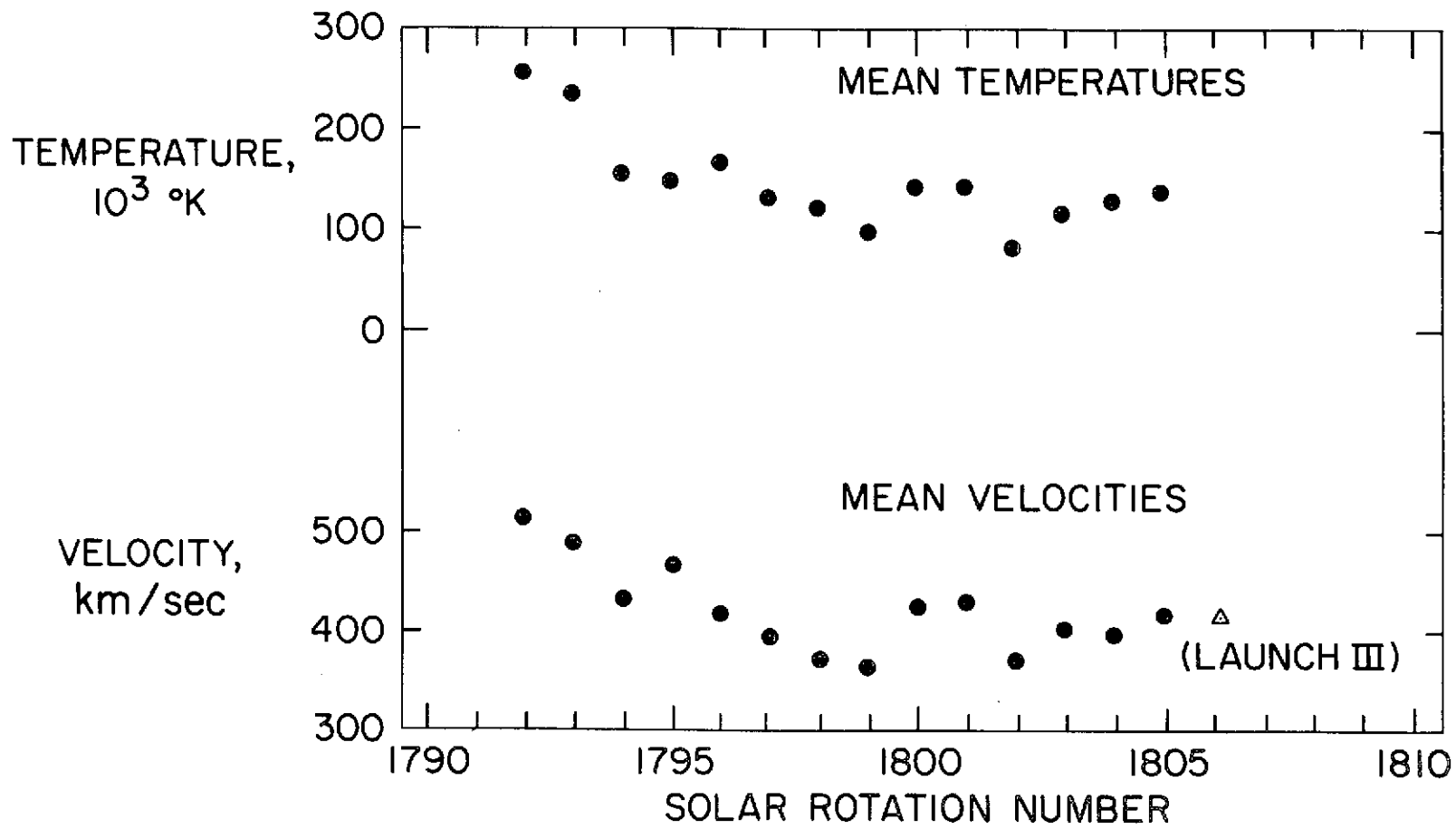


54

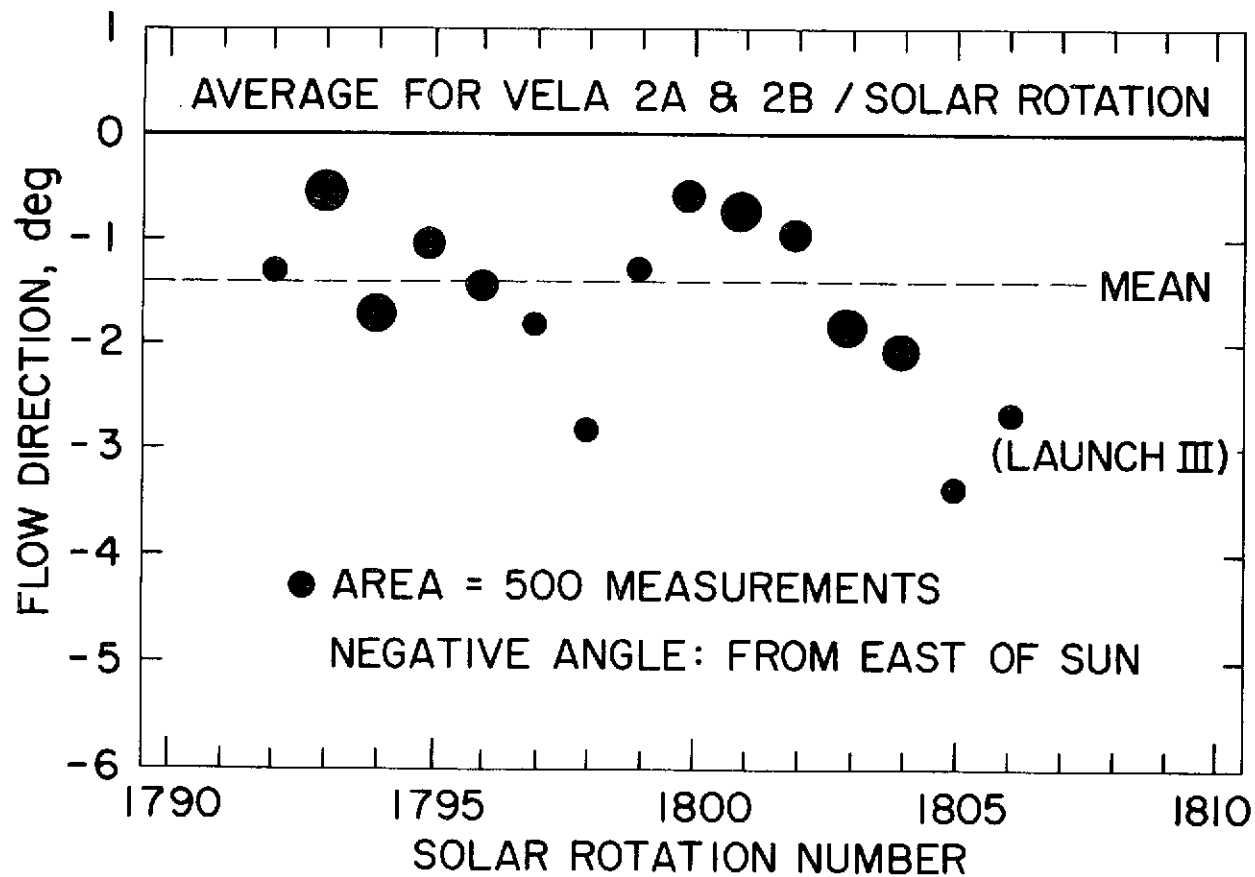
PIONEER 7
24 hr AVG'S
AUG 19, 1966 - SEPT 22, 1966
MAGNETIC FIELD SECTOR STRUCTURE



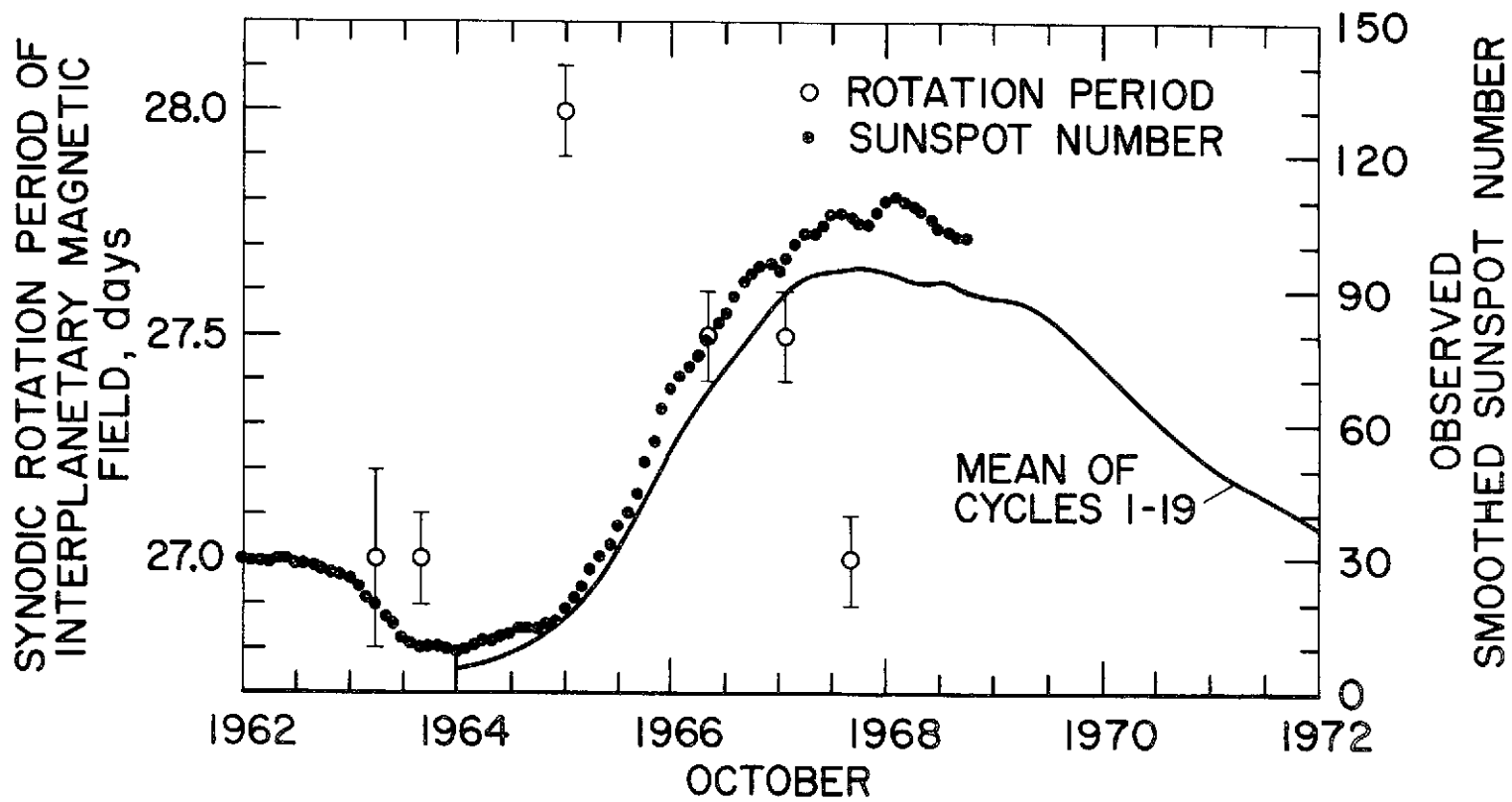
27
07



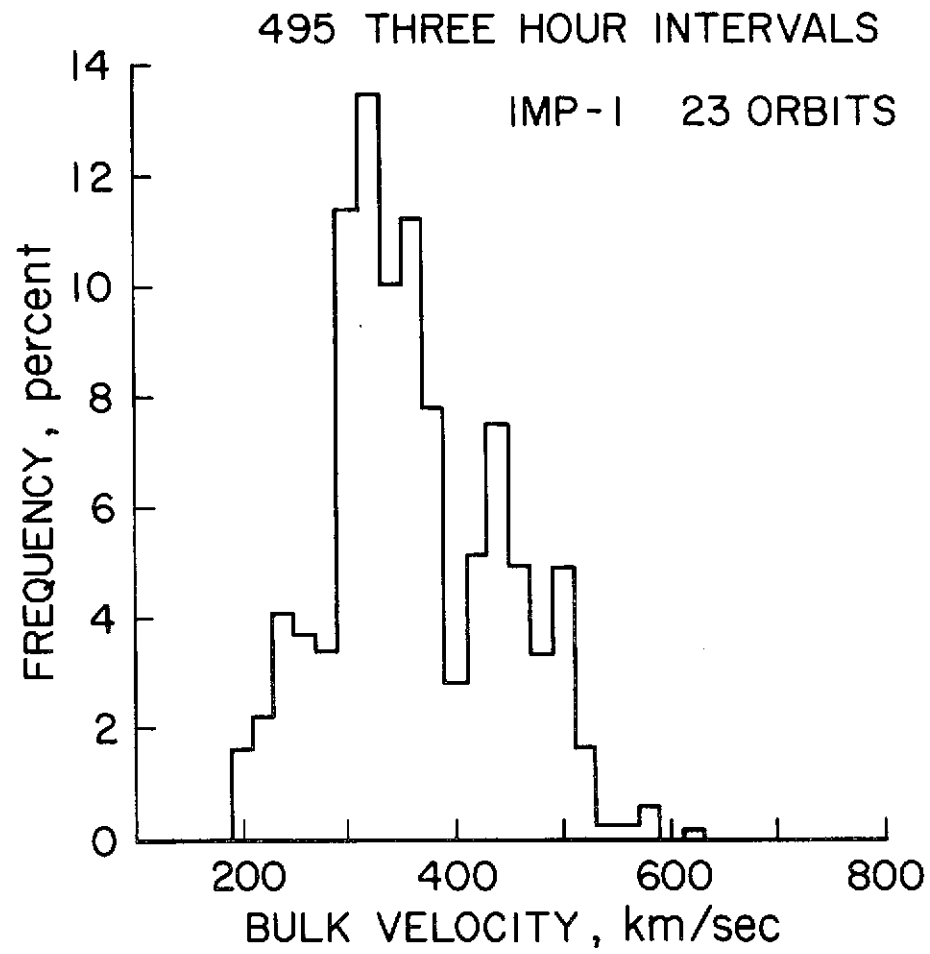
SOLAR - WIND DIRECTIONS FROM JULY 1964 TO JULY 1965



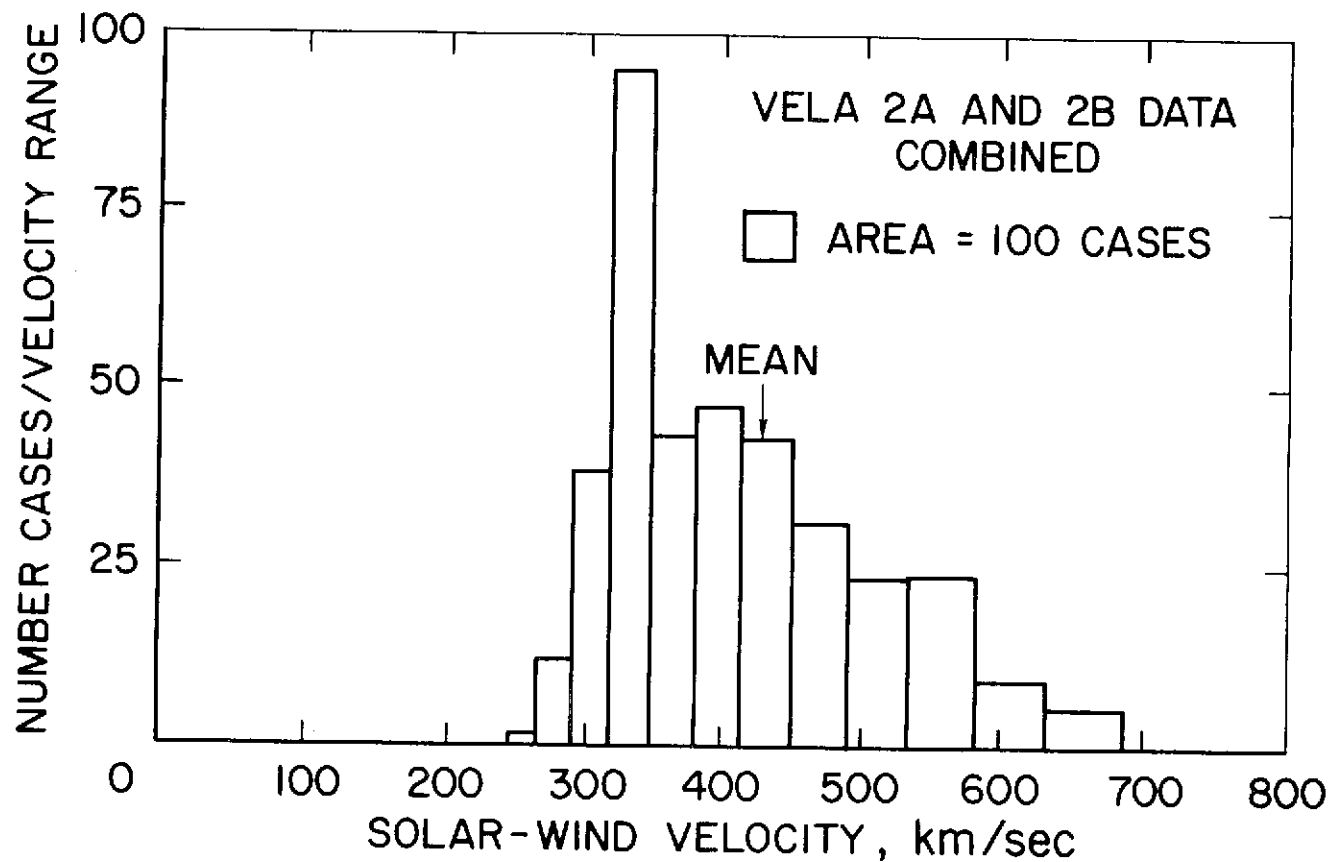
27
28

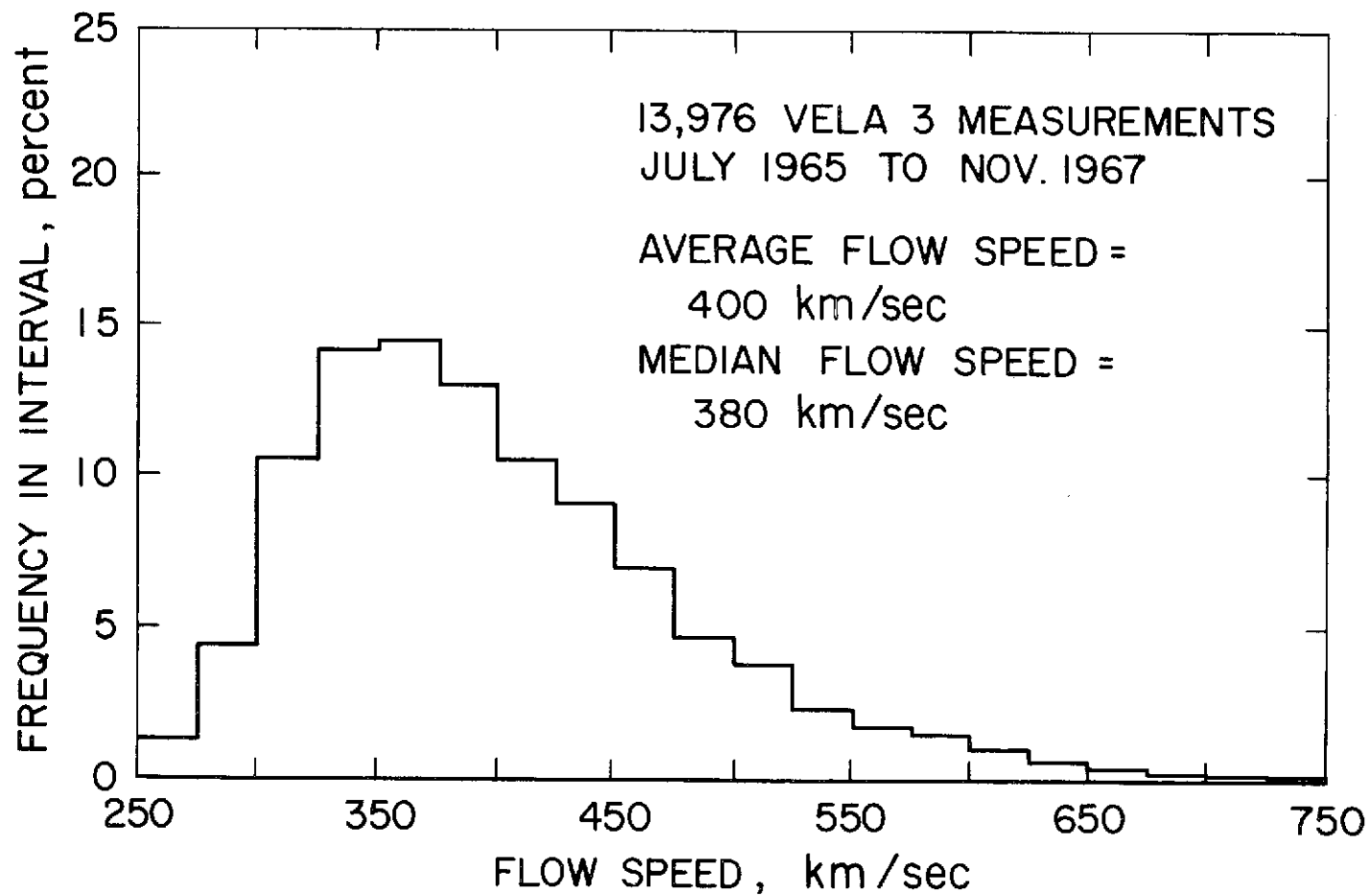


SPACECRAFT	INST.	V_{mp} , km/sec	V_{AV} , km/sec	N_{mp} , cm ⁻³	N_{AV} , cm ⁻³	T_{mp} , 10 ⁵ °K	T_{AV} , 10 ⁵ °K	ϕ deg	θ deg	~ DATE
MARINER - 2'	JPL		504		5.4		1.5 - 1.8			9/62 - 12/62
IMP - 1	MIT	330	360	4	7			+1.5		12/63 - 2/64
IMP - 1	ARC		378							12/63 - 2/64
VELA - 2	LASL	325	420			~0.5	1.4	-1.4		7/64 - 7/65
VELA - 3	LASL	~350	400	~4	7.7	~0.4	0.91	-2.5 -0.9		7/65 - 7/67
PIONEER - 6	MIT		430		6	0.38				12/65 - 2/66
PIONEER - 6	ARC	~340	422	~3.2	5.7	~0.4	1.0	+3.0	+0.56	12/65 - 2/66
PIONEER - 7	MIT		460		6	0.66				8/66 - 10/66
PIONEER - 7	ARC		455	~2.4	4.4	~0.5	1.6	+0.3	+0.34	8/66 - 10/66
EXPLORER - 34	GSFC	~390	438			0.46				6/67 - 12/67
HEOS - 1	ROME	~390	409	~2	4.3		0.66			12/68 - 1/70

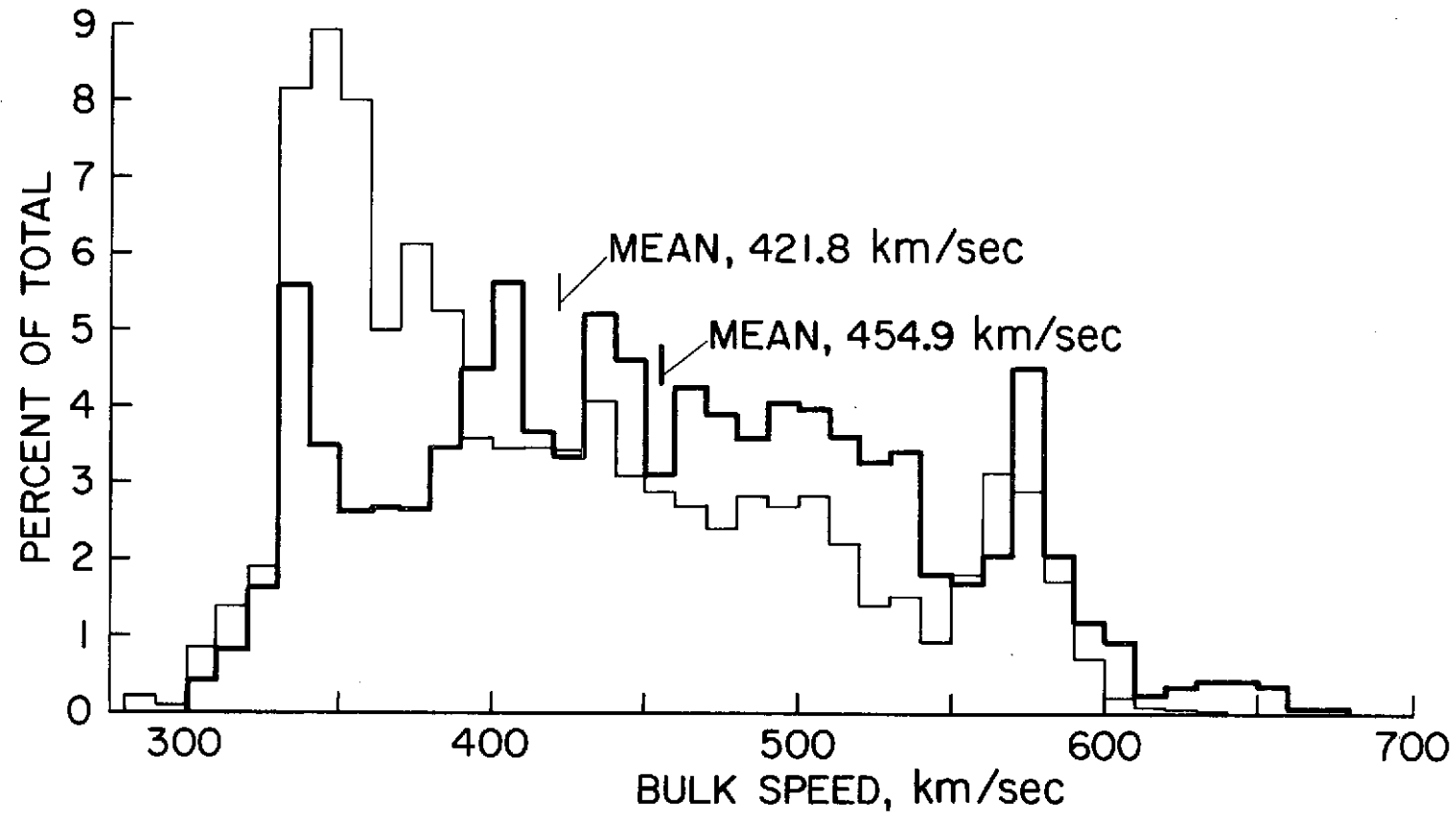


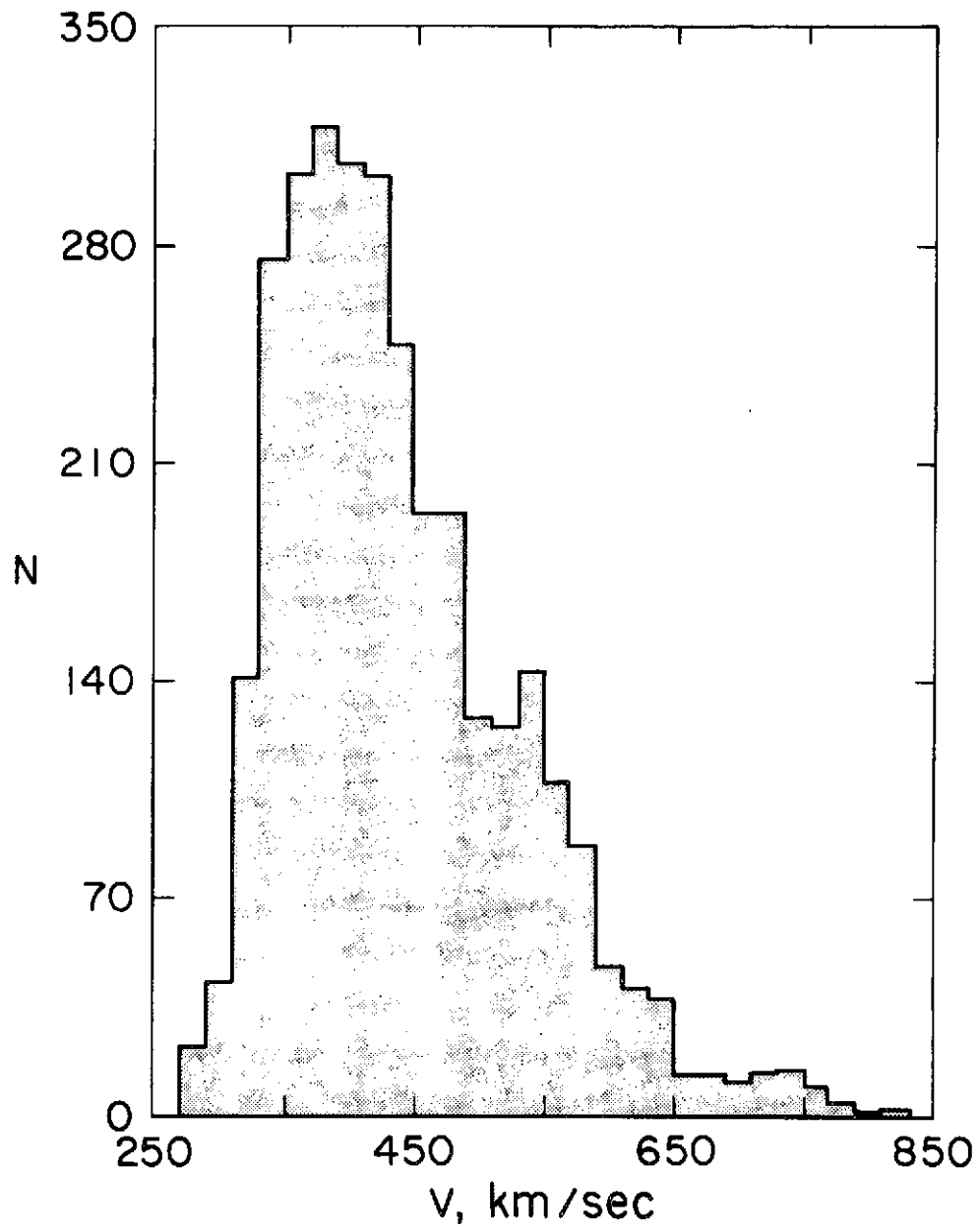
DISTRIBUTION OF SOLAR-WIND VELOCITY FROM JULY 1964 TO JULY 1965

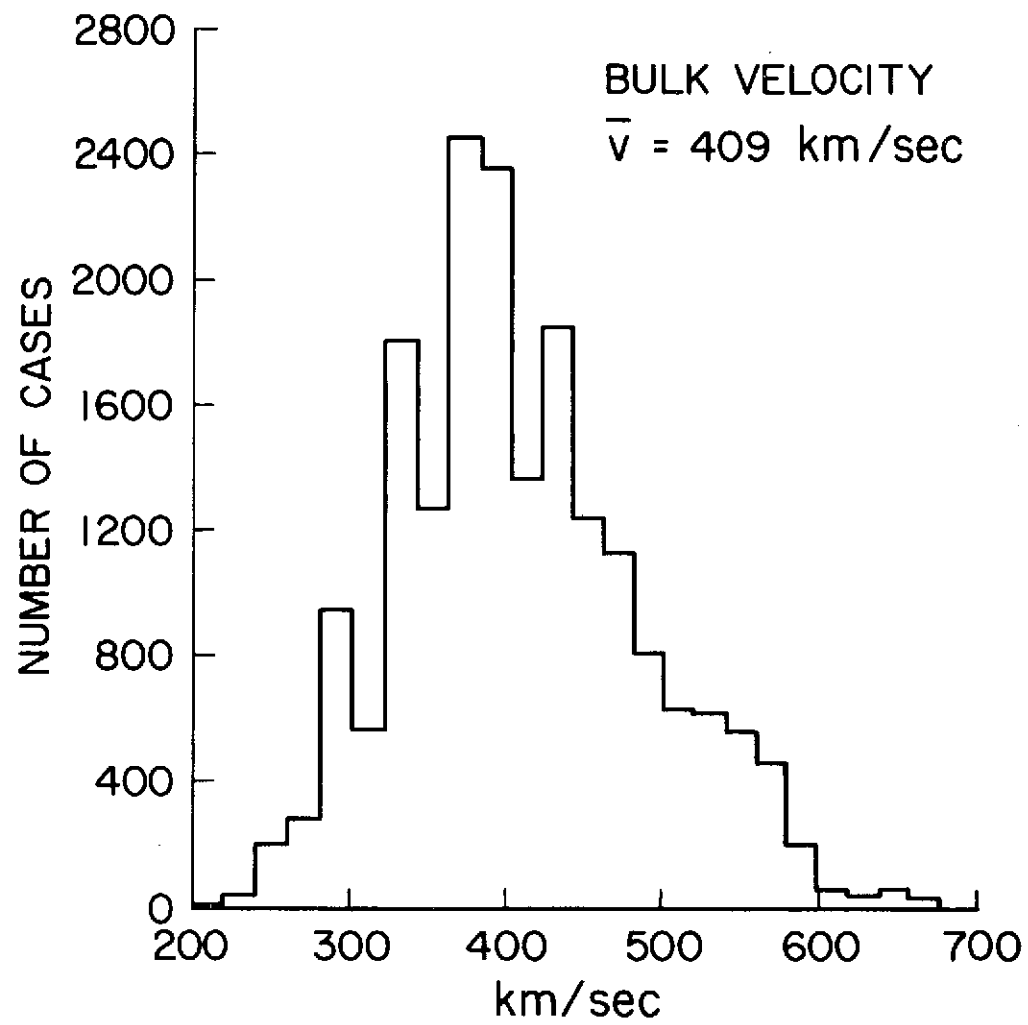


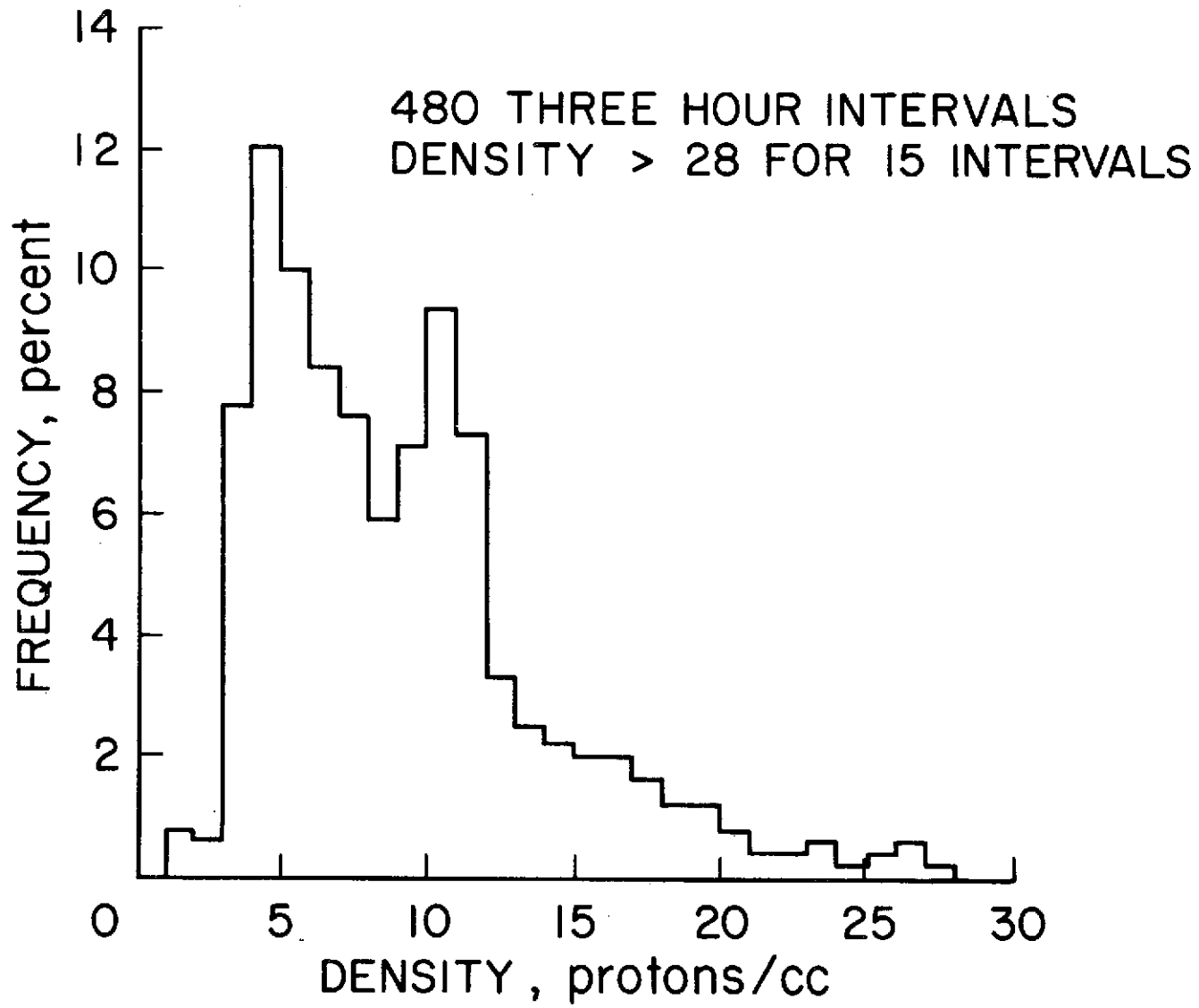


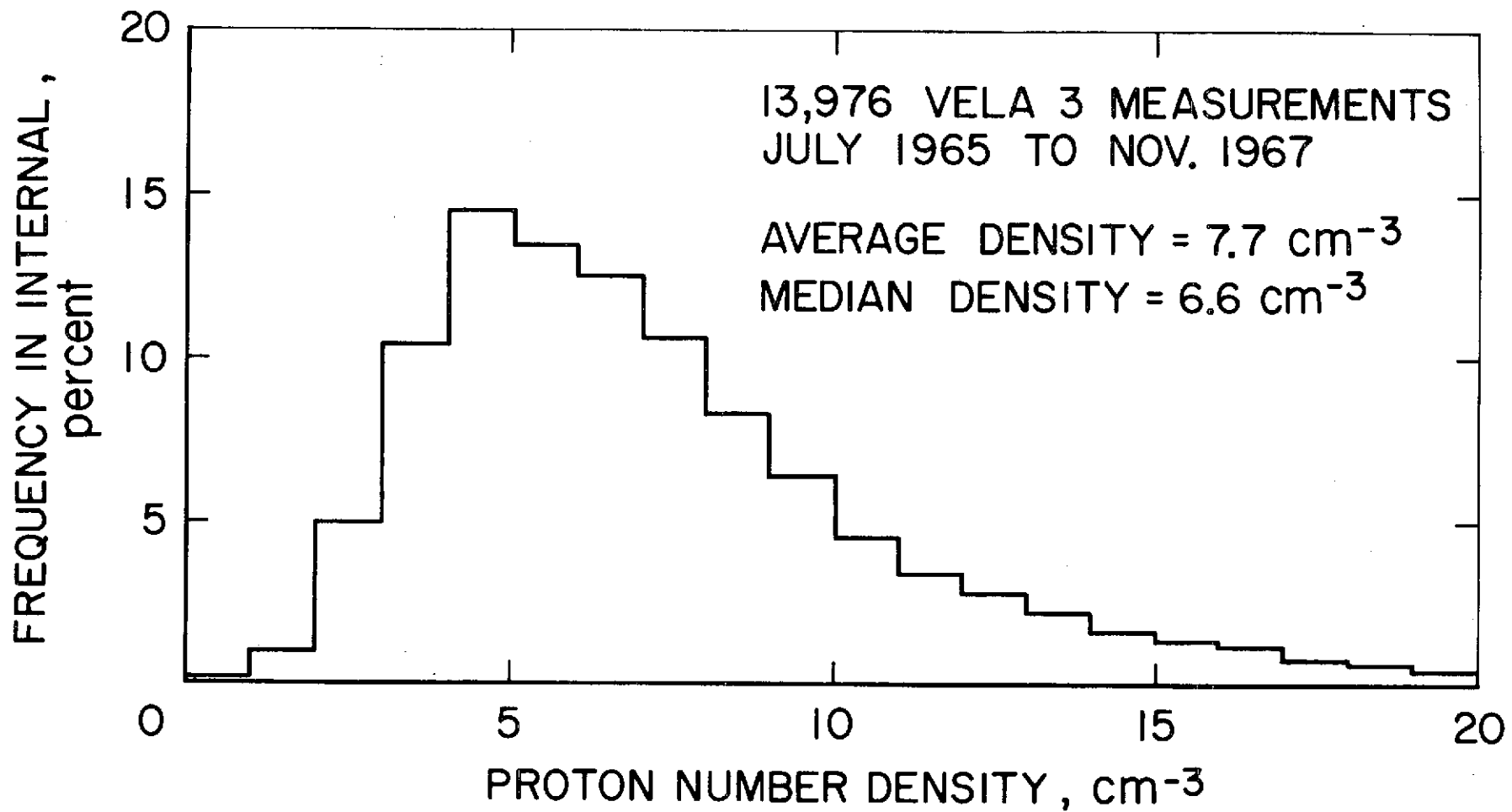
— PIONEER 6, 4702 SAMPLES
— PIONEER 7, 2400 SAMPLES

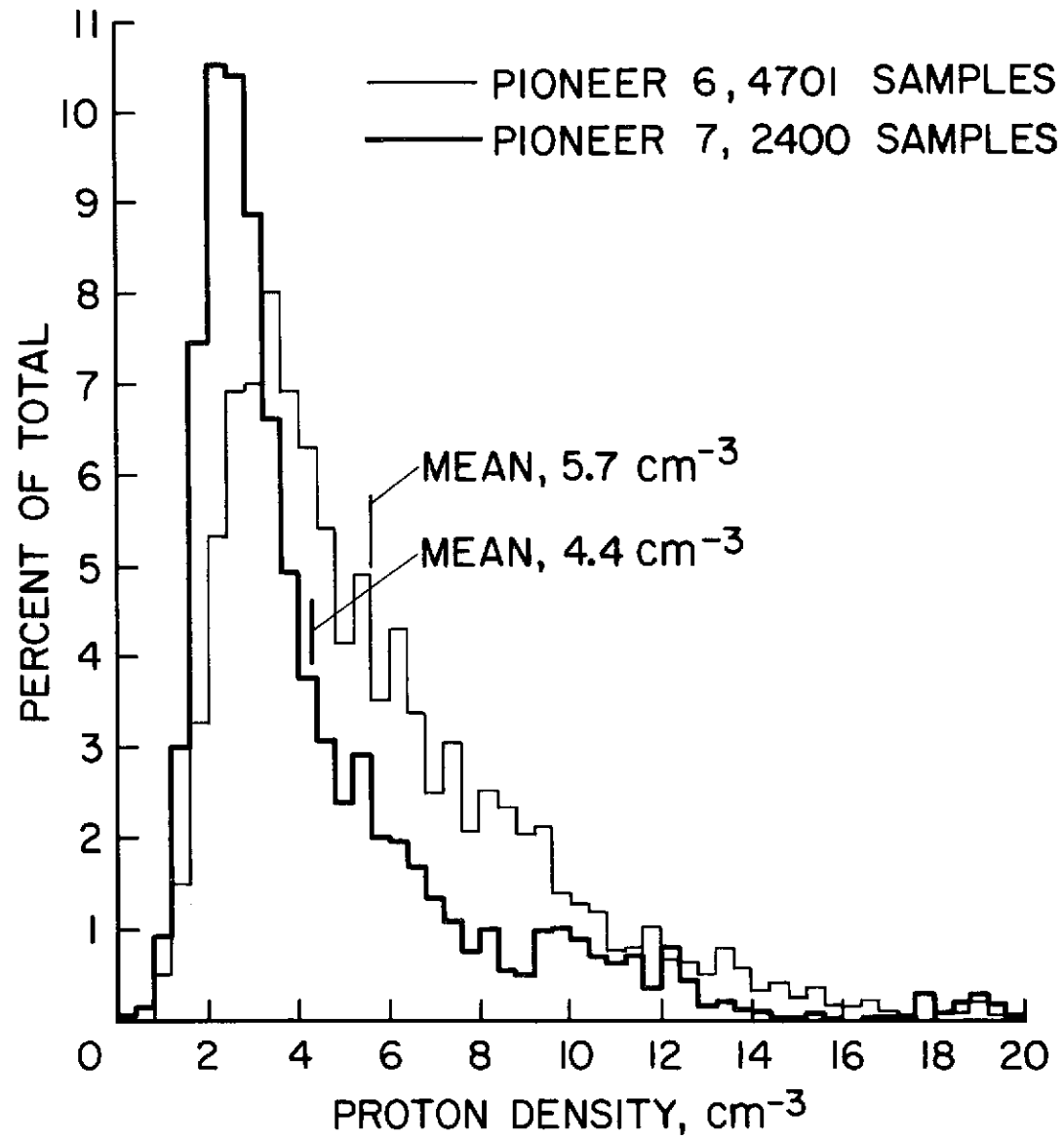


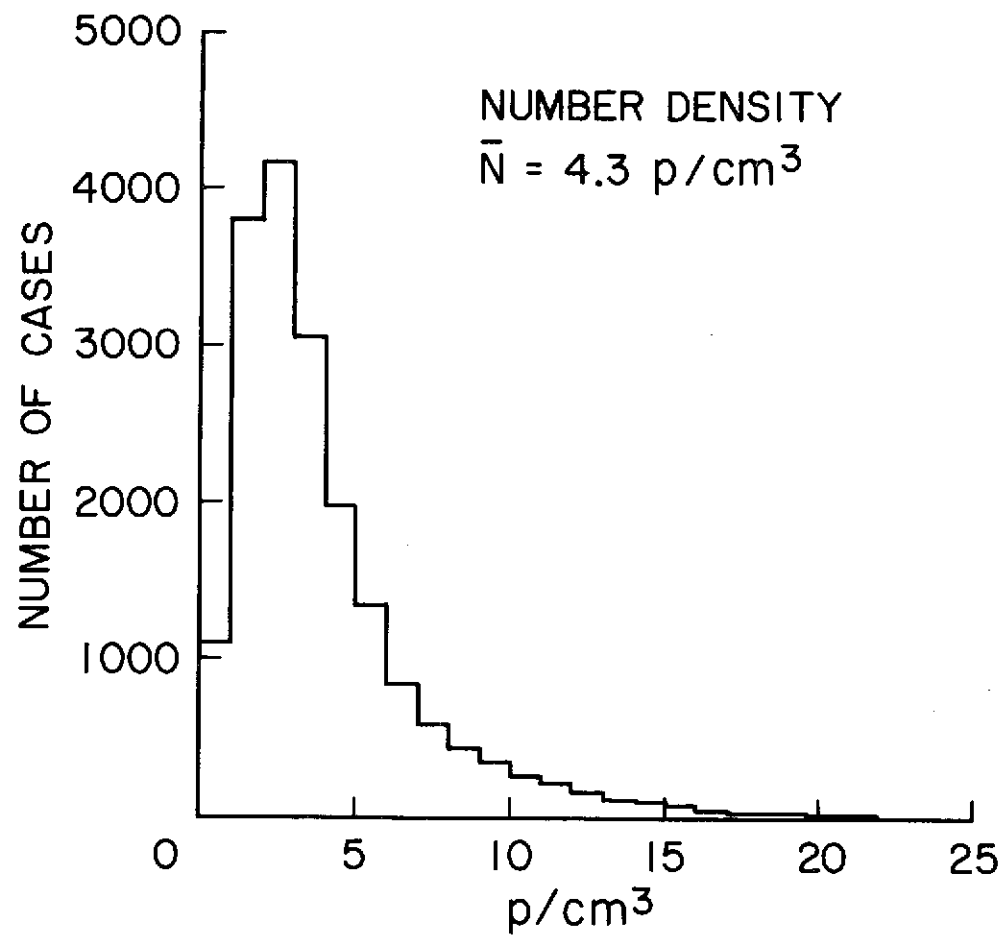




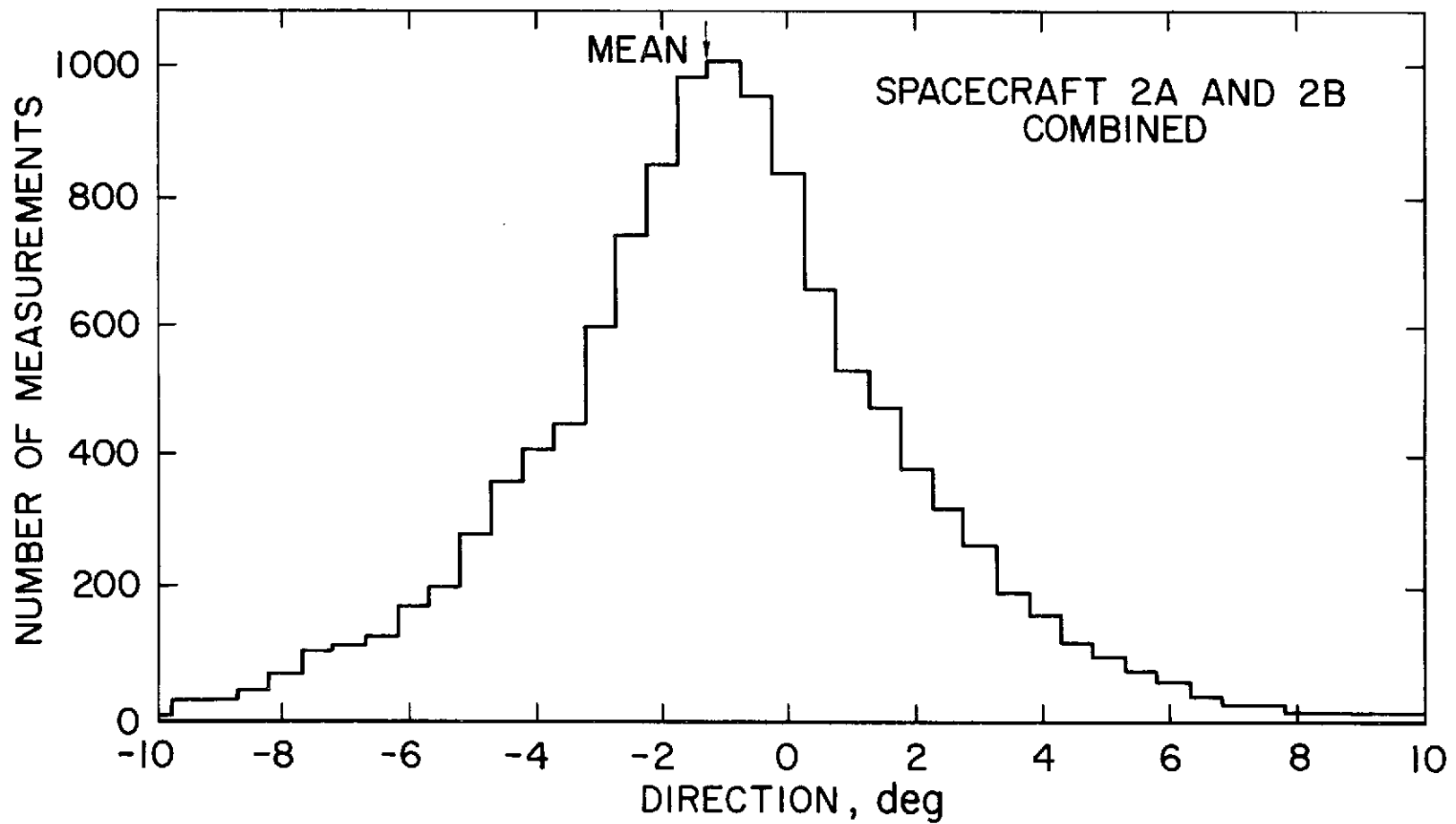


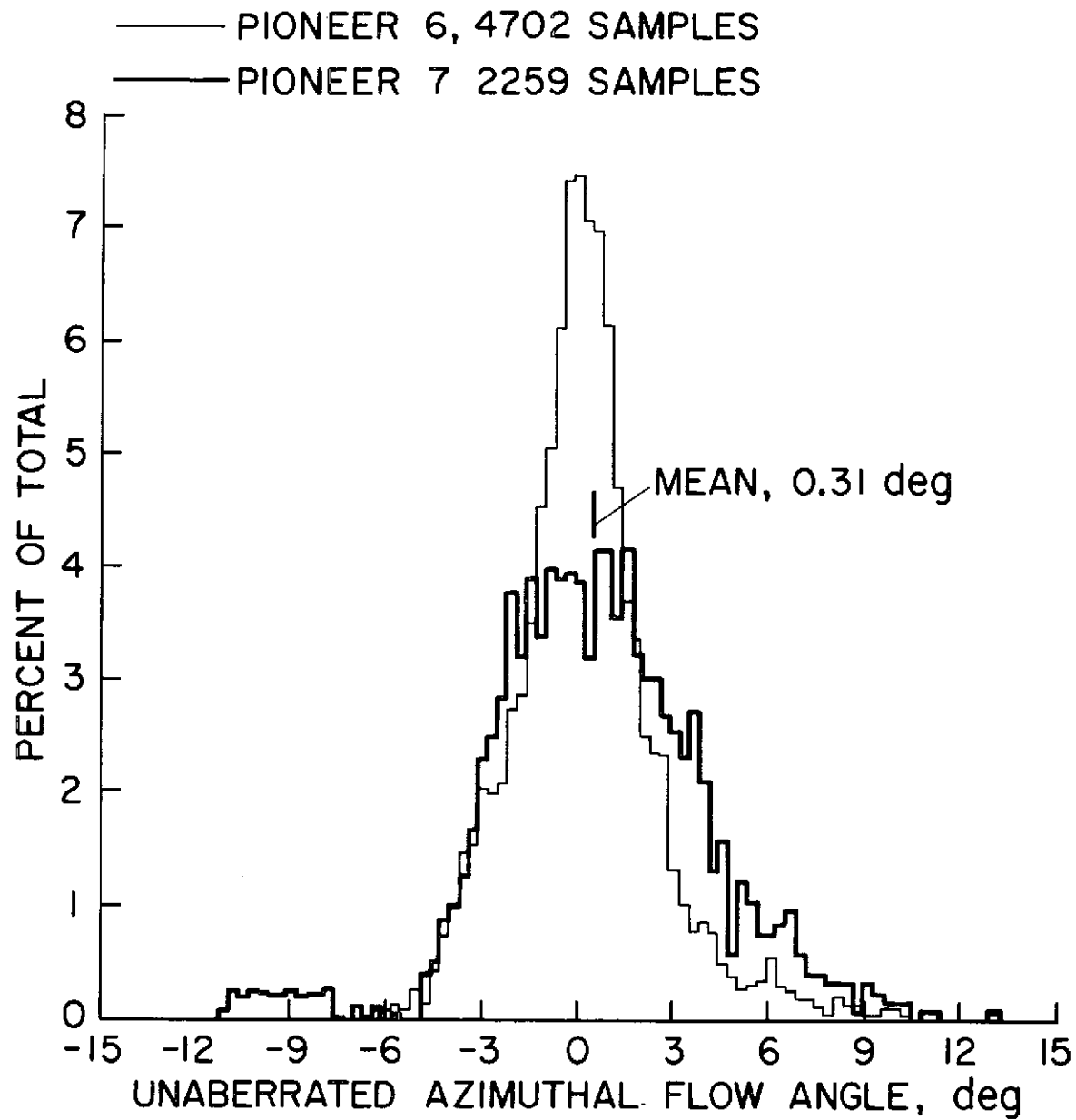


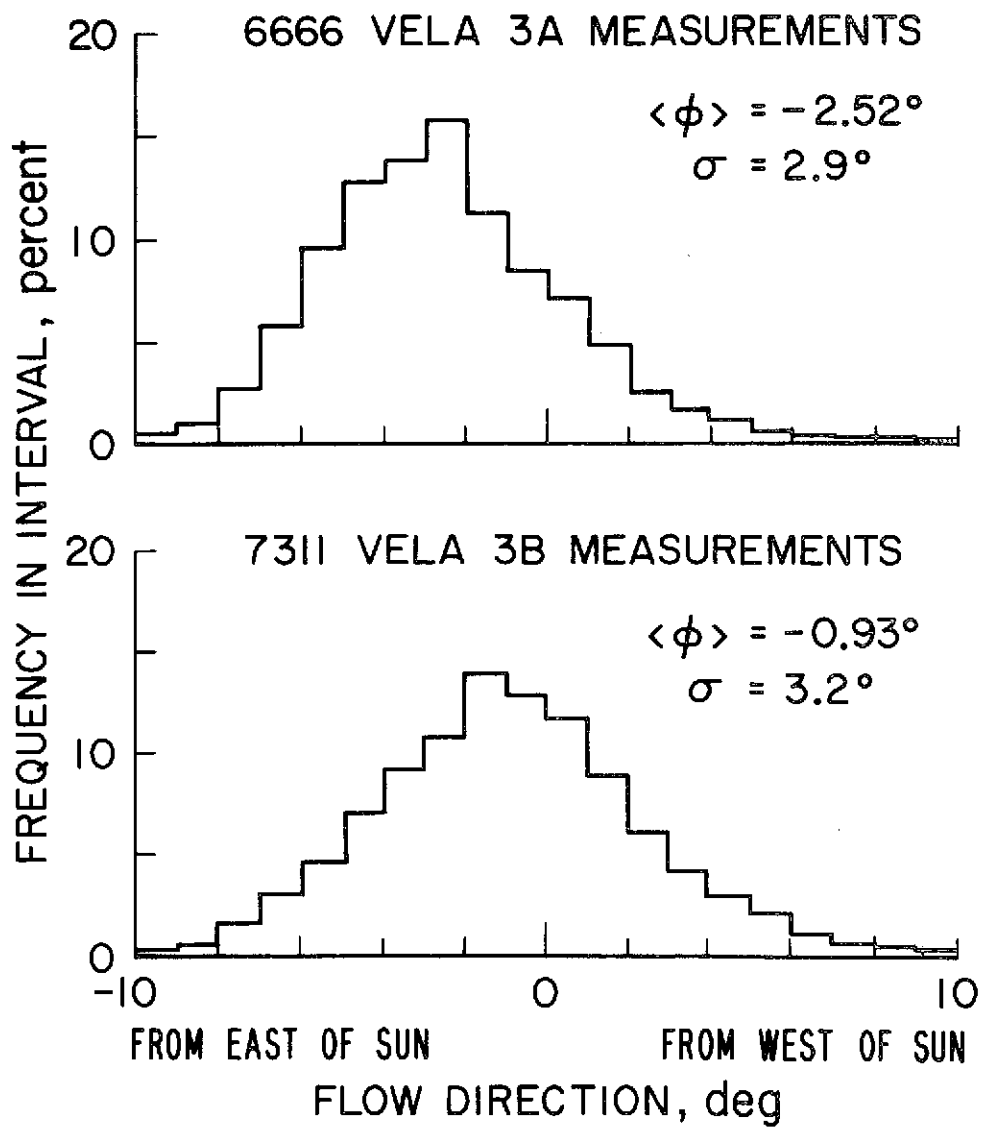


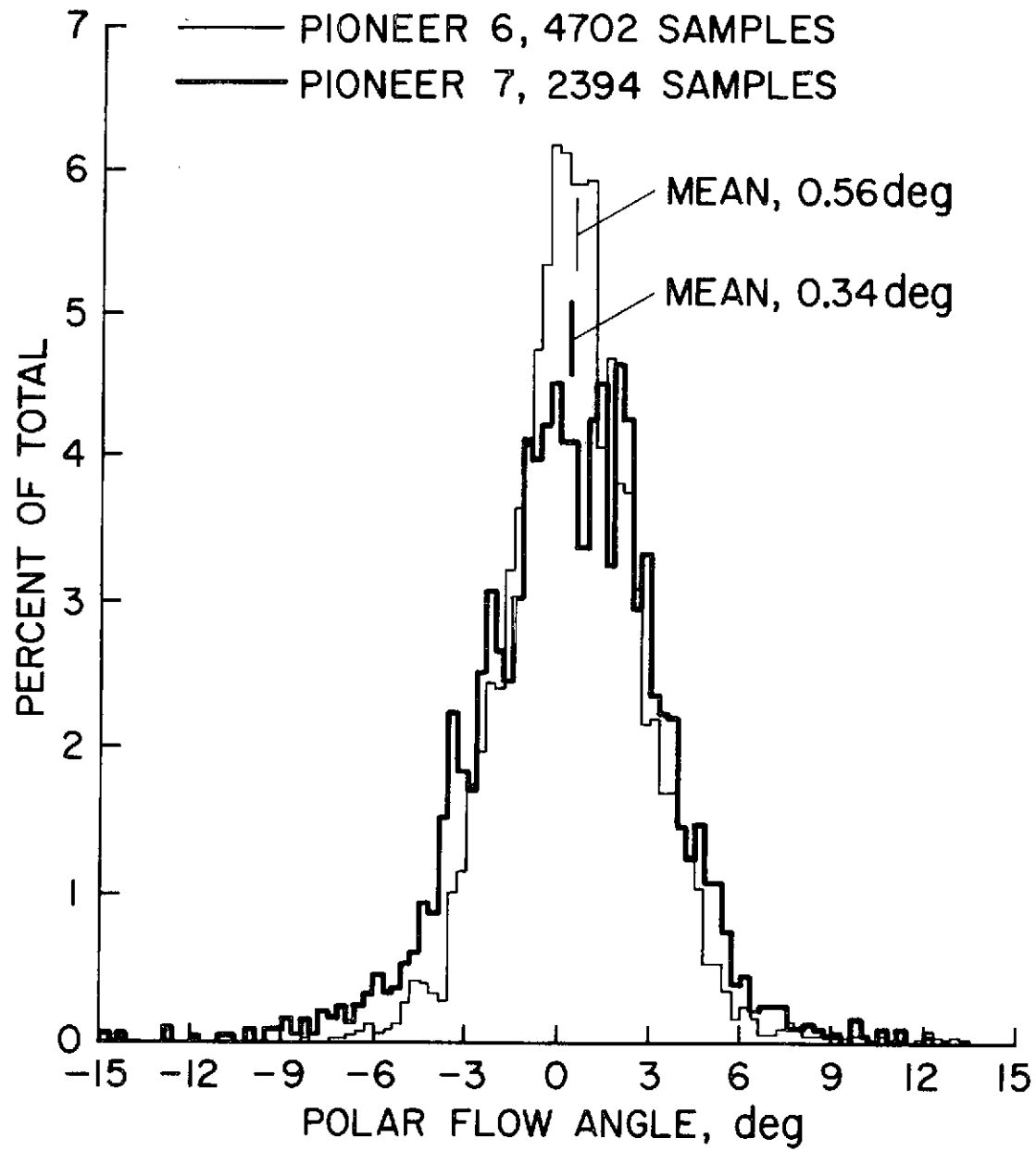


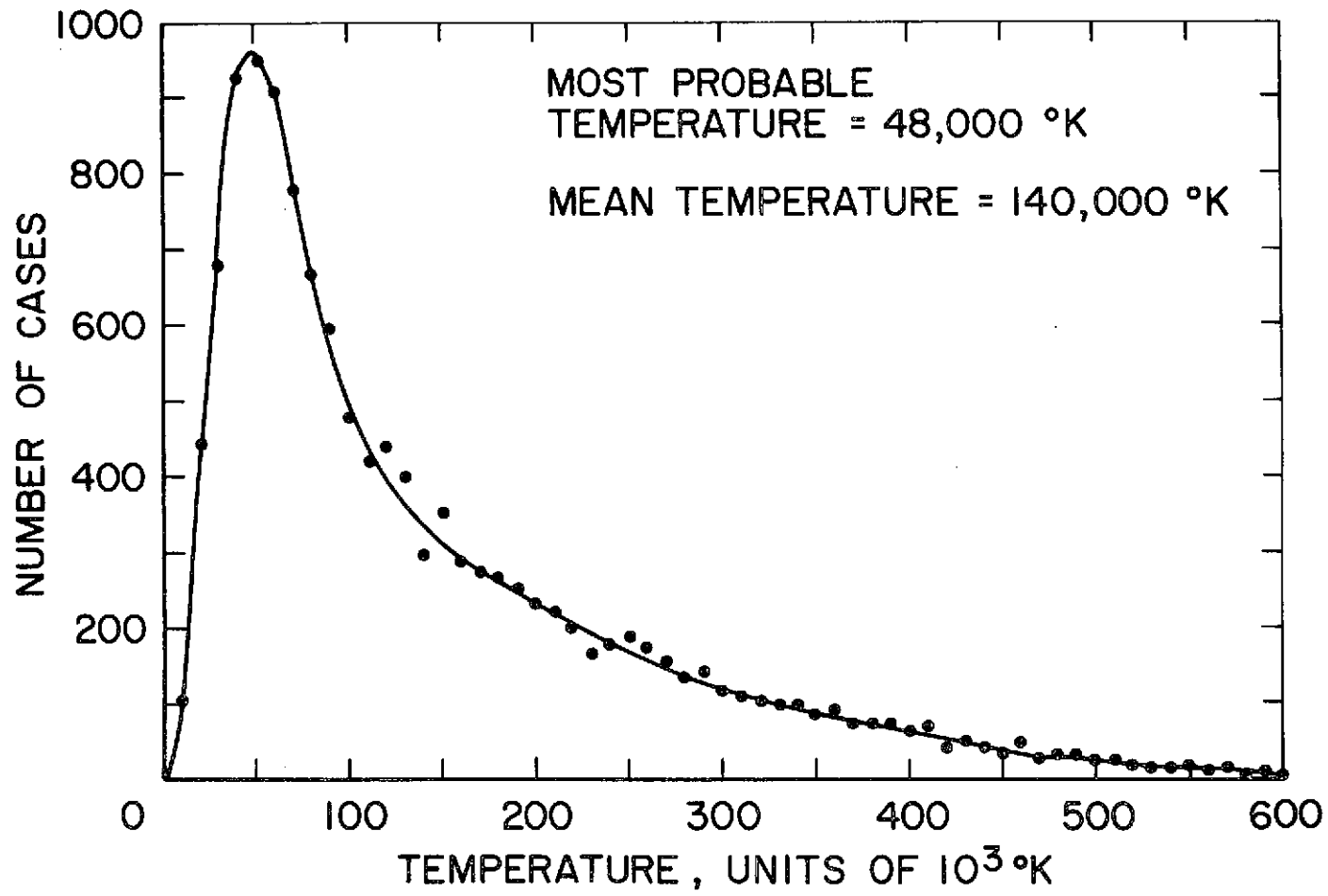
DISTRIBUTION OF SOLAR-WIND DIRECTIONS FROM
JULY 1964 TO JULY 1965

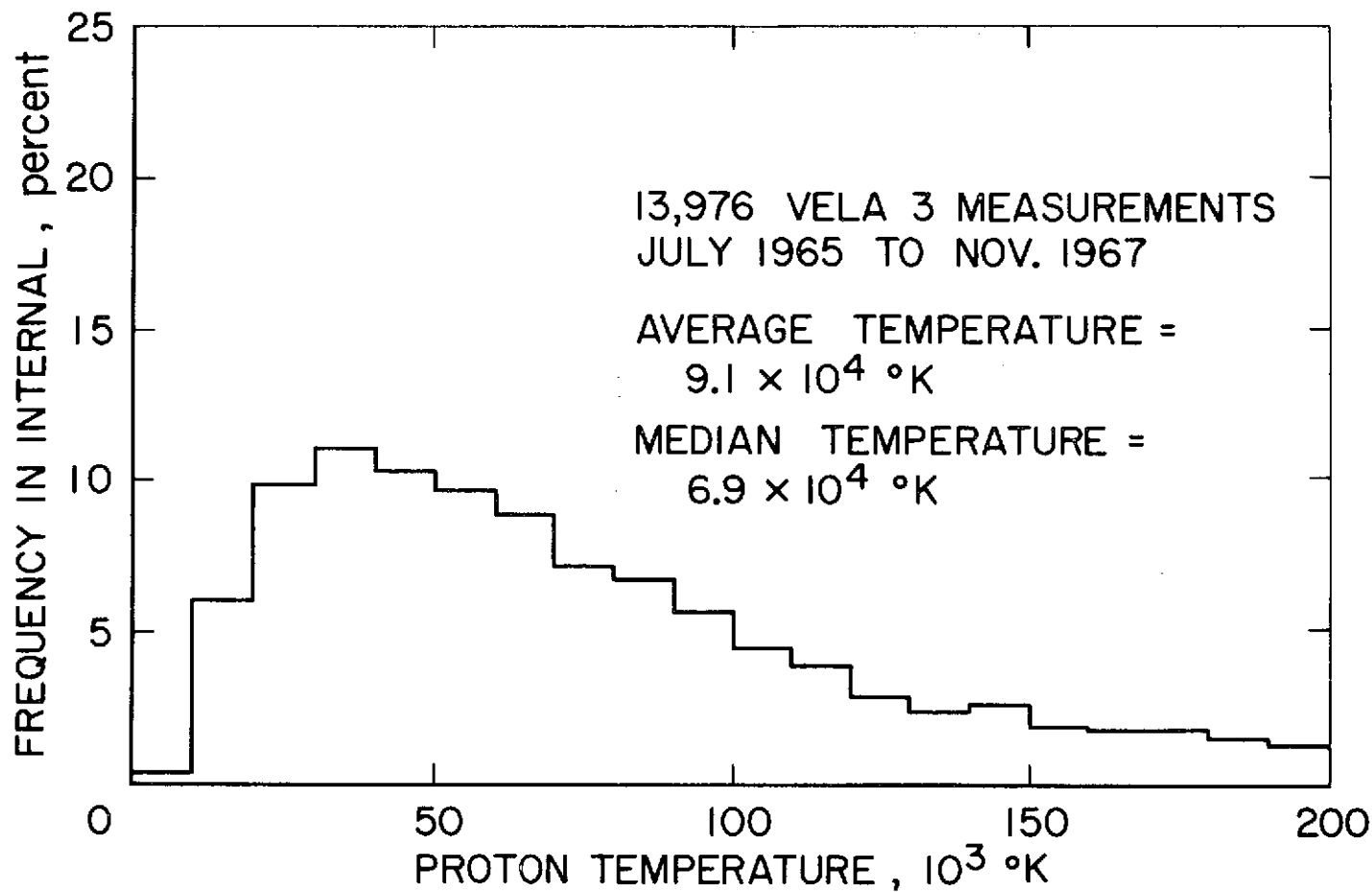




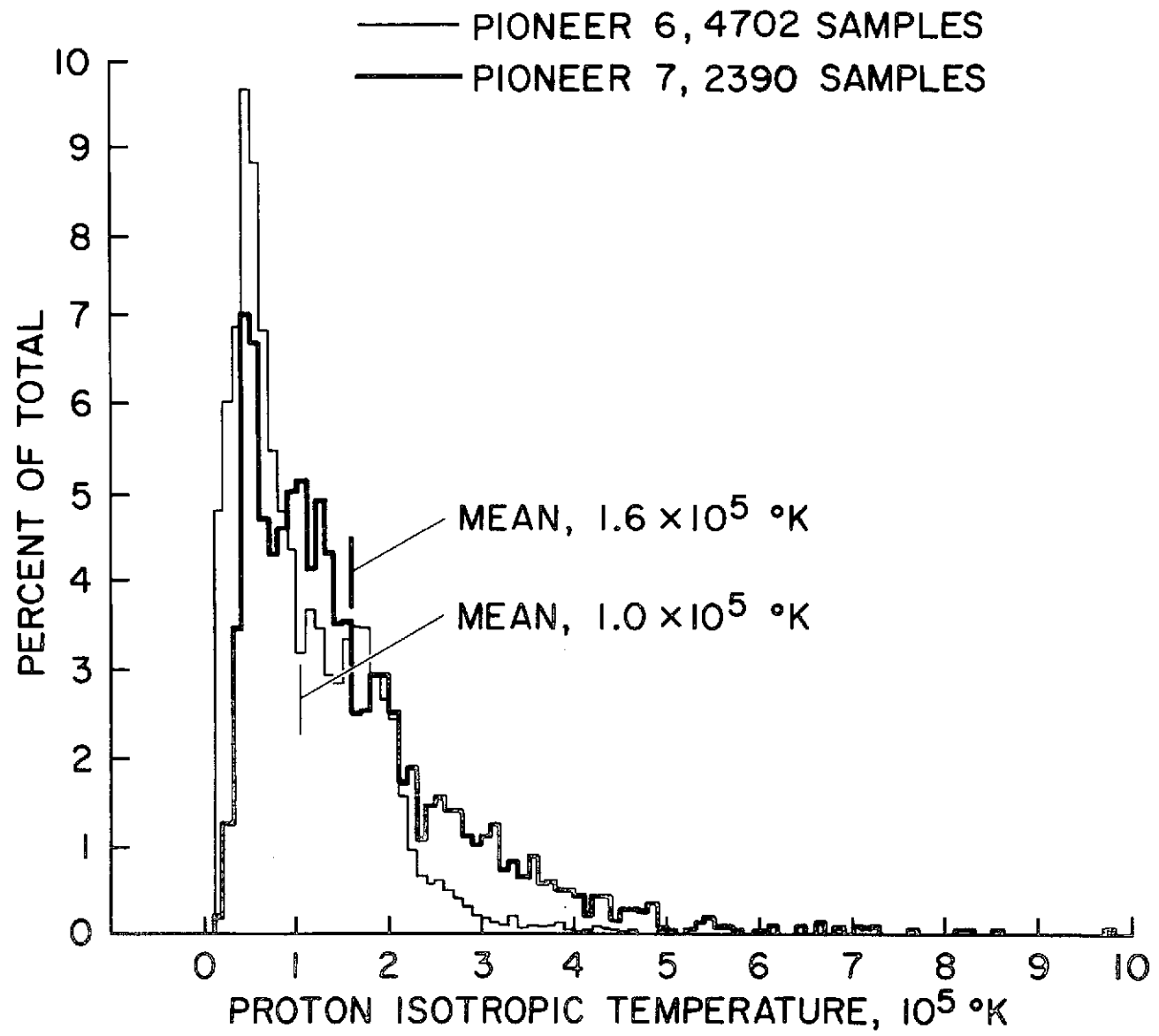


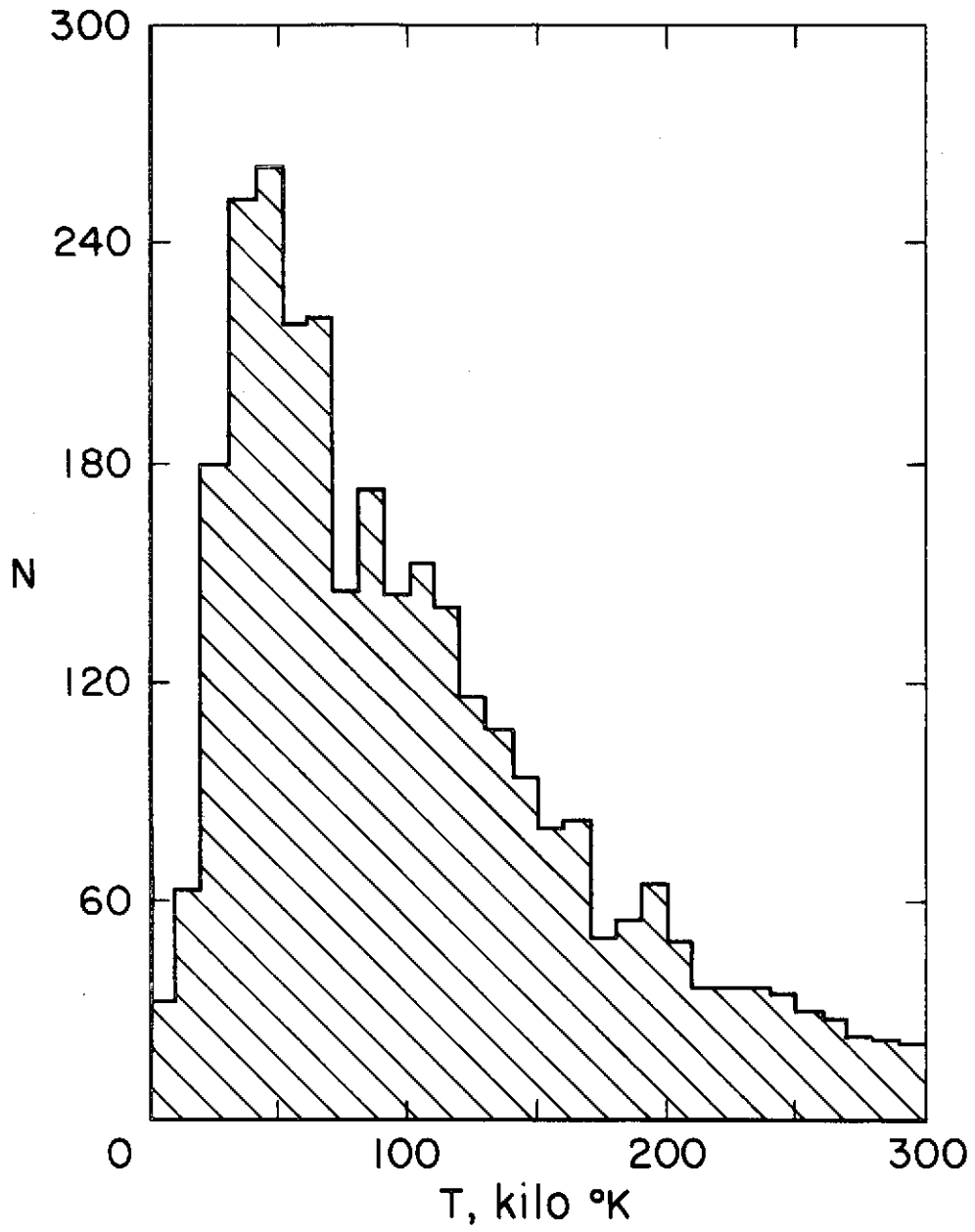




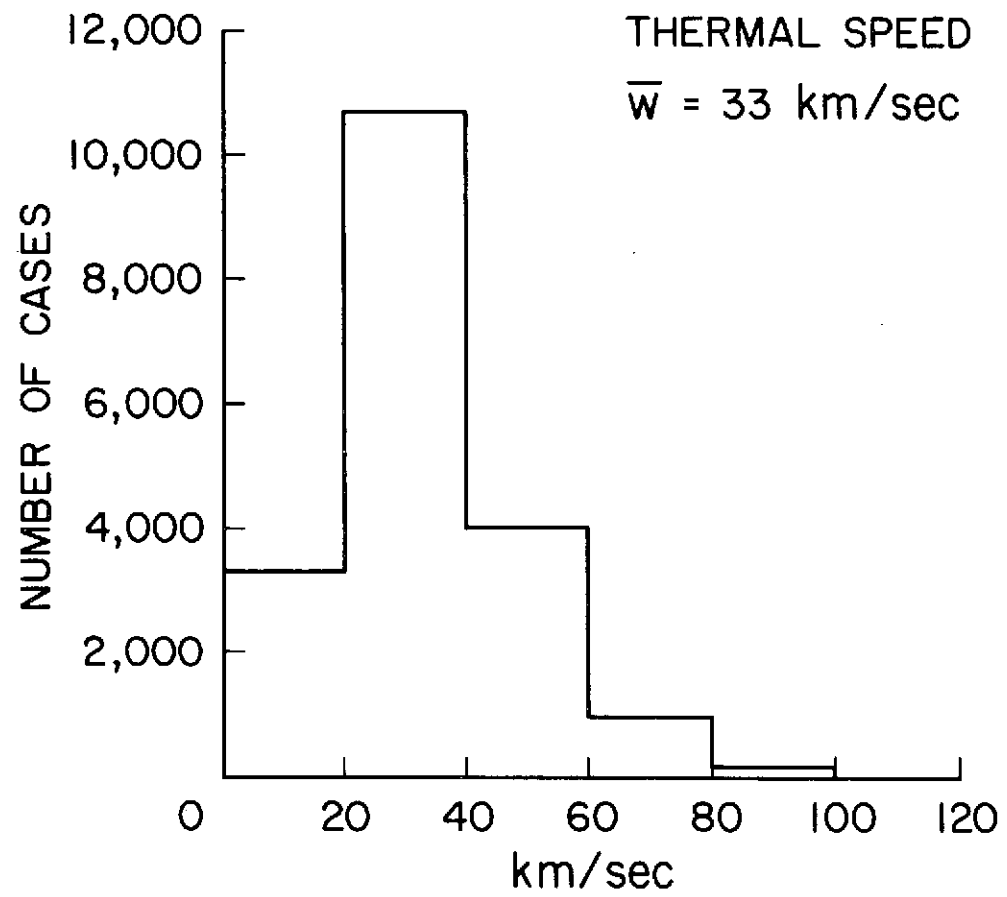


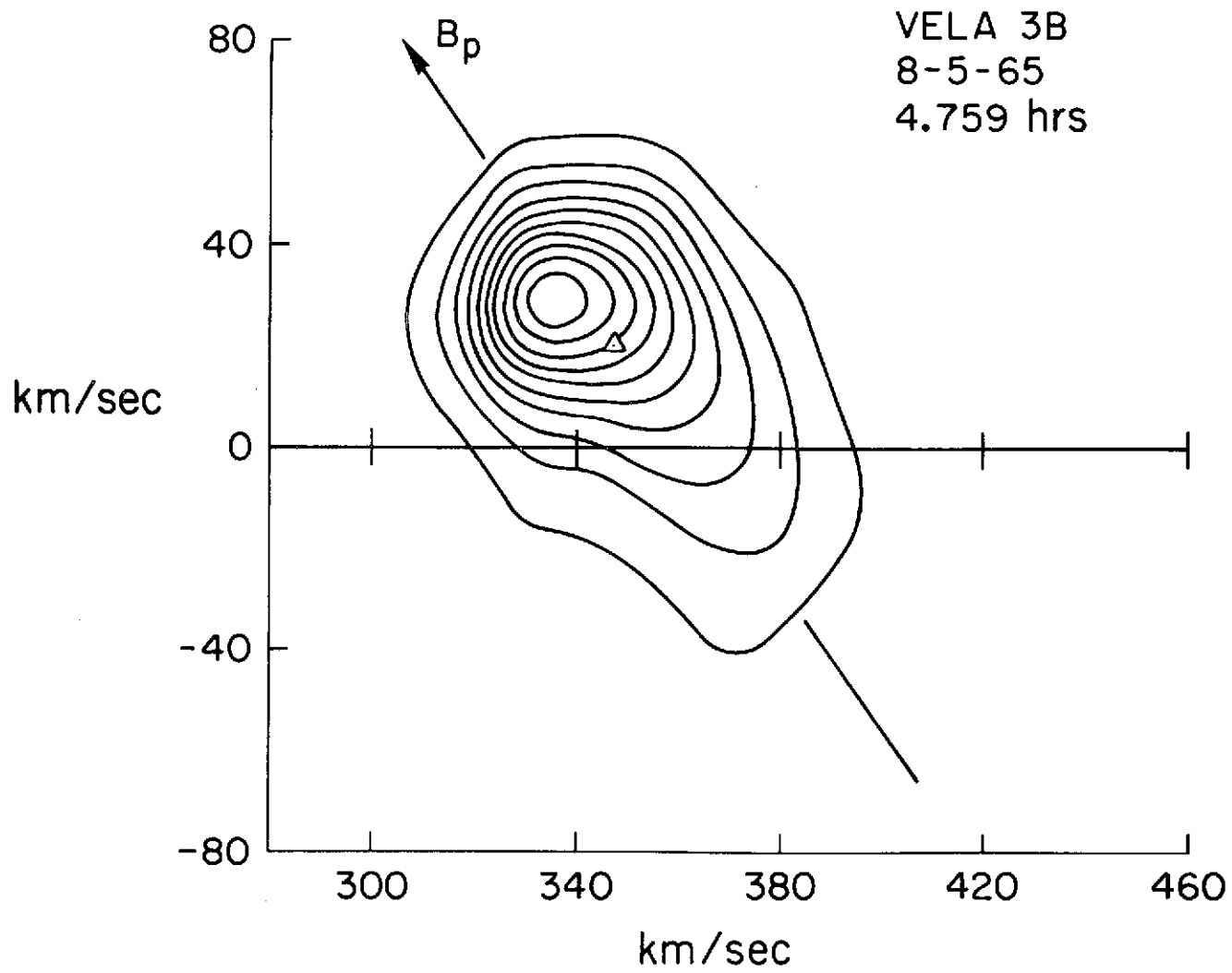
62

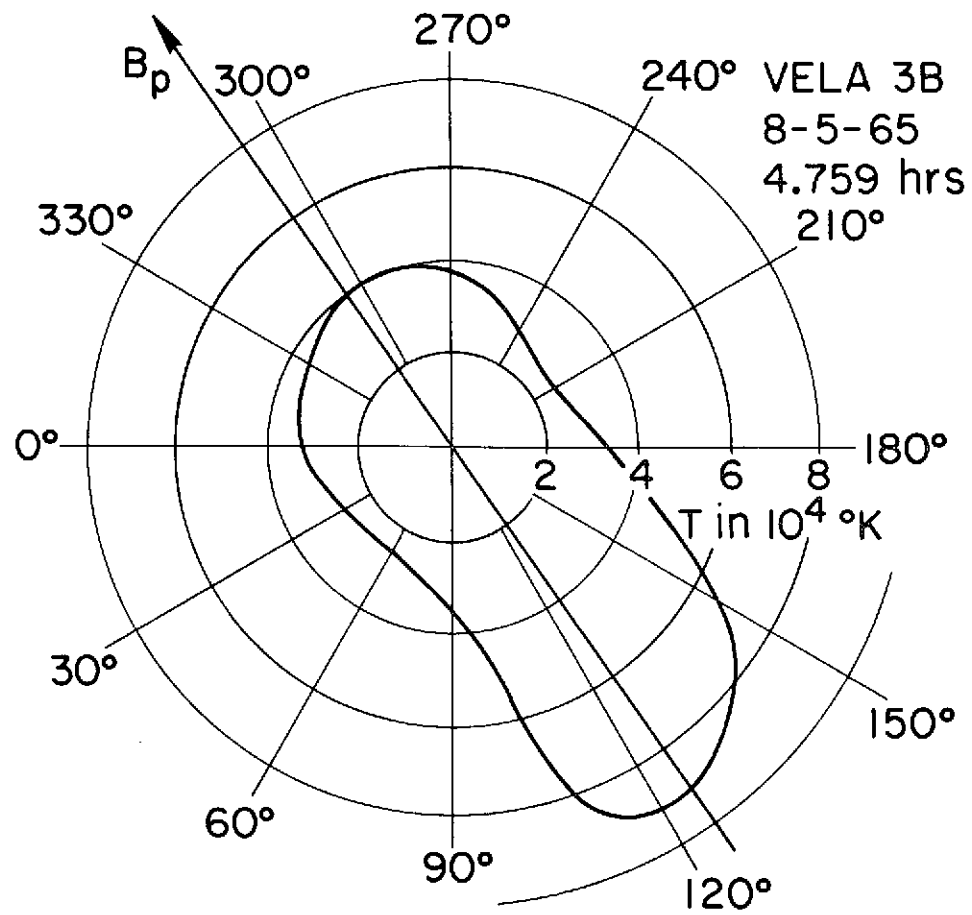


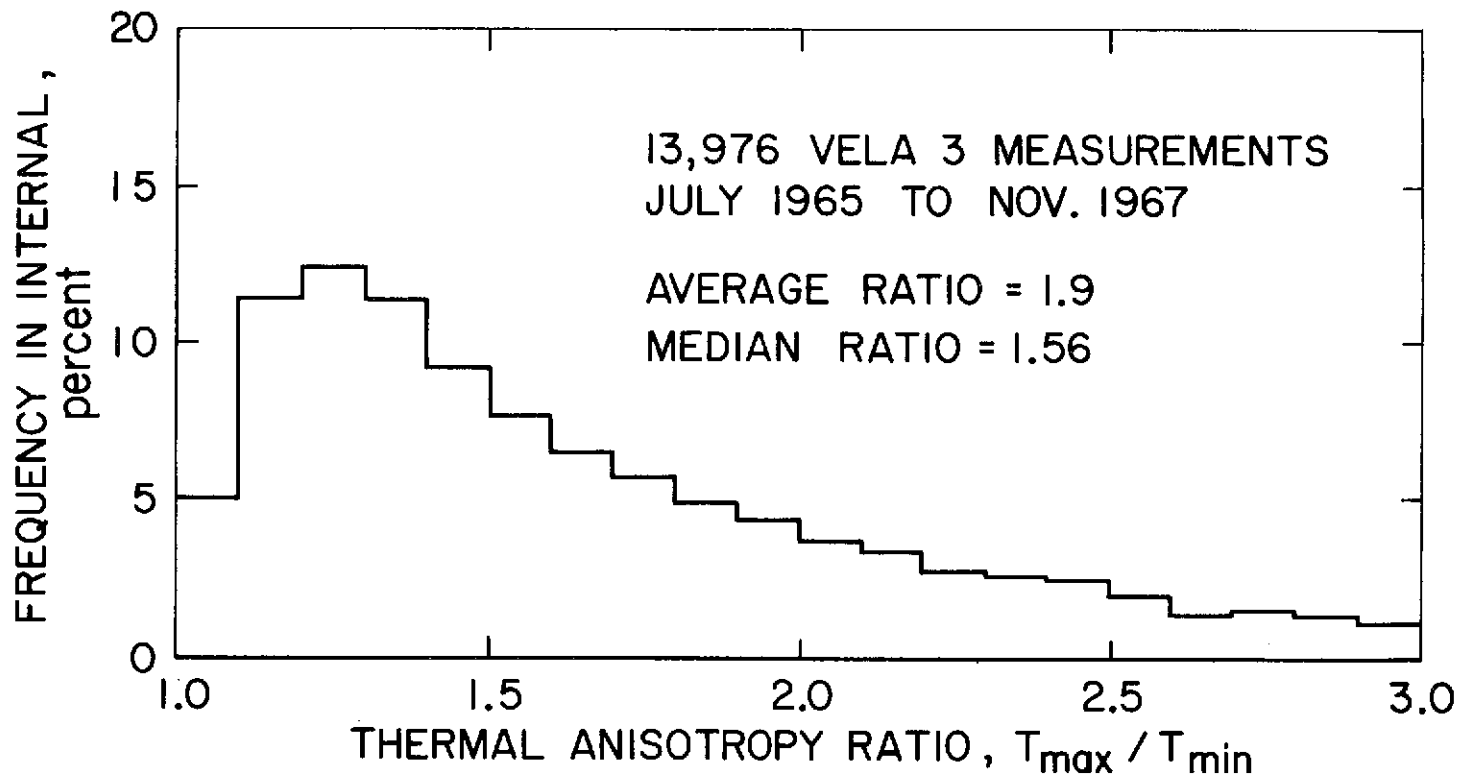


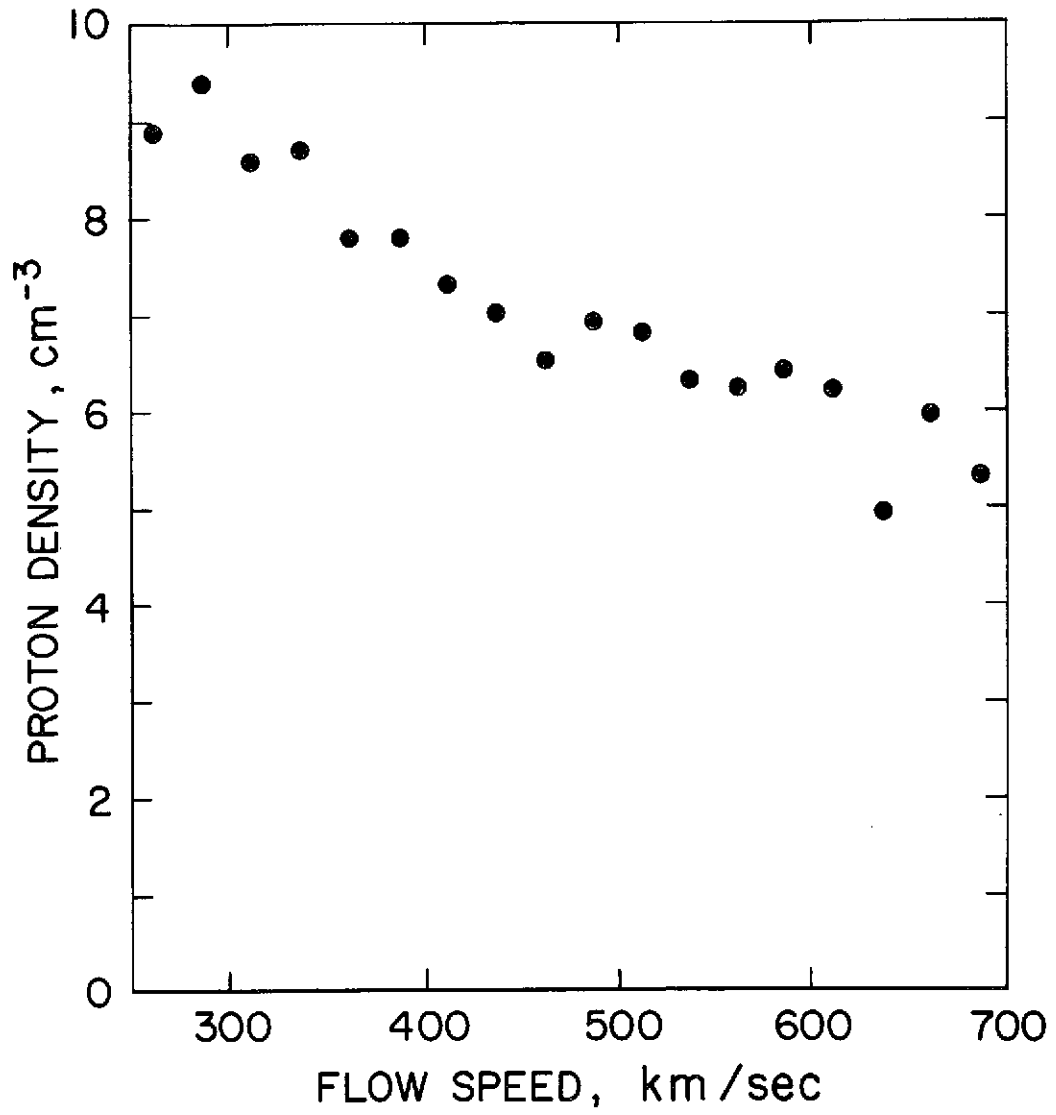
1AB709-7



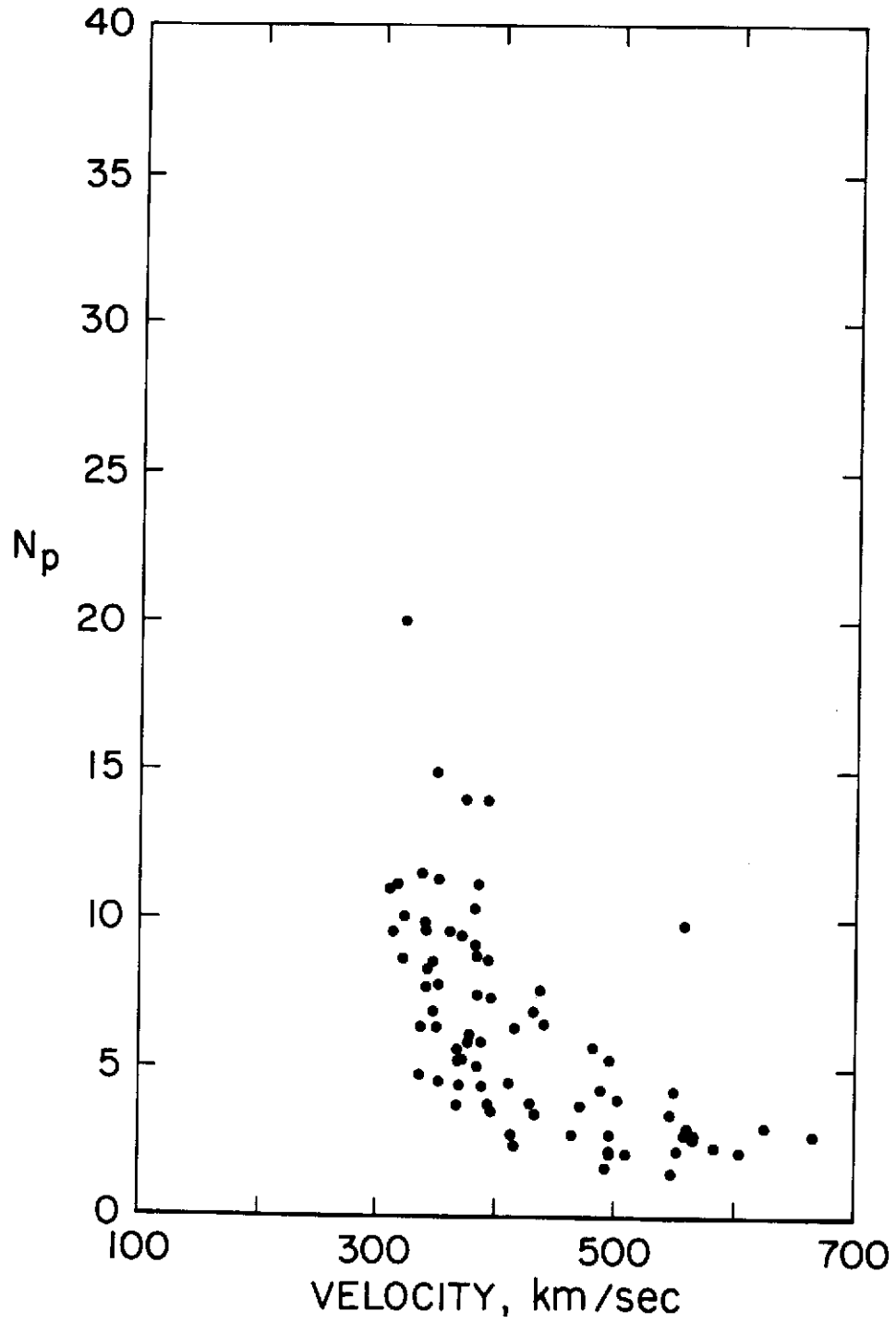


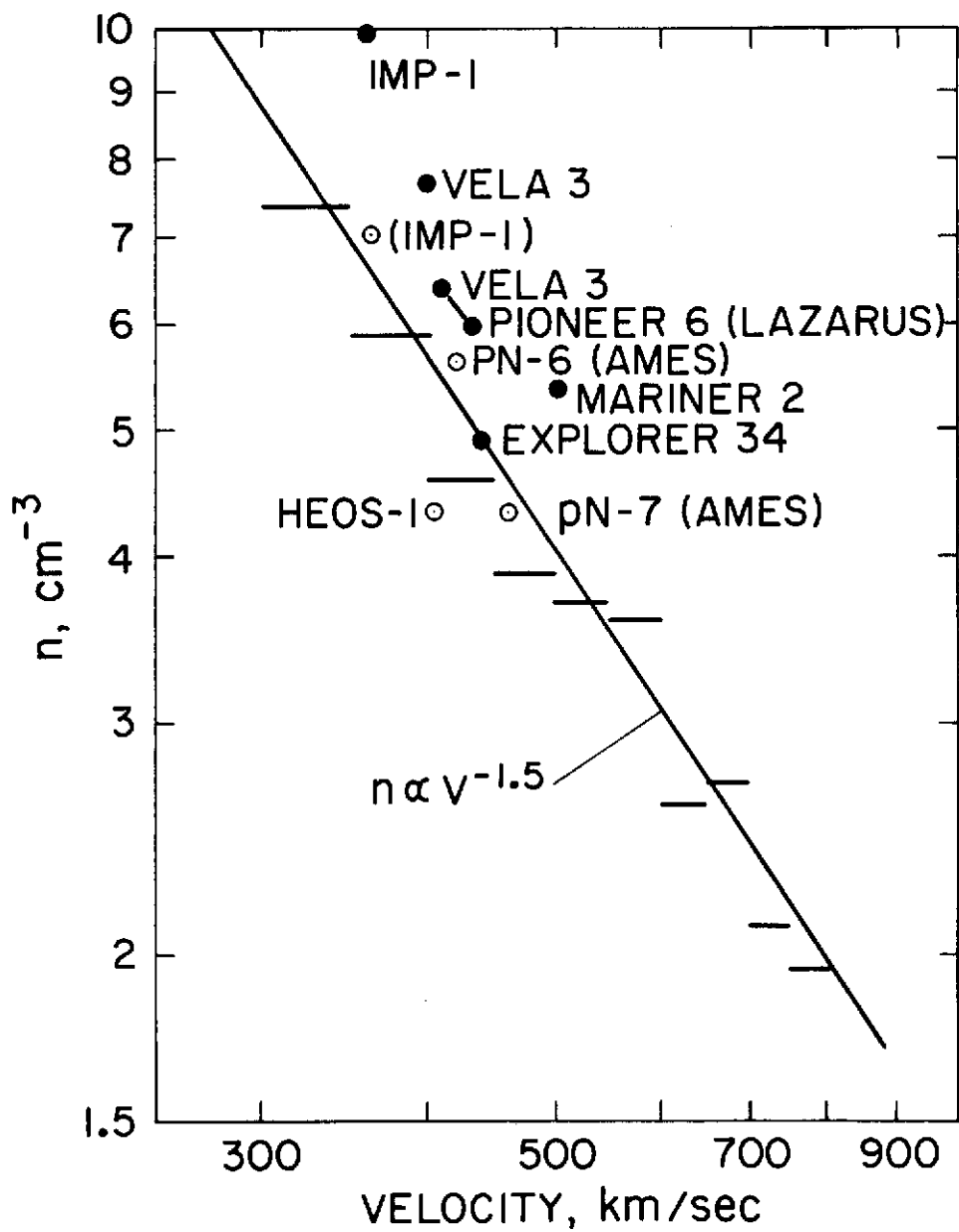


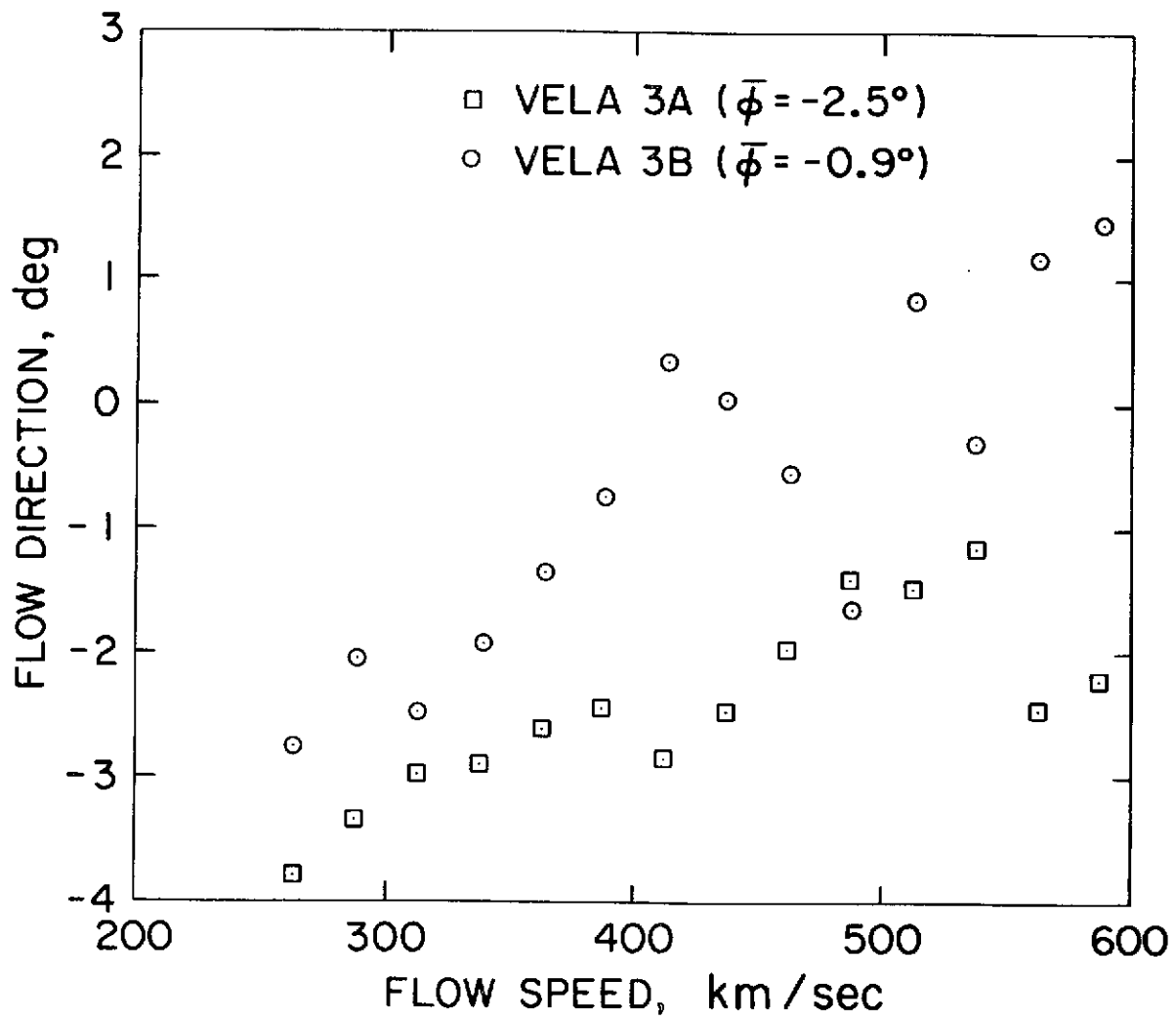




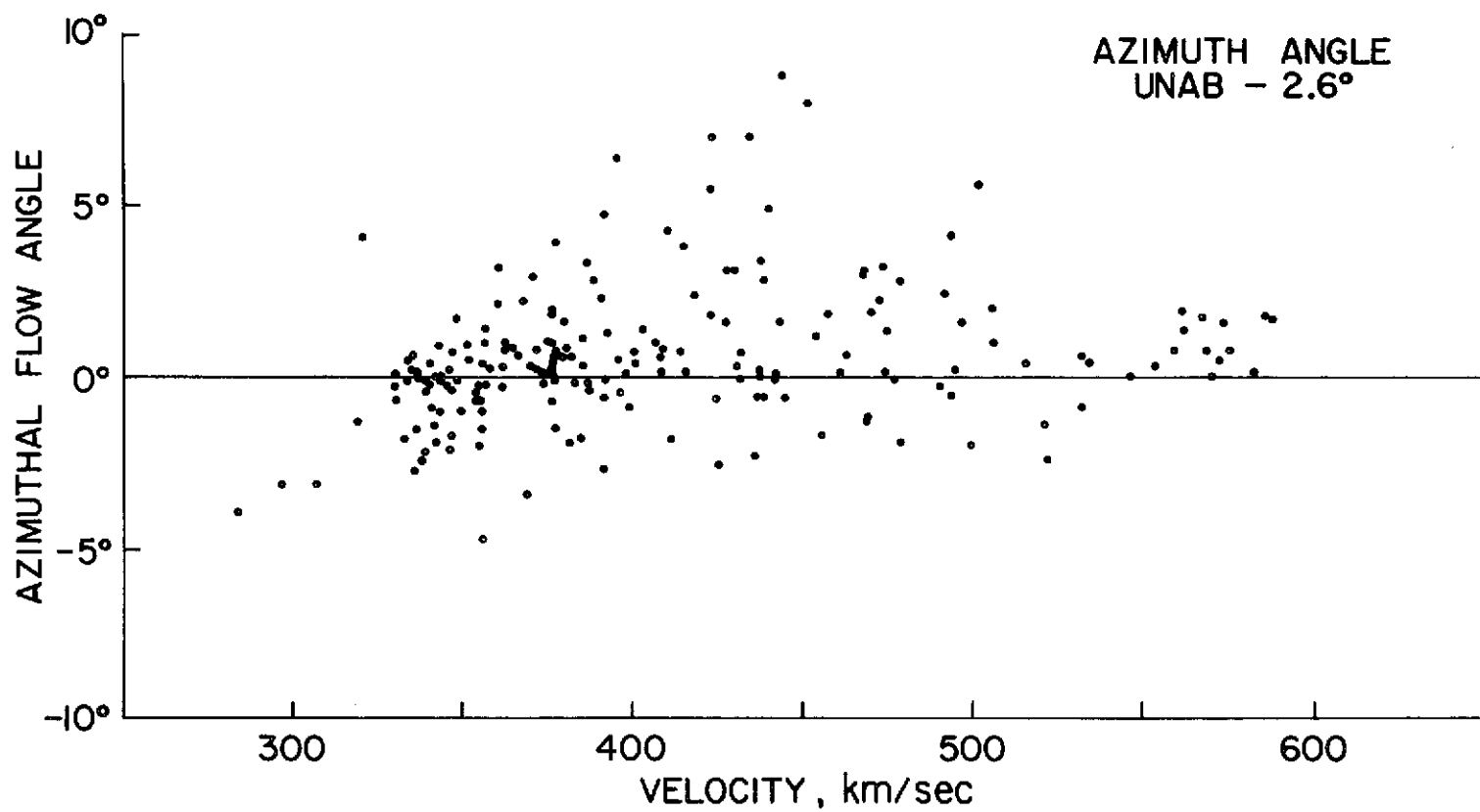
PIONEER 6
12/18/65 - 3/2/66



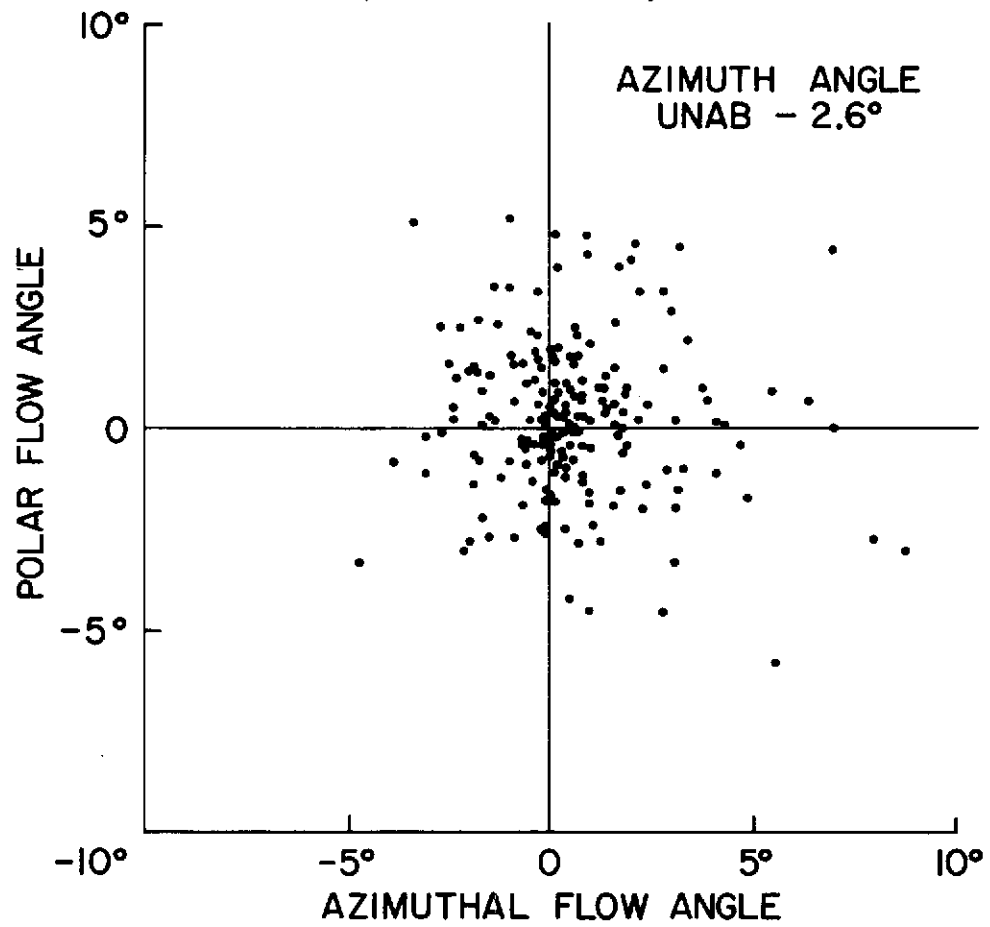




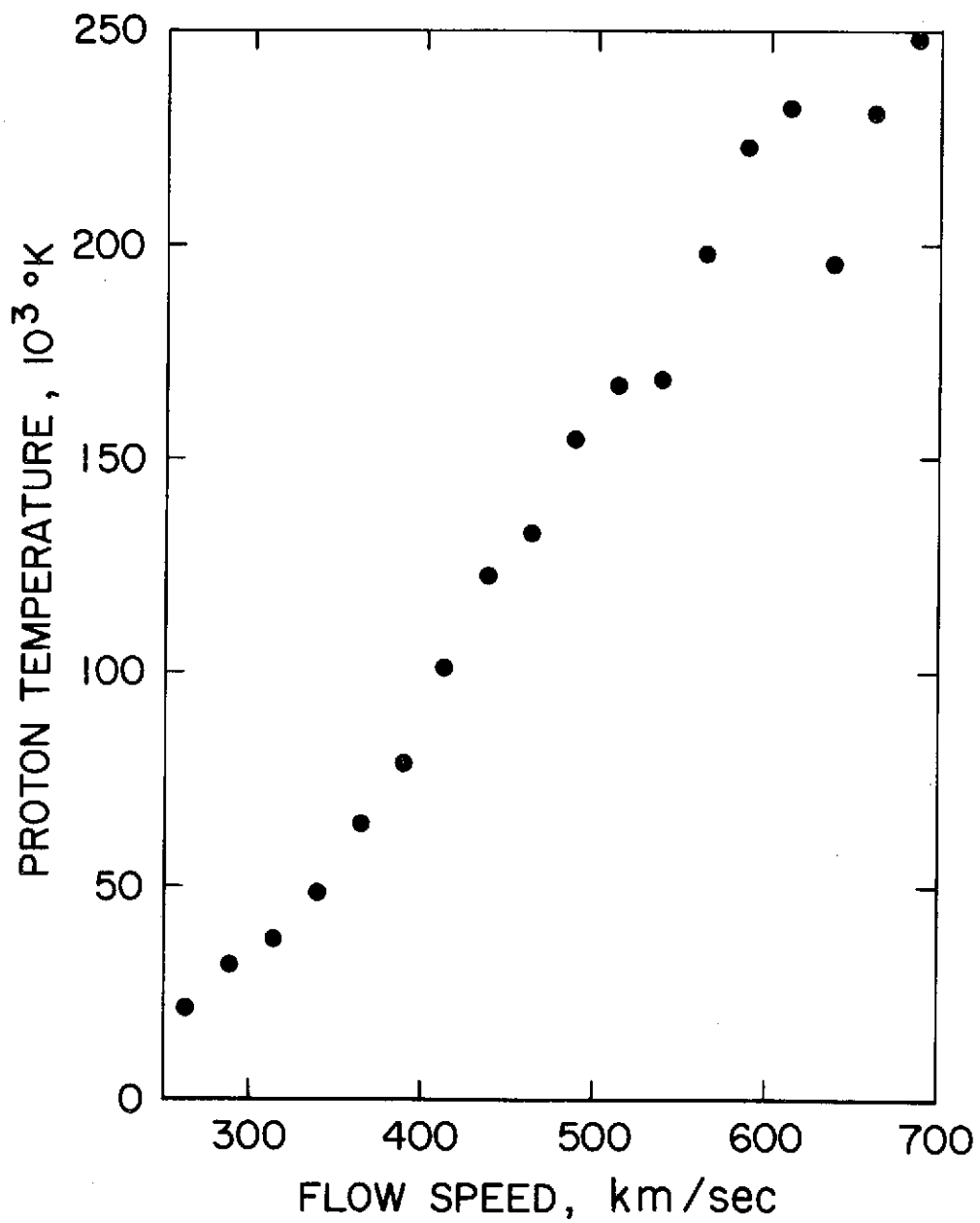
PIONEER 6
3 hr AVG's
DEC 18, 1965 - JAN 14, 1966



PIONEER 6
3 hr AVG's
DEC 18, 1965 - JAN 14, 1966

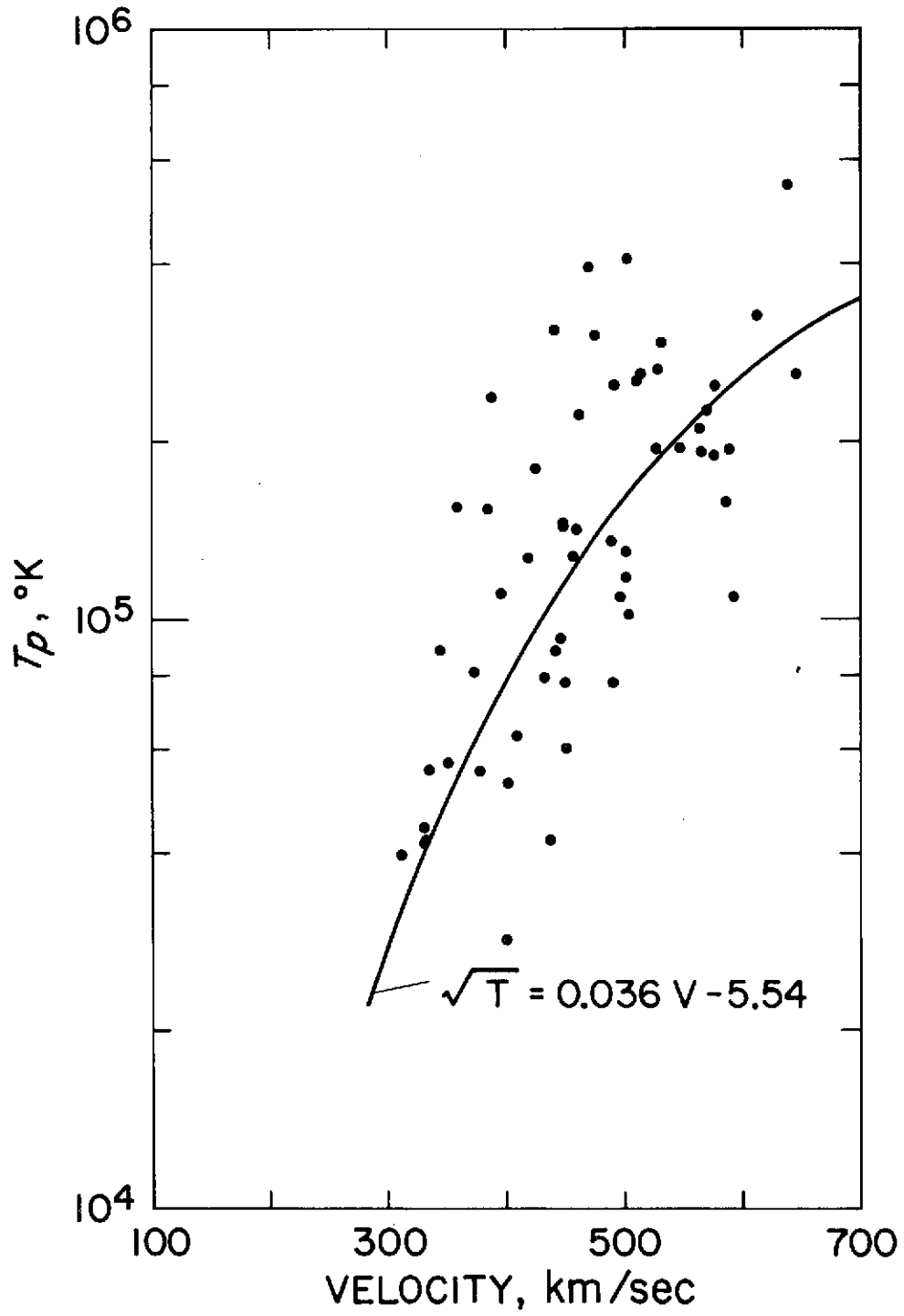


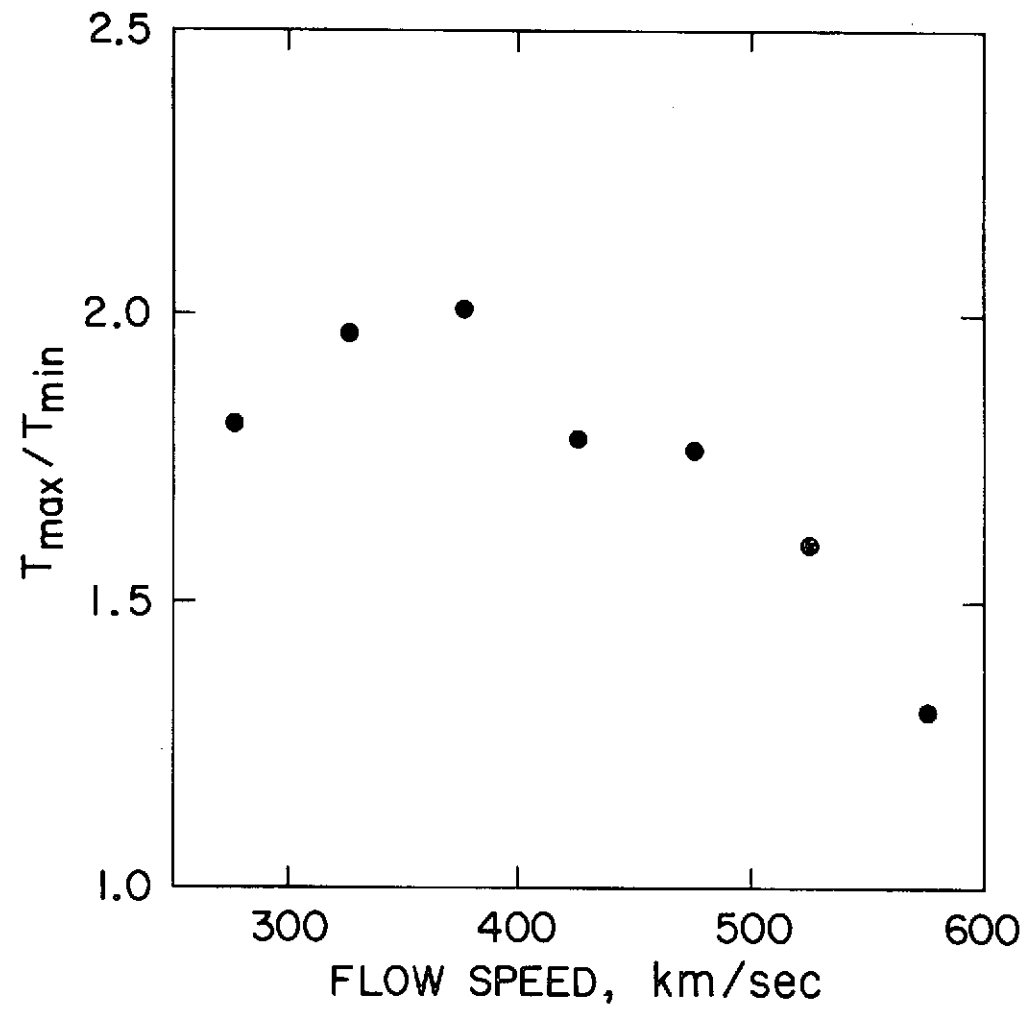
218

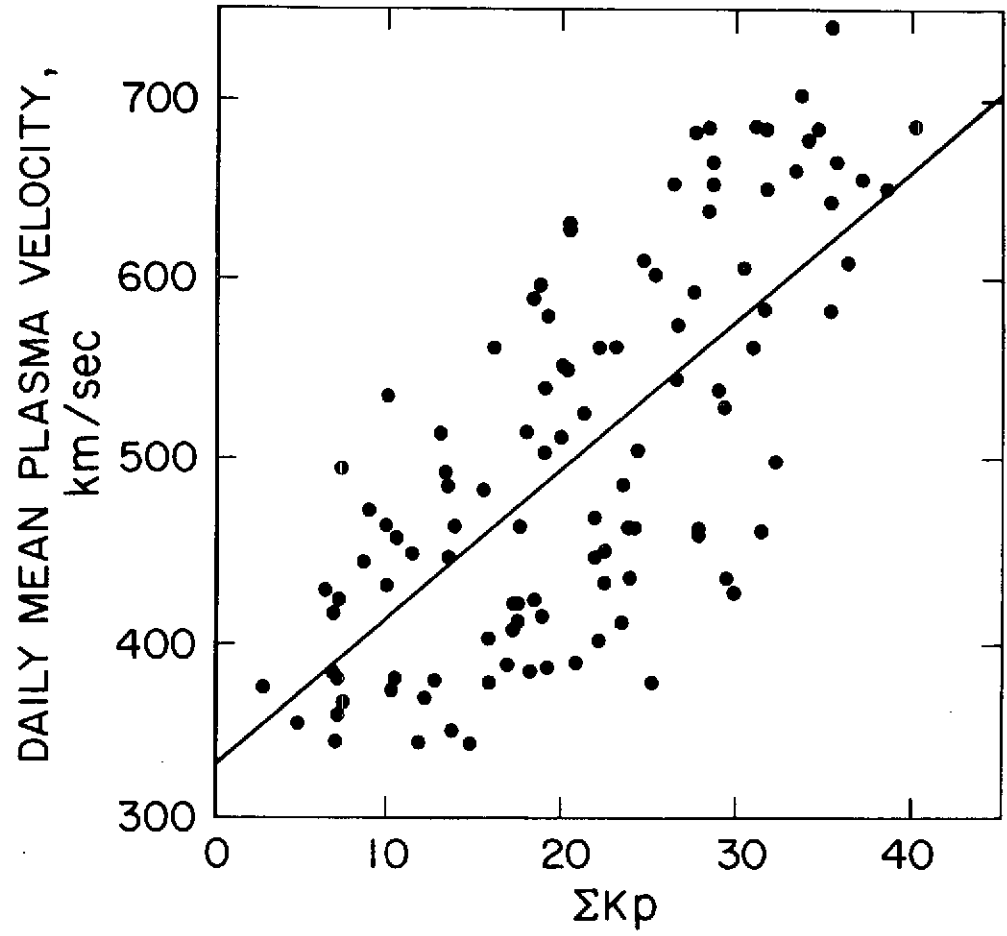


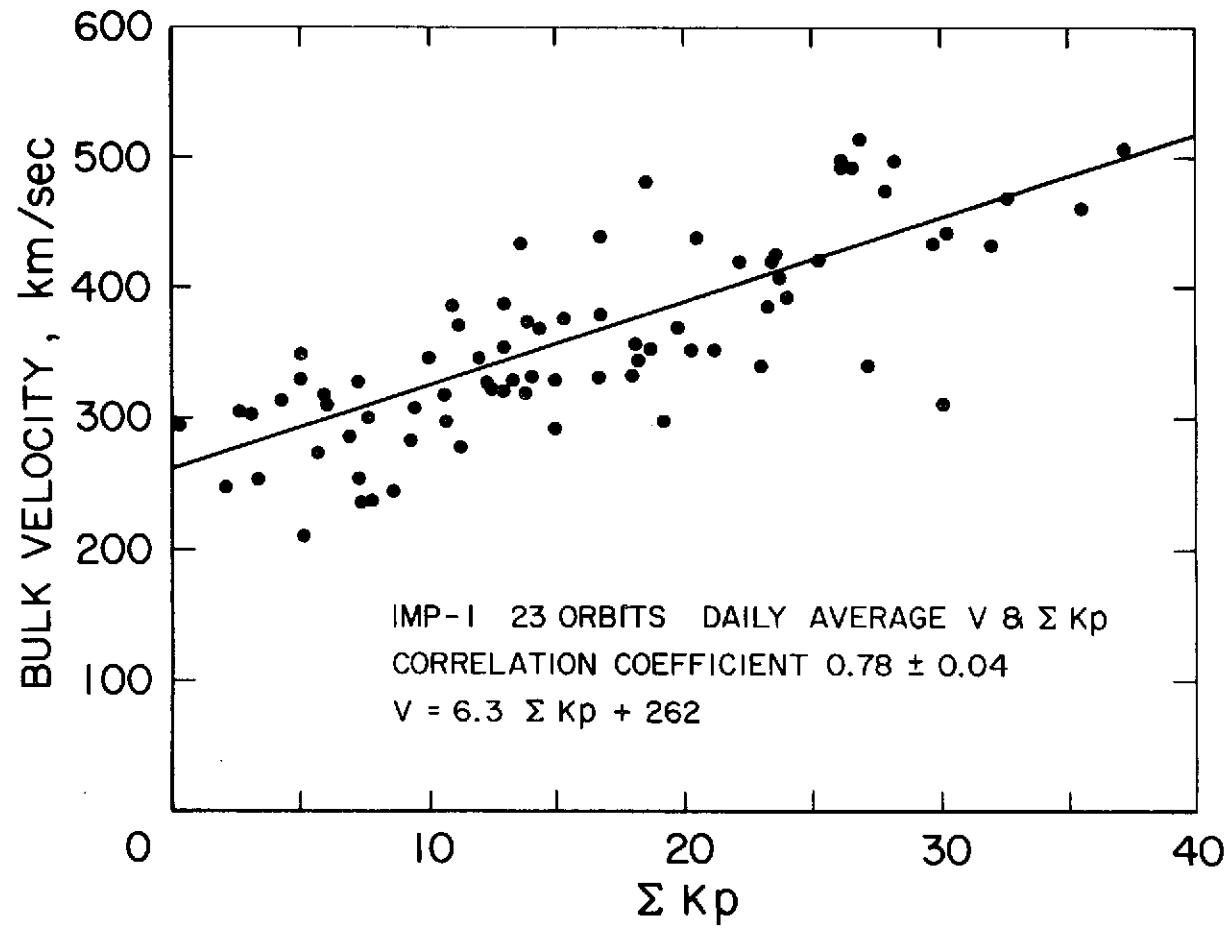
PIONEER 6

12/18/65 - 3/2/66

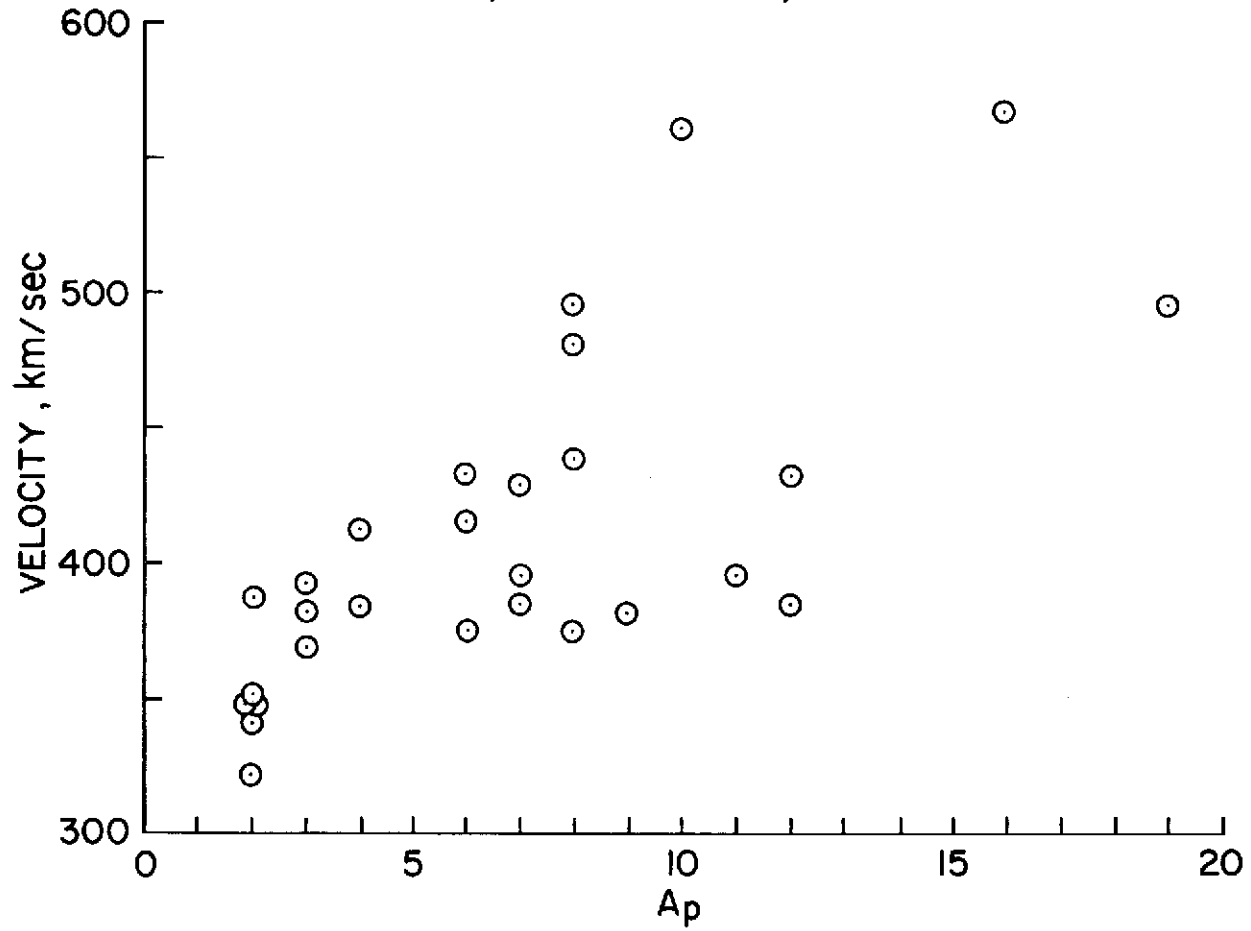




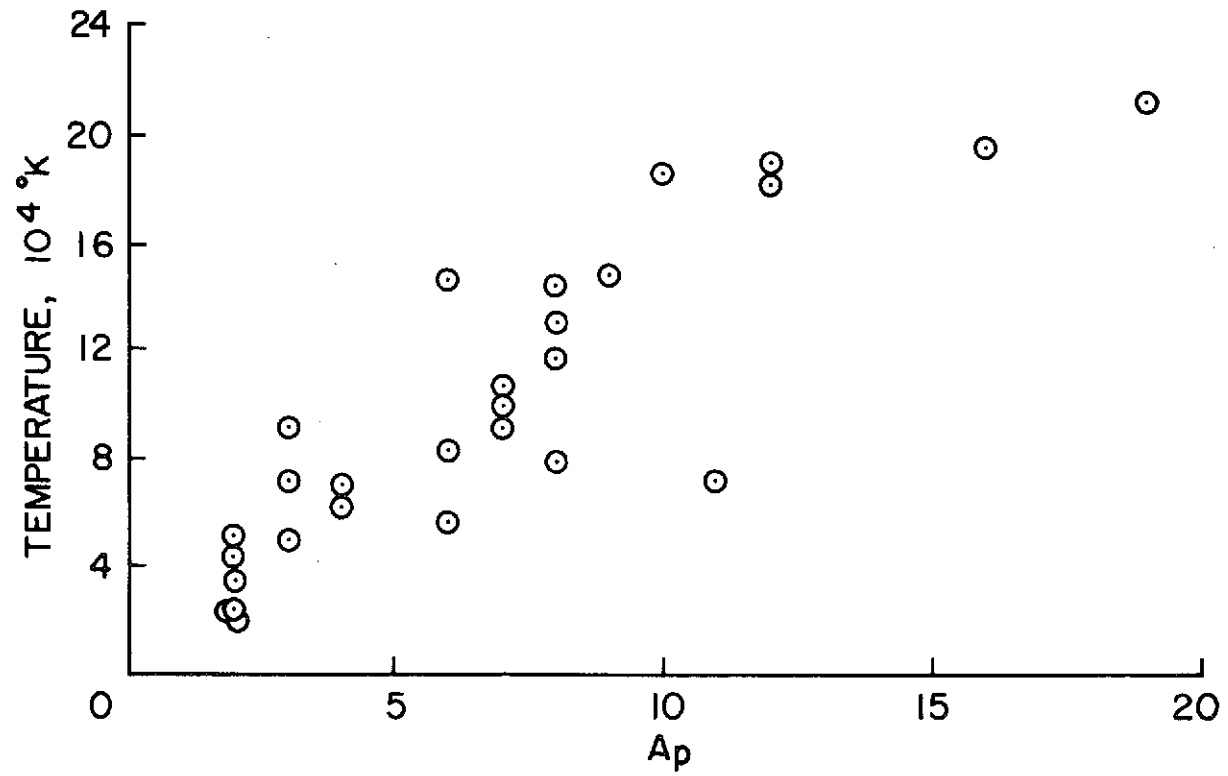




PIONEER 6
24 hr AVG's
DEC 18, 1965 - JAN 14, 1966

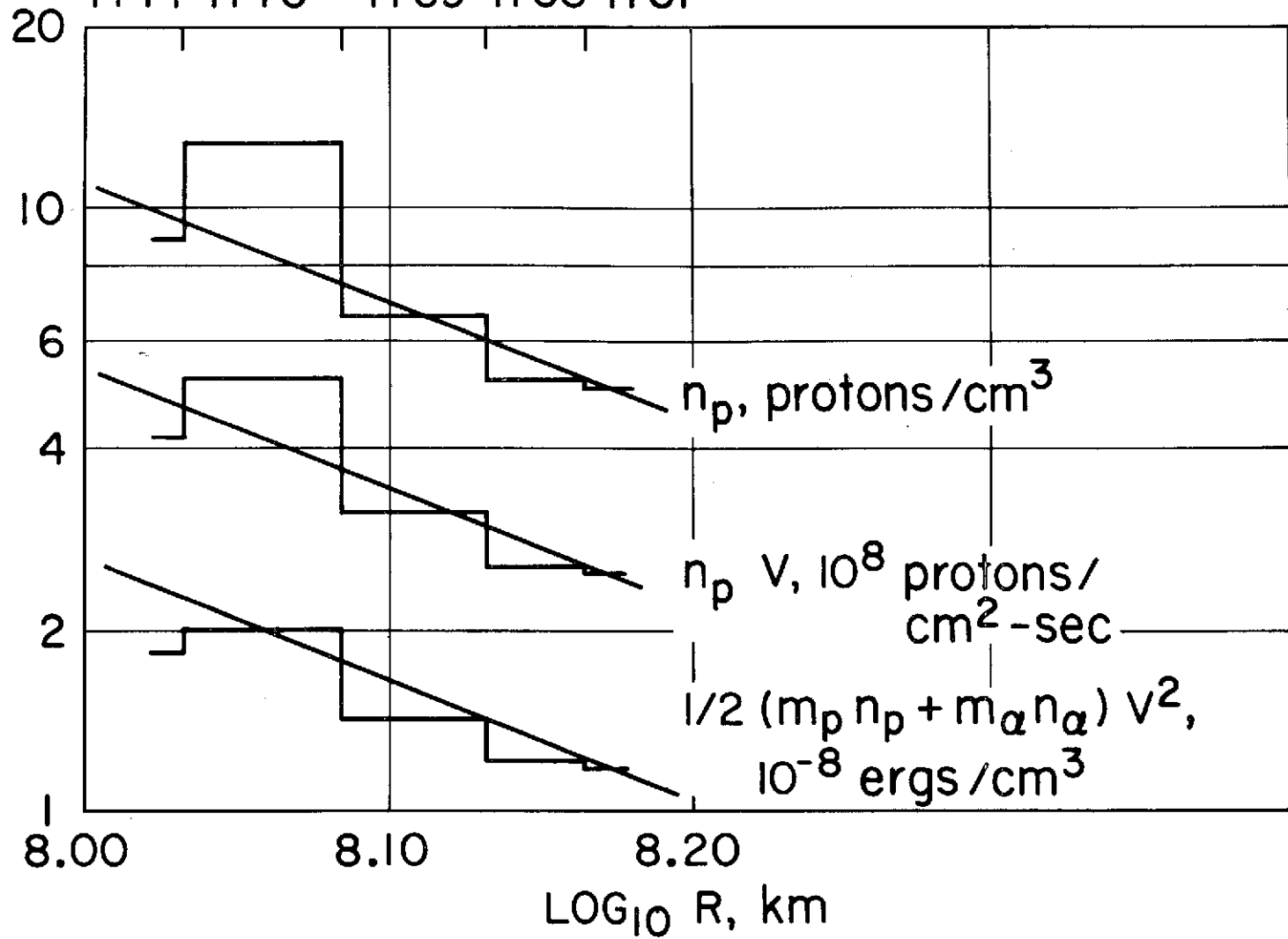


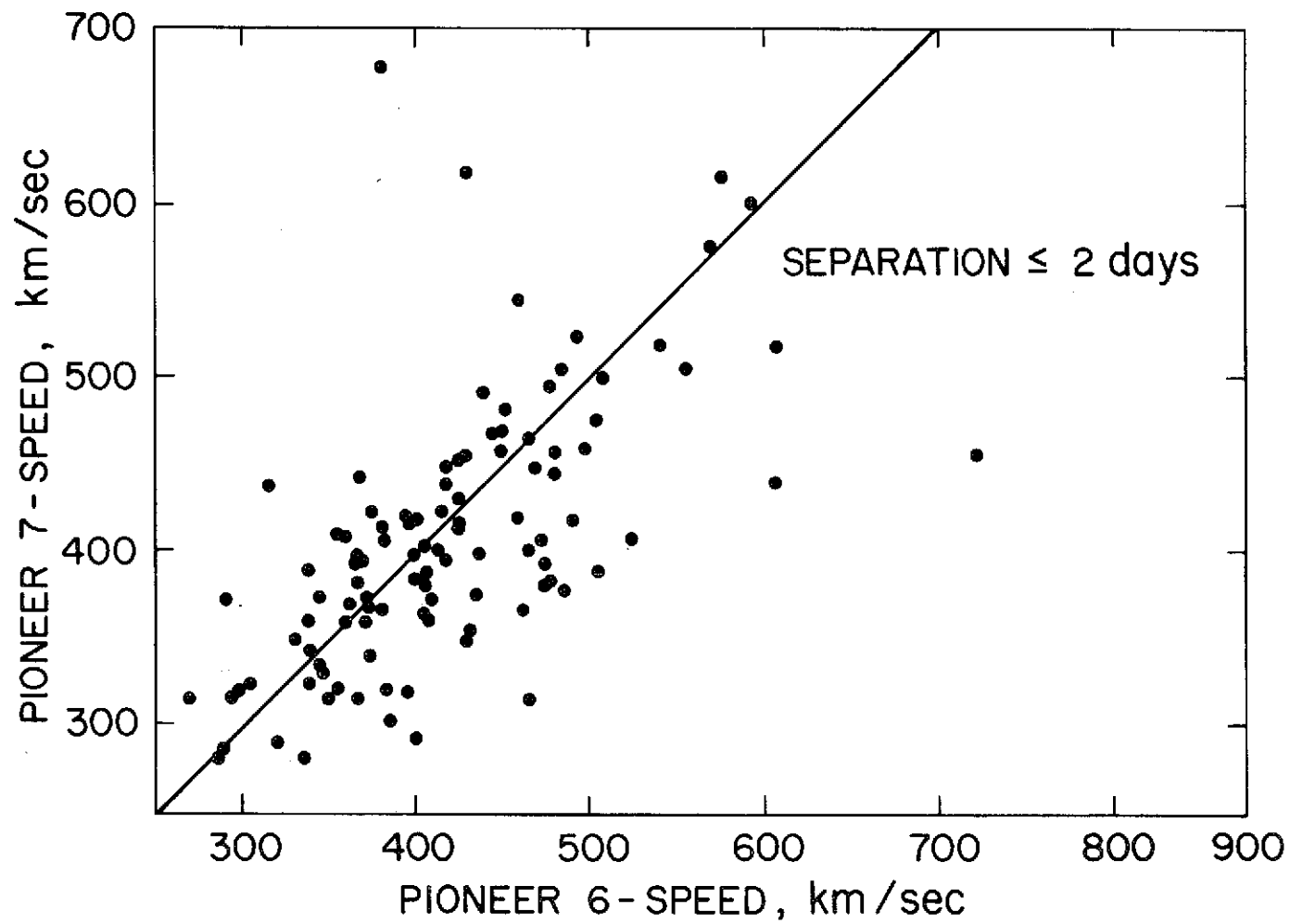
PIONEER 6
24 hr AVG's
DEC 18, 1965 - JAN 14, 1966



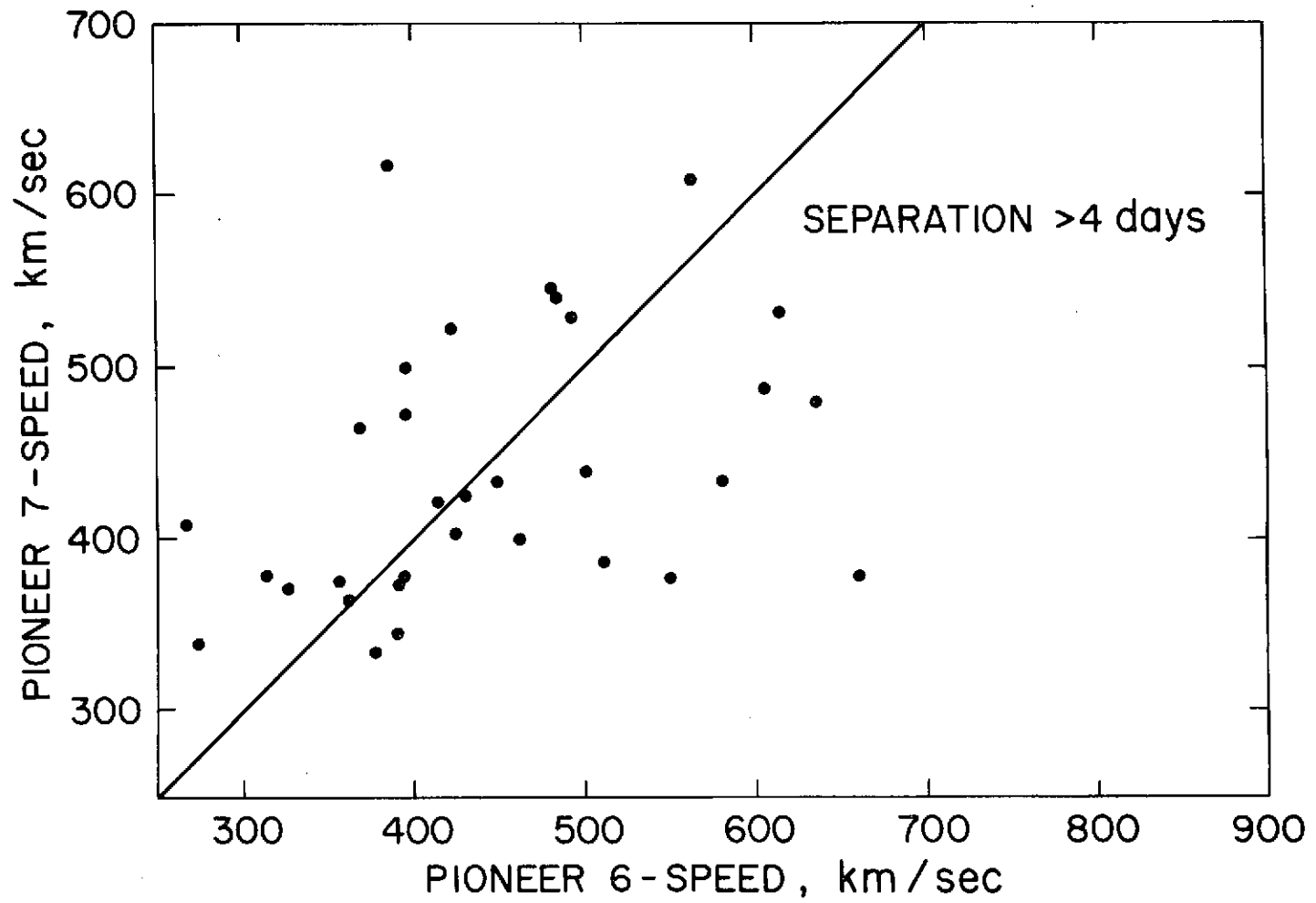
SOLAR ROTATION NUMBER

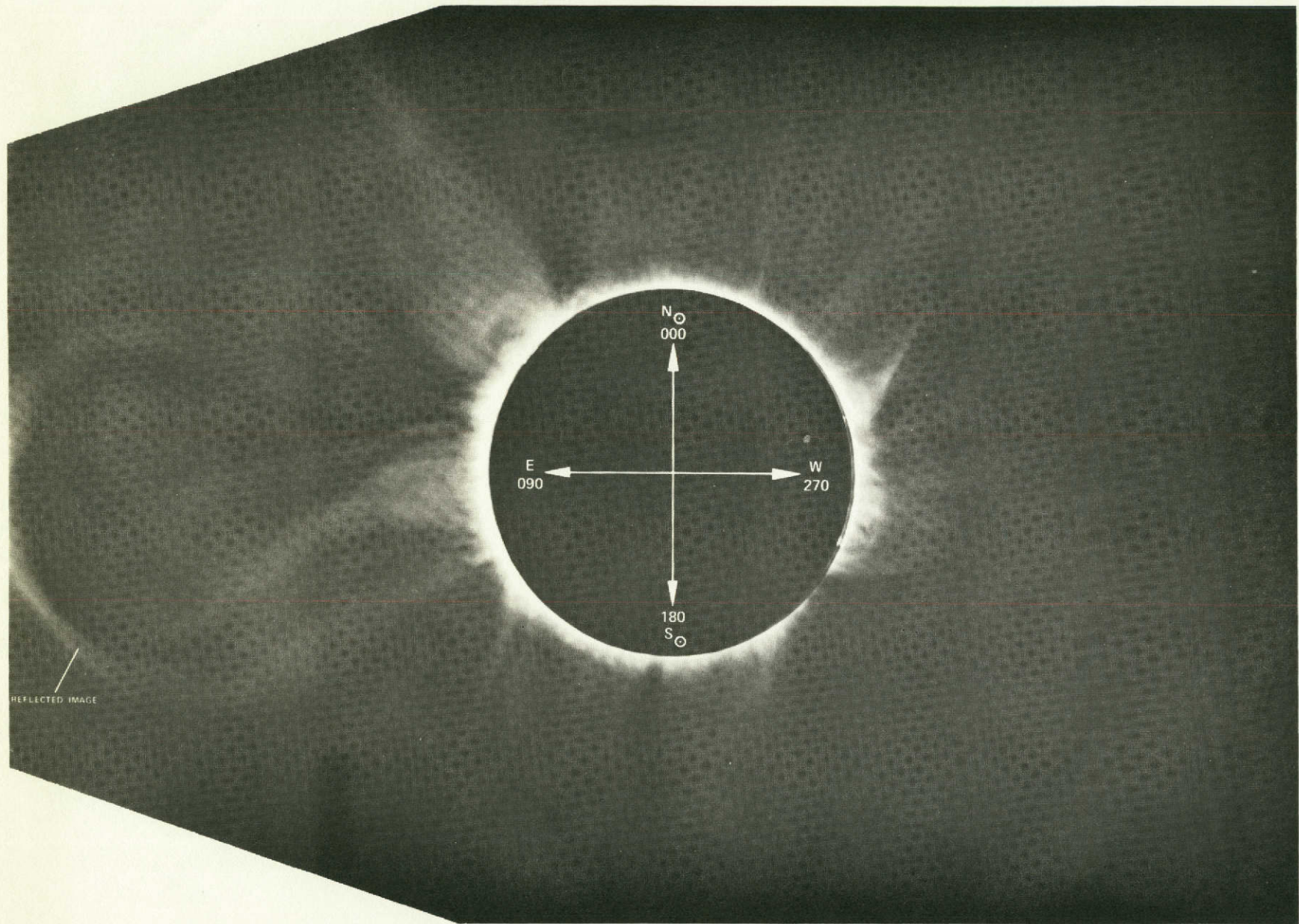
1771 1770 1769 1768 1767





20





S. M. SMITH
NASA — AMES RESEARCH CENTER
L. M. WEINSTEIN
NASA — LANGLEY RESEARCH CENTER